Investigation on the Relationship between Protein Aggregation and Neurodegeneration of Polyglutamine Disease in an Inducible Drosophila Model

THE CHINESE UNIVERSITY OF HONG KONG LIBRARY SYSTEM

WONG, Siu Lun

A Thesis Submitted in Partial Fulfillment
of the Requirements for the Degree of
Master of Philosophy
in
Molecular Biotechnology

© The Chinese University of Hong Kong
July 2007

The Chinese University of Hong Kong holds the copyright of this thesis. Any person(s) intending to use a part or whole of the materials in the thesis in proposed publication must seek copyright release from the Dean of the Graduate School.

香港中文大學
大學
統系館書圖
15 JUL 2008
UNIVERSITY
LIBRARY SYSTEM
THE CHINESE UNIVERSITY OF HONG KONG

Thesis/Assessment Committee

Professor TSUI, Kwok Wing (Chair)
Professor CHAN, Ho Yin (Thesis Supervisor)
Professor NGAI, Sai Ming (Committee Member)
Professor Cahir O'KANE (External Examiner)

DECLARATION

I declare that this dissertation is entirely my own work except where otherwise stated, either in the form of citation of published work, or acknowledgement of the source of any unpublished material.

Signed .....

Wong Siu-lun

ABSTRACT

Protein aggregation is a common pathologic feature of various neurodegenerative disorders including polyglutamine (polyQ) diseases. Disease-associated proteins that contain an expanded polyQ tract show a tendency to form aggregates and trigger neuronal dysfunction in polyQ-induced degeneration. Expanded polyQ proteins exist in various biophysical conformations that display different biochemical solubility properties. However, it remains unclear which forms of the expanded polyQ protein species cause neurodegeneration. In the present study, an inducible transgenic *Drosophila* model was established, and used to study the role of polyQ protein aggregates in neurodegeneration *in vivo*. Induction of expanded polyQ protein expression caused progressive degeneration of neurons in this model organism. Changes in levels of microscopically visible polyQ protein aggregates were not correlated with either pathogenic or protective effects on neuronal degeneration. However, biochemical analysis identified a distinct toxic fraction of expanded polyQ protein, which is sodium-dodecyl sulfate (SDS) insoluble and of size less than 220 nm. Atomic force microscopic analysis further defined such toxic expanded polyQ protein fraction to contain spherical oligomers with sizes of 5 to 20 nm. Collectively, this study provides *in vivo* evidence for the existence of spherical

polyQ oligomers that implicate neurotoxicity.

ABSTRACT (CHINESE VERSION)

蛋白聚集是多聚谷氨酰胺病 (polyglutamine diseases; polyQ diseases) 等多種神經退化性疾病的共同病理特徵。導致多聚谷氨酰胺病的蛋白帶有一段過度擴增的多聚谷氨酰胺序列，這類蛋白傾向形成蛋白聚集體 (aggregates)，並引起神經機能失常。多聚谷氨酰胺延伸的蛋白 (Expanded polyQ protein) 展示不同的物理形態和溶解程度，然而哪一種蛋白形態導致神經退化仍未有一個確切的定論。此研究以一個可誘導表達的基因改造果蠅爲模型去解構體內蛋白聚集體在神經退化過程中的角色。在這個研究模型中，多聚谷氨酰胺延伸蛋白的誘導表達逐漸引起神經元退化。改變於顯微鏡下可確認的蛋白聚集體的水平對神經元退化並不構成致病性抑或是保護性的作用。生化分析卻發現一種不溶於十二烷基硫酸鈉 (sodium dodecyl sulfate) 及粒徑小於二百二十納米的致病性多聚谷氨酰胺延伸蛋白。原子力顯微鏡分析進一步確定這種致病性蛋白呈球狀的形態 (spherical oligomers)，而粒徑則爲五至二十納米。總括而言，此項研究證實了球狀多聚谷氨酰胺延伸蛋白的存在，並強調其對於體內神經元退化的影響。

ACKNOWLEDGEMENTS

I would like express my deepest gratitude to my supervisor Dr. Edwin H. Y. Chan for his support and patient guidance in completing this project and writing up the thesis.

I sincerely thank all members of the Laboratory of *Drosophila* Research, CUHK, especially Ms. Priscilla W. M. Chan, Ms. Katy W. K. Chau, Ms. Gigi C. G. Choi, Dr. Macy N. Y. Huen, Ms. Jessica W. Lam, Ms. Angel Y. W. Lee, Ms. Azaria K. Y. Wong, Mr. Eric C. M. Chan, Mr. Steve T. W. Lo and Dr. Benny C. P. Yiu, and all labmates at MMW509, in particular Ms. L. M. Choi, Ms. Ivy H. Geng, Ms. Irene P. M. Lau, Ms. Peggy P. Y. Law, Ms. Teresa P. T. Tsang, Mr. M. Y. Liu and Mr. Wayne J. W. Zhou for their help, inspiring suggestions and encouragement in all the time of my research.

I am grateful to Mr. Andrew S. K. Li for his technical assistance and helpful discussion on AFM studies, and Dr. Martin E. Feder for anti-fly Hsp70 antibodies.

Particularly, I would like to give special thanks to my family and friends whose patience and continuous care enables me to complete this work.

LIST OF ABBREVIATIONS

Abbreviation used	Term
AFM	Atomic Force Microscopy
APS	Ammonium Persulfate
CBP	cAMP-response-element Binding Protein
cDNA	complementary Deoxyribonucleic Acid
DAPI	4'-6-Diamidino-2-phenylindole
dpe	days post-eclosion
dpi	days post-induction
DNase	Deoxyribonuclease
DNA	Deoxyribonucleic acid
DEPC	Diethyl Pyrocarbonate
dNTPs	Deoxynucleoside Triphosphates
DRPLA	Dentatorubropallidoluysian Atrophy
DTT	Dithiothreitol
ECL	Enhanced Chemiluminescent
EDTA	Ethylenediaminetetraacetic Acid
EGFP	Enhanced Green Fluorescent Protein
FA	Formic Acid
FITC	Fluorescein Isothiocyanate
GAL80^{ts}	Temperature-sensitive GAL80
GFP	Green Fluorescent Protein
gmr	*glass multiple reporter*
HA	Hemagglutinin
Tris-HCl	Tris-Hydrochloric Acid
HD	Huntington's Disease
HRP	Horseradish Peroxidase
Hsc70	Heat shock cognate 70
Hsp70	Heat shock protein 70
IgG	Immunoglobulin G
KCl	Potassium Chloride
KH_2PO_4	Potassium Phosphate Monobasic Anhydrous
$MgCl_2$	Magnesium Chloride
MJD	Machado-Joseph Disease

$Na_2HPO_4 \cdot 7H_2O$	Sodium Phosphate Dibasic Heptahydrate
NA	Numerical Aperture
NaCl	Sodium Chloride
NP-40	Nonidet P-40
O.C.T.	Optimum Cryosectioning Temperature
PBS	Phosphate-Buffered Saline
PBS-T	Phosphate-Buffered Saline-Triton X-100
PBS-GS	Phosphate-Buffered Saline-Goat Serum
PMSF	Phenylmethanesulphonylfluoride
PolyQ	Polyglutamine
PVDF	Polyvinylidene Fluoride
RNase	Ribonuclease
RNA	Ribonucleic Acid
RT-PCR	Reverse Transcription-Polymerase Chain Reaction
SBMA	Spinobulbar Muscular Atrophy
SCA	Spinocerebellar Ataxia
SDS	Sodium Dodecyl Sulfate
SDS-PAGE	Sodium Dodecyl Sulfate-Polyacylamide Gel Electrophoresis
s.e.m.	*standard error of the mean*
Taq	*Thermus aquaticus*
TARGET	Temporal And Regional Gene Expression Targeting
TBE	Tris-Borate-EDTA
TBS	Tris-Buffered Saline
TBS-T	Tris-Buffered Saline-Tween-20
TCA	Trichloroacetic Acid
TEMED	N,N,N',N'-Di-(dimethylamino)ethane
***tub*P**	*tubulin* Promoter
UAS	Upstream Activator Sequence

LIST OF TABLES

LIST OF FIGURES

TABLE OF CONTENTS

1. INTRODUCTION

1.1 Neurodegenerative disorders – a brief overview

Neurodegenerative disorders are neurological diseases that are often characterized by accumulation of microscopically visible protein aggregates in neurons (reviewed by Ross and Poirier, 2004) and progressive malfunctioning and/or death of neurons (reviewed by Bredesen et al., 2006; Palop et al., 2006). Common examples include Alzheimer's disease, Parkinson's disease, amyotrophic lateral sclerosis, and various types of unstable triplet repeat expansion diseases (reviewed by Gatchel and Zoghbi, 2005; Hardy and Gwinn-Hardy, 1998). Despite the peculiar characteristics of each pathologic condition, neurodegenerative disorders are often diagnosed by loss of memory and mobility in patients (reviewed by Palop et al., 2006). Since these disease symptoms cannot be clinically recognized until substantial deterioration of neuronal function has occurred, pre-symptomatic neuronal dysfunction exists (reviewed by Rubinsztein, 2006). Potential mechanisms of neuronal dysfunction include dysregulation of neuronal excitation (reviewed by Doble, 1999), malfunctioning of mitochondria (reviewed by Lin and Beal, 2006) and impairment of intracellular protein degradation machineries (reviewed by Rubinsztein, 2006).

1.2 Polyglutamine diseases

Polyglutamine (PolyQ) diseases are neurodegenerative disorders caused by unstable triplet repeat expansion in the genome which results in an expansion of the existing glutamine-coding triplet (CAG) repeats in the coding region of affected genes (reviewed by Zoghbi and Orr, 2000). At least nine polyQ diseases have been identified thus far, and they are Huntington's disease (HD), spinobulbar muscular atrophy (SBMA), dentatorubropallidoluysian atrophy (DRPLA) and several types of spinocerebellar ataxia (SCA) including SCA 1, 2, 3, 6, 7 and 17 (reviewed by Gatchel and Zoghbi, 2005). The CAG repeat expansion results in the production of an expanded polyQ tract in the respective disease protein (Table 1). Disease protein with an expanded polyQ tract shows a tendency to form microscopically visible aggregates in neurons (Figure 1; reviewed by Ross and Poirier, 2004).

Similar to most other neurodegenerative disorders, polyQ diseases usually strike in midlife, trigger progressive neuronal dysfunction, and eventually lead to cognitive impairment, motor deficits, as well as neuronal cell loss (reviewed by Zoghbi and Orr, 2000). An interesting trait of polyQ diseases is that the size of the glutamine repeat expansion is correlated with lower age of onset and the severity of the disease (reviewed by Zoghbi and Orr, 2000). For most polyQ diseases, the threshold repeat

Table 1. Molecular characterization of polyglutamine diseases.

Disease	Gene locus	Gene product	Normal CAG(n)	Expanded CAG(n)	Protein localization	Special features	Brain regions most affected
DRPLA	12q	Atrophin-1	6–36	49–84	Cytoplasmic		Cerebellum, cerebral cortex, basal ganglia, Luys body
HD	4p16.3	Huntingtin	6–34	36–121	Cytoplasmic	Intermediate alleles: 29–35	Striatum, cerebral cortex
SBMA	Xq11-12	Androgen receptor	9–36	38–62	Nuclear and cytoplasmic		Anterior horn and bulbar neurons, dorsal root ganglia
SCA1	6p22-23	Ataxin-1	6–44	39–82	Nuclear in neurons	Normal alleles >21 repeats interrupted with 1–4 CAT units	Cerebellar Purkinje cells, dentate nucleus; brainstem
SCA2	12q23-24	Ataxin-2	15–31	36–63	Cytoplasmic	Normal alleles interrupted with 1–2 CAA units	Cerebellar Purkinje cells, brain stem, fronto-temporal lobes
SCA3/ MJD	14q24.3-31	Ataxin-3	12–41	62–84	Cytoplasmic		Cerebellar dentate neurons, basal ganglia, brain stem, spinal cord
SCA6	19p13	CACNA1A	4–18	21–33	Cell membrane		Cerebellar Purkinje cells, dentate nucleus, inferior olive
SCA7	3p12-p21.1	Ataxin-7	4–35	37–306	Nuclear	Intermediate alleles: 28–35	Cerebellum, brain stem, macula, visual cortex
SCA17	6q27	TATA-binding protein	25–42	47–63	Nuclear		Cerebellar Purkinje cells

(Modified from Zoghbi and Orr (2000) and Gatchel and Zoghbi (2005)).

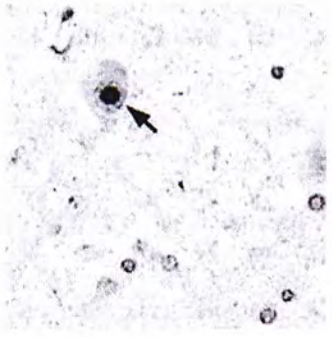

Figure 1. Presence of microscopically visible aggregates in brain tissues of patients with polyglutamine disease. A hallmark feature of polyglutamine diseases is the formation of microscopically visible disease protein aggregates in affected neurons. The image shown is the occurrence of nuclei-containing disease protein aggregates (indicated by arrow) in a brain tissue section of a patient with spinocerebellar ataxia type 3. (Adapted from Paulson et al. (1997)).

number for pathogenesis is around 40 (Table 1).

Most polyQ diseases show a dominant pattern of inheritance (reviewed by Zoghbi and Orr, 2000). It has been suggested that the glutamine repeat expansion would cause a loss-of-function of the wild type disease protein in which its activity can be reduced up to 50 percent (reviewed by Cattaneo et al., 2001). However, polyQ diseases are not caused by a simple loss-of-function mechanism (reviewed by Rubinsztein, 2006). In fact, expanded polyQ protein also provokes a common toxic gain-of-function mechanism which has significant implications on disease pathogenesis (reviewed by Di Prospero and Fischbeck, 2005). Toxicity conferred by the glutamine repeat expansion is directly supported by that comparable disease phenotypes occur, even if the expanded polyQ tract is carried by unrelated cellular proteins such as hypoxanthine phosphoribosyltransferase (Ordway et al., 1997) and enhanced green fluorescent protein (EGFP; Lam and Chan, unpublished data), or is expressed without any adjoining sequence (Adachi et al., 2001; Lievens et al., 2005; Marsh et al., 2000). A toxic gain-of-function mechanism could potentially be mediated through the aberrant interaction between the expanded polyQ protein and various cellular factors (see below, section 1.3).

It is well documented that expanded polyQ proteins interfere with the gene transcription (reviewed by Butler and Bates, 2006; Riley and Orr, 2006), protein folding (reviewed by Brignull et al., 2007; Huen et al., 2007), and protein degradation (reviewed by Rubinsztein, 2006) machineries. For example, a number of cAMP-response-element Binding Protein (CBP)-dependent transcriptional activities (Jiang et al., 2006; McCampbell et al., 2000; Nucifora et al., 2001; Wyttenbach et al., 2001), the level of various molecular chaperones (Chang et al., 2005; Hay et al., 2004; Huen and Chan, 2005; Tsai et al., 2005; Wen et al., 2003) and the activity of the ubiquitin-proteasome system (Bence et al., 2001; Bennett et al., 2005) are depleted in polyQ pathogenesis. Such interference provides the basis for neuronal dysfunction to occur (reviewed by Brignull et al., 2007; Butler and Bates, 2006; Gatchel and Zoghbi, 2005; Rubinsztein, 2006). This is further supported by that over-expression of transcription regulators like CBP (Jiang et al., 2006; McCampbell et al., 2000; Nucifora et al., 2001; Taylor et al., 2003b) and molecular chaperones (Chan et al., 2000; Cummings et al., 2001; Fernandez-Funez et al., 2000; Kazemi-Esfarjani and Benzer, 2000; Kobayashi et al., 2000; Warrick et al., 1999) suppresses polyQ-mediated toxicity. Puzzlingly, while most disease proteins are widely expressed throughout the brain and other tissues, only subsets of neurons are susceptible to dysfunction (Table 1). Up till now, the mechanisms by which neuronal

dysfunction instigated in particular cell types remain unclear (reviewed by Michalik and Van Broeckhoven, 2003).

1.3 Microscopically visible polyglutamine protein aggregates and its relation to toxicity

Neurodegenerative disorders including polyQ diseases are frequently characterized by accumulation of microscopically visible protein aggregates in affected neurons (Figure 1; reviewed by Ross and Poirier, 2004). The involvement of these protein aggregates in polyQ pathogenesis has been extensively studied for over a decade (reviewed by Michalik and Van Broeckhoven, 2003; Ross and Poirier, 2005; Slow et al., 2006).

To resolve the role of microscopically visible polyQ protein aggregates, some researchers have attempted to ascertain their composition. These aggregates are not solely composed of the respective expanded polyQ disease protein; a range of cellular factors are also present in them (reviewed by Michalik and Van Broeckhoven, 2003). Sequestration of cellular factors to polyQ aggregates has been speculated to compromise their normal activities and eventually lead to neuronal dysfunction. For example, various transcription regulators, including CBP (McCampbell et al., 2000;

Steffan et al., 2000), localize to microscopically visible polyQ aggregates. Recruitment of CBP to these aggregates may account for the down-regulation of a number of CBP-dependent transcriptional activities observed in polyQ pathogenesis (Jiang et al., 2006; McCampbell et al., 2000; Nucifora et al., 2001; Wyttenbach et al., 2001). Other cellular proteins include molecular chaperones, ubiquitin and proteasome subunits have also been identified in these polyQ aggregates (Chai et al., 2001; Doi et al., 2004; Jana et al., 2001; Mitsui et al., 2002; Stenoien et al., 1999; Suhr et al., 2001; Warrick et al., 1999). Molecular chaperones assist proper folding of proteins as well as their degradation when the proteins cannot be folded properly (reviewed by Bukau et al., 2006; Young et al., 2004), whereas ubiquitin and proteasome subunits are involved in the degradation and clearance of misfolded proteins (reviewed by Rubinsztein, 2006). Co-aggregation of these cellular factors with polyQ aggregates has been proposed to limit cellular protein folding and degradation machineries, which in turn lead to accumulation of misfolded and damaged proteins.

Recruitment of cellular proteins to microscopically visible polyQ aggregates does not necessarily mean that they are irreversibly trapped. Indeed, some studies have revealed that certain recruited proteins including CBP (Stenoien et al., 2002),

molecular chaperone Heat shock protein 70 (Hsp70; Kim et al., 2002) and proteasome subunits (Stenoien et al., 2002) were only transiently associated with these aggregates. It has also been demonstrated that transcription factors including CBP are not depleted by polyQ aggregates (Yu et al., 2002). Whether or not the recruitment of cellular proteins into polyQ aggregates will bring about neuronal toxicity remains disputed.

Cell death has been reported to occur devoid of microscopically visible aggregates (Schiffer et al., 2007). Formation of microscopically visible polyQ aggregates is correlated with reduced cell death in cultured neurons (Arrasate et al., 2004). It is plausible to speculate that the recruitment of molecular chaperones and components of the ubiquitin-proteasome system into these aggregates is indeed a cellular defensive mechanism to assist proper folding and degradation of the expanded polyQ protein, and that aggregate formation prevents the toxic polyQ protein species from forming aberrant interactions with other cellular proteins (reviewed by Michalik and Van Broeckhoven, 2003; Ross and Poirier, 2005; Slow et al., 2006). It is yet to confirm the protective role of microscopically visible protein aggregates in polyQ pathogenesis.

The link between protein aggregation and polyQ pathogenesis has long been recognized, but a causal relationship has not been unequivocally established. One concern is that polyQ protein aggregates develop progressively with time, and so they have been speculated to have multiple roles during disease progression (Morton et al., 2000). In addition, the composition of microscopically visible polyQ aggregates varies considerably among different cell types (Wanderer and Morton, 2007), from cell to cell of the same type (Wanderer and Morton, 2007) and even within an individual cell at different times (Takahashi et al., 2002; Wanderer and Morton, 2007). The role of protein aggregates in polyQ pathogenesis still awaits further examination.

1.4 Polyglutamine protein conformers and their relation to toxicity

Expanded polyQ protein has been proposed to form stable β-sheet-rich structures, through intra- and inter-molecular hydrogen bonds (Perutz et al., 1994). Multiple biophysical conformations have been reported for the expanded polyQ protein, which include monomers (Nagai et al., 2007), spherical oligomers (Ehrnhoefer et al., 2006; Mukai et al., 2005; Wacker et al., 2004), annular oligomers (Wacker et al., 2004), amorphous aggregates (Muchowski et al., 2000; Wacker et al., 2004), protofibrils (Diaz-Hernandez et al., 2004; Li et al., 2006; Poirier et al., 2002)

and fibrils (Dahlgren et al., 2005; Muchowski et al., 2000; Poirier et al., 2002; Scherzinger et al., 1999; Wacker et al., 2004). Temporal analyses have demonstrated a sequential occurrence of spherical oligomers, protofibrils and fibrils (Figure 2; Poirier et al., 2002; Wacker et al., 2004). When the fibrils are large enough, they become microscopically visible (reviewed by Ross and Poirier, 2005). Possible pathways for the formation of these polyQ conformers are illustrated in Figure 3, in which the aggregation process is initiated by a β-sheet conformational transition of the expanded polyQ protein monomer from its native state (Nagai et al., 2007). The exact mechanisms by which these polyQ protein conformers form are however uncertain.

Disease proteins with stable β-sheet-rich structures are generally believed to trigger cellular toxicity in various neurodegenerative disorders (reviewed by Frid et al., 2007; Ross and Poirier, 2004). Expanded polyQ protein species in form of monomers of β-sheet conformation (Nagai et al., 2007), spherical oligomers (Ehrnhoefer et al., 2006) and protofibrils (Diaz-Hernandez et al., 2004; Li et al., 2006) have been proposed to associate with toxicity in several polyQ disease models. First, expanded polyQ protein monomers of β-sheet conformation initiated cytotoxicity when injected into cultured cells (Nagai et al., 2007). Second, treatment of cells with

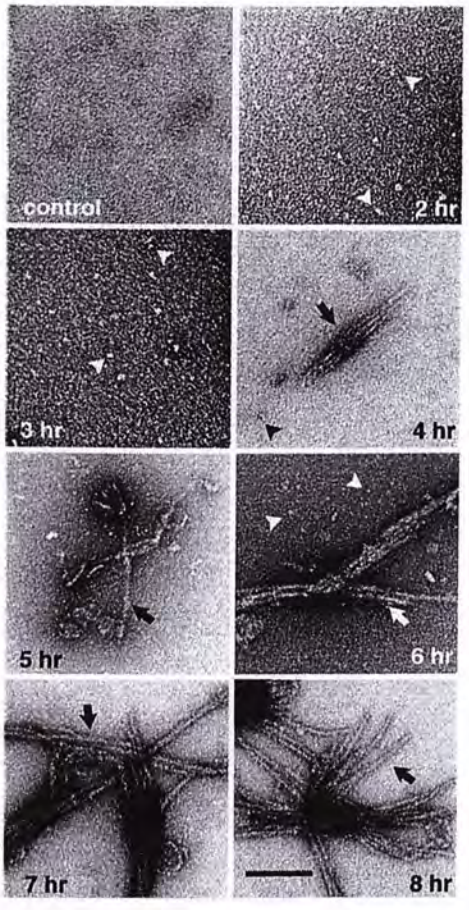

Figure 2. Sequential occurrence of polyglutamine oligomers, protofibrils and fibrils. Time course of polyglutamine disease protein aggregation *in vitro* monitored under transmission electron microscopy. Spherical oligomers (indicated by arrowheads) were observed at 2 and 3 hr after the enzymatic initiation of the aggregation process. Spherical oligomers (indicated by arrowheads) and protofibrils (indicated by arrows) co-existed from 4 to 6 hr. By 7 and 8 hr, only fibrils (indicated by arrows) were detected. The fibrils were seen bundled together. Scale bar represents 200 nm. (Adapted from Poirier et al. (2002)).

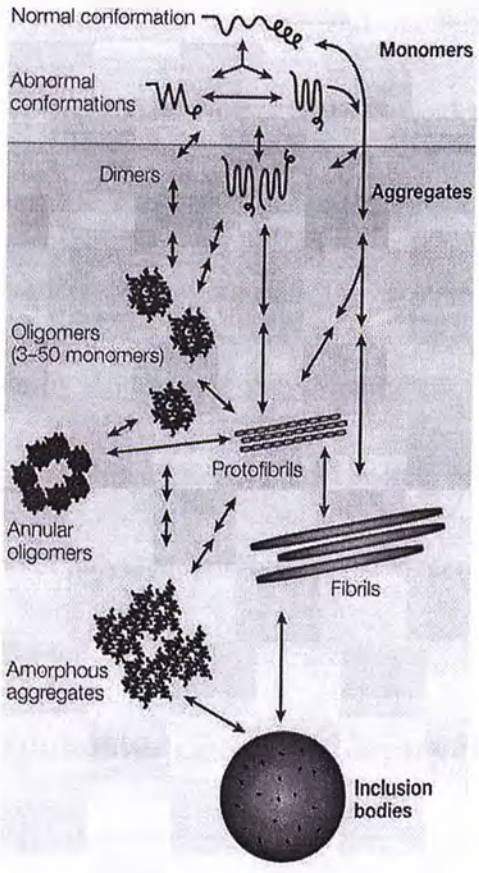

Figure 3. A schematic diagram of the proposed model of polyglutamine protein aggregation pathways. Expanded polyglutamine disease protein exists in several conformations. The expanded polyglutamine protein monomers adopt abnormal conformations and initiate the aggregation process. Fibrils are formed by addition of monomers to the growing fiber, or through intermediate species such as oligomers and protofibrils, of which trigger the formation of annular ring structures (annular oligomers) and amorphous aggregates. When fibrils or amorphous aggregates become large enough, they can be visualized under light microscopy. These microscopically visible aggregates are also termed inclusion bodies. (Adapted from Ross and Poirier (2005)).

chemical compounds like green tea polyphenol (-)-epigallocatechin-3-gallate was shown to suppress polyQ-mediated toxicity and modulate spherical oligomer formation (Ehrnhoefer et al., 2006). Further, both castration (Li et al., 2006) and reduction of polyQ transgene expression (Diaz-Hernandez et al., 2004) in mice prevented neurodegeneration and eliminated the accumulation of protofibrils. However, the mechanism by which these polyQ conformers cause toxicity remains unaddressed. It is yet too preliminary to have any concrete conclusion on the distinct biophysical conformation of polyQ protein species that underlie neurodegeneration.

1.5 Modeling polyglutamine diseases in *Drosophila*

1.5.1 GAL4/UAS spatial transgene expression system in *Drosophila*

Many human diseases are tissue-specific in nature so that regional expression of transgene would better mimic the pathologic conditions in patients. A bipartite spatial transgene expression system can therefore be used to restrict the expression of a transgene in particular *Drosophila* cell types (Figure 4; Brand and Perrimon, 1993). Two kinds of transgenic flies must first be generated: one line carries a cell type-specific promoter/enhancer sequence fused upstream to the yeast transcriptional activator *GAL4* gene (driver line), and a second line carries the transgene which is placed downstream of the yeast upstream activator sequence (UAS) binding site

Figure 4. GAL4/UAS spatial transgene expression system in *Drosophila.* The GAL4 protein is expressed in cells of which the endogenous promoter/enhancer sequence is active. The GAL4 protein then binds to its binding sequence UAS that is located upstream to the transgene, and activates transcription of the transgene. (Modified from McGuire et al. (2004)).

(target line). In the progeny of the driver and target lines, the yeast GAL4 transactivator would be expressed in cells which the endogenous promoter/enhancer sequence are active. Since the transgene is located downstream of the GAL4 binding sequence (UAS), expression of UAS-transgene would then be detected. For example, multiple copies of the *glass* gene promoter sequence have been placed upstream of the yeast *GAL4* gene, and this *glass multiple reporter* (*gmr)*-GAL4 line can be used to direct expression of UAS-transgene in all eye cells posterior to the morphogenetic furrow, including photoreceptor neurons and eye pigment cells (Ellis et al., 1993). The driver and target lines are carried in different parental transgenic fly strains. This ensures the viability of the parental fly strains especially when cytotoxic proteins are studied, and also enables the use of the same target line to study the effect of the transgene in different tissues simply by performing genetic crosses with different driver lines.

1.5.2 Temporal control of GAL4/UAS transgene expression system in *Drosophila*

The GAL4/UAS system controls only the spatial expression pattern of the gene of interest (section 1.5.1). One limitation of the GAL4/UAS system is the lack of temporal regulation over the transgene expression. Additional approaches have been developed over the conventional GAL4/UAS system to tackle this issue in

Drosophila. They include the Gene-Switch system (Han et al., 2000; Osterwalder et al., 2001; Roman et al., 2001) and the temporal and regional gene expression targeting (TARGET) system (McGuire et al., 2003).

In the Gene-Switch system (Figure 5A), fly strain with a promoter/enhancer sequence located upstream of a *GAL4*-hormonal receptor fusion gene is constructed as the driver line. In the absence of hormone, the GAL4-containing fusion protein is expressed but adopts an inactive conformation such that it cannot bind to UAS to trigger transcriptional activation. Upon hormonal exposure, the fusion protein converts into an active conformation, binds to UAS, and activates transgene expression. Induction of transgene expression is therefore determined by the hormonal exposure on flies.

Another approach to aid temporal transgene expression is the TARGET system (Figure 5B). In yeast, the GAL4-mediated transcriptional activation can be repressed by the GAL80 protein (reviewed by Lohr et al., 1995). The GAL80 protein can also repress the GAL4/UAS-mediated transgene expression in *Drosophila* (Lee and Luo, 1999). McGuire et al. (2003) further established a temperature-sensitive GAL80 ($GAL80^{ts}$) mutant to regulate the GAL4 activity in a temperature-dependent manner

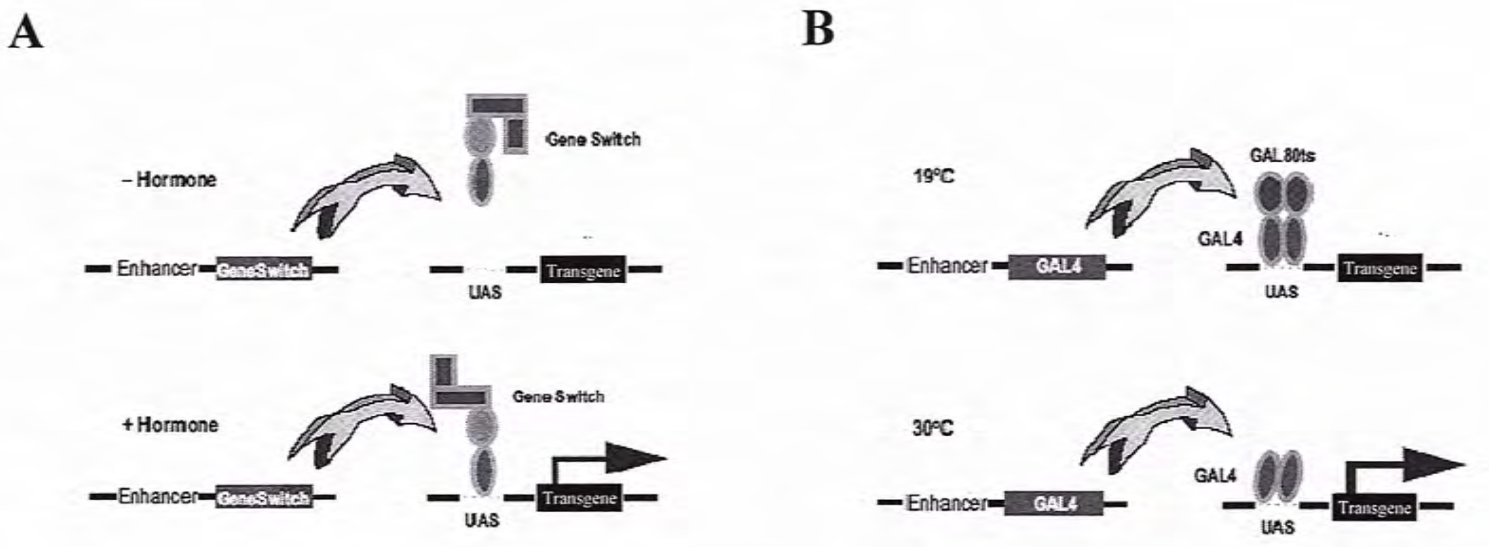

Figure 5. Temporal control on the GAL4/UAS transgene expression system in *Drosophila.* (**A**) Gene-Switch system. The DNA binding domain of the GAL4 protein is fused to a hormonal receptor (Gene Switch). In the absence of hormone, the Gene Switch molecule adopts an inactive conformation that does not bind to the UAS sequence. In the presence of hormone, the Gene Switch molecule changes to an active conformation in which it binds to the UAS sequence and activates transcription of transgene. (**B**) Temporal and regional gene expression targeting (TARGET) system. The conventional GAL4-UAS system (Figure 4) is conditionally regulated by a temperature-sensitive GAL80 (GAL80ts) protein. At a permissive temperature for the action of GAL80ts (i.e. under 19°C), the GAL80ts protein binds to the GAL4 protein and represses the transcription of transgene. Such repression is relieved by a temperature shift to a non-permissive temperature for the action of GAL80ts (i.e. 30°C), which inactivates the GAL80ts protein and thus allows the GAL4-mediated transgene expression. (Modified from McGuire et al. (2004)).

in *Drosophila*, which grounds the basis of the TARGET system. Fly strain with a *tubulin* promoter sequence placed upstream of a *GAL80^{ts}* gene is constructed as an additional driver line to aid ubiquitous expression of GAL80^{ts} protein. When flies with the GAL80^{ts} driver are crossed to flies bearing both the GAL4 driver and UAS-transgene, at a permissive temperature for the action of GAL80^{ts} (i.e. under 19°C), the GAL80^{ts} protein binds to the transcriptional activation domain of the GAL4 protein and prevent the GAL4-mediated transcriptional activation. At a non-permissive temperature for the action of GAL80^{ts}, GAL80^{ts} adopts an inactive conformation and the GAL80-mediated transcriptional repression is thus relieved. In this way, induction of transgene expression can be controlled by raising flies at desired temperature.

1.5.3 *Drosophila* as a model to study human pathologies

For a number of reasons that the fruit fly *Drosophila melanogaster* emerges as one of the most popular model organisms to study various biological mechanisms (reviewed by Arbouzova and Zeidler, 2006; Casanova, 2007; Sanchez-Soriano et al., 2007; Wager-Smith and Kay, 2000). Most importantly, flies have a relatively short life cycle (Figure 6; about 10 days at 25°C), and that a large number of progeny can be produced to enable large-scale analysis. Their anatomy and physiology are also

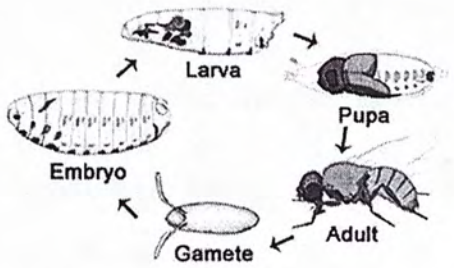

Figure 6. The life cycle of *Drosophila*. Developmental stages of *Drosophila* include gamete, embryo, larva, pupa and adult. The entire developmental cycle takes about 10 days at 25°C. (Modified from Flybase ImageBrowse (http://flybase.bio.indiana.edu/static_pages/imagebrowser/imagebrowser10.html)).

extensively studied to facilitate phenotypic examination. All these, together with well-developed transgene expression systems (section 1.5.1; section 1.5.2) and the genome-wide collection of transgenic fly stocks (reviewed by Ryder and Russell, 2003; Venken and Bellen, 2005) allow rapid *in vivo* analysis of gene functions. Furthermore, comparison between the *Drosophila* and human genomes revealed a high degree of conservation in fundamental biological pathways (Rubin et al., 2000), and that over 60 percent of human disease genes have orthologs in flies (Reiter et al., 2001). This makes *Drosophila* a suitable organism to study human disease-related biological mechanisms. Overall, these features have made *Drosophila* an attractive model for studies of human diseases (reviewed by Bier and Bodmer, 2004; Bilen and Bonini, 2005; Garesse and Kaguni, 2005; Marsh and Thompson, 2006; O'Kane, 2003; Sang and Jackson, 2005; Vidal and Cagan, 2006).

1.5.4 *Drosophila* as a model to study polyglutamine diseases

Drosophila has a complex nervous system with an architecture similar to that of the mammalian nervous system (reviewed by Yoshihara et al., 2001), and has been used to study various neurodegenerative disorders including polyQ diseases (reviewed by Bilen and Bonini, 2005; Marsh and Thompson, 2006; Sang and Jackson, 2005; Shulman et al., 2003). The polyQ disease was initially modeled in

Drosophila by over-expression of a truncated form of human SCA 3, also known as Machado-Joseph disease (MJD), disease protein using the conventional GAL4/UAS spatial transgene expression system (Warrick et al., 1998). Directed expression of the truncated form of expanded MJD protein with 78 glutamine repeats (MJDtrQ78) in all neurons in *Drosophila* led to premature death (Warrick et al., 1998). Constitutive expression of MJDtrQ78, but not the truncated form of unexpanded MJD protein with 27 glutamine repeats (MJDtrQ27), in the fly eye under the control of *gmr*-GAL4 caused late-onset progressive degenerative phenotypes such as depigmentation and collapse of internal retinal morphology (Figure 7A, C; Warrick et al., 1998). Besides, the pathogenic expanded MJDtrQ78 protein was found to accumulate in form of microscopically visible protein aggregates (Figure 7B; Warrick et al., 1998). Both the severity of degenerative phenotypes and the onset of microscopically visible protein aggregates mediated by the expanded MJD protein were shown to correlate well with both the expression level and the glutamine repeat length of the protein (reviewed by Bilen and Bonini, 2005).

Drosophila models of other polyQ diseases have also been successfully established by the over-expression of respective human polyQ disease proteins. They include huntingtin protein for HD (Jackson et al., 1998), androgen receptor protein

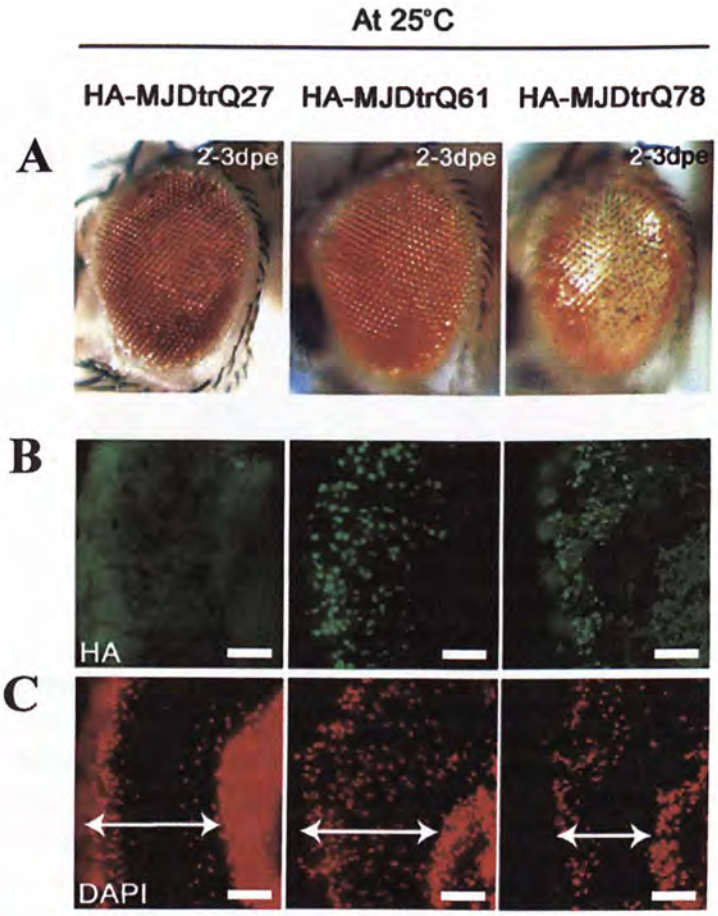

Figure 7. Constitutive expression of the MJD protein in *Drosophila*. (**A**) Observation of the adult external fly eye. Constitutive expression of MJDtrQ78, but not MJDtrQ27 and MJDtrQ61, caused eye depigmentation at 2 to 3 days post-eclosion (dpe). (**B**) Immunofluorescence analysis of the adult fly retina. Constitutive expression of MJDtrQ61 and MJDtrQ78 resulted in the formation of polyQ aggregates (shown in green) at 2 to 3 dpe. (**C**) Monitoring of adult fly retinal morphology under fluorescence microscopy. Constitutive expression of MJDtrQ78, but not MJDtrQ27 and MJDtrQ61, led to a reduction in the depth of the retina (indicated by double-headed arrows) at 2 to 3 dpe. DAPI was used to stain the cell nuclei (shown in red). This method has been commonly used to assess retinal cell death (Boeddrich et al. (2006); Fernandez-Funez et al. (2000); Warrick et al. (2005)). Scale bars represent 30 μm.

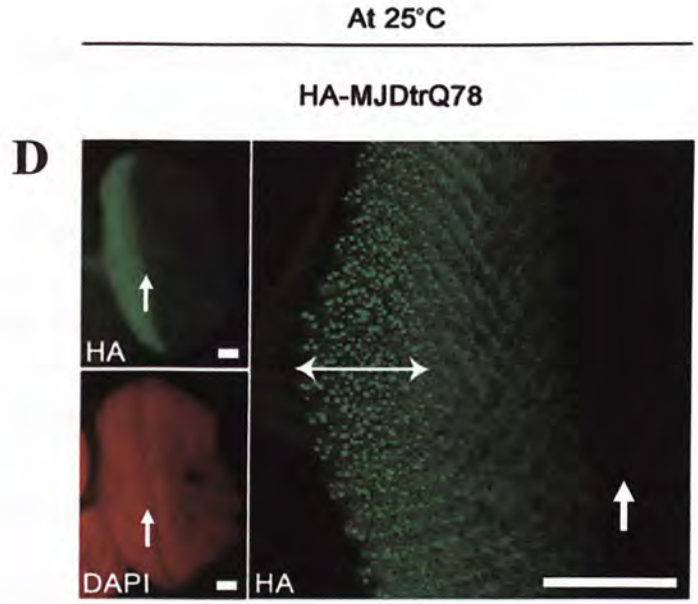

Figure 7 (continued). (D) Immunofluorescence analysis of the larval imaginal eye disc. Constitutive expression of MJDtrQ78 led to the formation of polyQ aggregates (shown in green). DAPI was used to label the cell nuclei (shown in red). In this constitutive expression system, *gmr*-GAL4 drives UAS-transgene (i.e. *UAS-MJDtrQ78(s)*) expression in all cells posterior to the morphogenetic furrow in the larval imaginal eye disc (Ellis et al. (1993)) and a new row of eye disc cells would start to express UAS-transgene in roughly every 2 hr. Ten eye discs were examined to determine cell rows with polyQ aggregates (right panel; indicated by double-headed arrows) and polyQ aggregates (shown in green) were found to appear from about 8 rows of cells from the furrow (indicated by arrows). Scale bars represent 50 μm. The larva and flies were of genotypes *w*; *gmr-GAL4 UAS-MJDtrQ27*/+; +/+, *w*; *gmr-GAL4 UAS-MJDtrQ61*/+; +/+ and *w*; *gmr-GAL4 UAS-MJDtrQ78(s)*/+; +/+.

for SBMA (Chan et al., 2002; Takeyama et al., 2002), atrophin-1 protein for DRPLA (Charroux et al., 2006), ataxin-1 protein for SCA 1 (Fernandez-Funez et al., 2000) and ataxin-7 protein for SCA 7 (Latouche et al., 2007). The various *Drosophila* models of polyQ diseases have provided primary insights to link a range of cellular pathways to polyQ-mediated neuronal dysfunction. Examples include protein folding (Warrick et al., 1999), transcriptional regulatory (Steffan et al., 2001), cell signaling (Chen et al., 2003), apoptotic (Sang et al., 2005) and microRNA regulatory (Bilen et al., 2006) pathways. *Drosophila* emerges as a valuable model organism to find out biological pathways that underlie polyQ-mediated neurodegeneration.

To conclude, transgenic polyQ disease fly models exhibit disease characteristics that resemble pathologic conditions observed in patients (reviewed by Bilen and Bonini, 2005; Marsh and Thompson, 2006); *Drosophila* would therefore be a useful model to elucidate pathogenic mechanisms in polyQ diseases *in vivo*.

1.6 Aims of study

Aggregation of disease protein is a feature shared among neurodegenerative disorders including polyQ diseases (reviewed by Ross and Poirier, 2004). Over the last decade, the involvement of polyQ disease protein aggregation in neuronal degeneration has been a central area of research (reviewed by Michalik and Van Broeckhoven, 2003; Ross and Poirier, 2005; Slow et al., 2006). Disease protein with an expanded polyQ tract exists in multiple aggregated forms such as oligomers, protofibrils and fibrils (reviewed by Ross and Poirier, 2005); the pathogenic form of the expanded polyQ protein remains yet to be explicitly defined and characterized. This project aims to reveal the relationship between polyQ disease protein aggregation and neurodegeneration, and with the intention to uncover the pathogenic form of polyQ protein species that cause neurodegeneration. The experimental model used in this study is *Drosophila,* a model organism that allows rigorous examination on the pathogenic mechanisms of polyQ disease *in vivo*.

2. MATERIALS AND METHODS

2.1 *Drosophila* culture and manipulation

2.1.1 *Drosophila* culture

Fly stocks and crosses were raised in cotton-plugged plastic vials containing cornmeal-yeast-glucose-agar medium (section 2.10.1) in temperature-controlled incubators (LMS). All genetic crosses were maintained at either 18°C or 25°C. For each cross, around 4 male and 6 female virgin flies were put together in a fly vial supplemented with dry yeast. For collection of virgin females, adult flies were first removed from the vial, and virgin female flies were collected in the following 8 hr at 25°C or 16 hr at 18°C.

2.1.2 Phenotypic examination of adult external eye degeneration

Adult fly eyes of appropriate genotype and age were examined under a stereomicroscope (Olympus SZE-12). External eye images were captured by a SPOT Insight CCD camera (Diagnostic Instruments Inc.) using SPOT Advanced software (version 4.1; Diagnostic Instruments Inc.). The images were optimized for their brightness and contrast on Adobe Photoshop 7.0 (Adobe) and such manipulations were applied across the entire image.

2.1.3 Pseudopupil assay of adult retinal degeneration and observation of green fluorescent protein in adult eyes

Adult fly heads of appropriate genotype and age were decapitated, put on a glass slide, and immersed in a drop of immersion oil (Olympus). Around 5 fly heads were aligned in a straight line on each glass slide in an orientation that antennae were facing upward and ocelli were facing forward. With two glass cover slips served as spacers on both sides, a third glass cover slip was carefully placed on top of the fly heads. The glass cover slip junction was then sealed with nail polish. Ommatidia were examined under a light microscope (Olympus CX31) using a 60X oil objective with numerical aperture (NA) of 1.25. To visualize ommatidia and green fluorescent protein (GFP) signals simultaneously in the fly eye, a fluorescence microscope (Olympus BX51) equipped with a 60X/ NA 1.4 oil objective was used. Ommatidial images were captured by a SPOT Insight CCD camera (Diagnostic Instruments Inc.) using SPOT Advanced software (version 4.1; Diagnostic Instruments Inc.). The images were optimized for their brightness and contrast on Adobe Photoshop 7.0 (Adobe) and such manipulations were applied across the entire image.

The ommatidia integrity was revealed by the number of rhabdomeres per ommatidium. In each experiment, at least 100 ommatidia were counted at random

from 5 to 10 fly eyes, and the average number of rhabdomeres per ommatidium count was determined. Each experiment was repeated independently for three times. For pseudopupil analysis along with GFP signal detection, at least 80 ommatidia were randomly counted from 8 fly eyes. Two independent experiments were performed. Sample mean value and standard error of the mean (*s.e.m.*) were calculated to determine the variation among individual flies. Mean differences of average numbers of rhabdomeres per ommatidium count between samples were compared by Mann-Whitney U-test (SPSS 12.0 for Windows). Statistical significance was demonstrated by p-value of less than 0.05.

The Image Pro Plus imaging software (version 5.1; Media Cybernetics) was used to determine the area occupied by GFP-positive polyQ aggregates in an ommatidium. For each of the 80 ommatidia, the area of GFP signals was measured. The area occupied by the GFP-positive polyQ aggregates in each ommatidium was calculated by dividing the total area of GFP signals by the overall area of a single ommatidium.

Linear regression (SPSS 12.0 for Windows) was performed to determine the correlation between the area occupied by GFP-positive polyQ aggregates and the

average number of rhabdomeres per ommatidium count.

2.2 Semi-quantitative Reverse Transcription-Polymerase Chain Reaction

2.2.1 RNA extraction from adult *Drosophila* heads

Ribonucleic acid (RNA) was extracted from adult fly heads using TRIZOL reagent (Invitrogen). Sixteen fly heads were homogenized in 800 µl of TRIZOL reagent with a motorized plastic pestle (Kontes). Homogenates were first centrifuged at 12,000 X *g* for 10 min at 4°C to remove cell debris. Supernatant was then transferred to a fresh tube and incubated for 5 min at room temperature. A volume of 160 µl of chloroform was added to the supernatant and incubated for another 2 min at room temperature. The sample mixture was centrifuged at 12,000 X *g* for 15 min at 4°C. The aqueous upper phase was collected in a fresh tube, and 400 µl of isopropanol was added to precipitate the RNA overnight at -20°C. The sample was centrifuged at 12,000 X *g* for 10 min at 4°C, and the supernatant was discarded. The resultant RNA pellet was washed with 1 ml of 70% ethanol, and centrifuged again at 12,000 X *g* for 10 min at 4°C. Ethanol was then removed; the pellet was air-dried at room temperature and dissolved in 50 µl of diethyl pyrocarbonate (DEPC)-treated water (section 2.10.2).

2.2.2 DNase treatment of extracted RNA

Ribonuclease (RNase)-free deoxyribonuclease (DNase; Promega) was used to digest the residual deoxyribonucleic acid (DNA) left in the extracted RNA. A reaction mixture of 50 µl of total RNA, 6 µl of 10X DNase buffer (Promega), 3 µl of DNase (1 U/µl; Promega) and 1 µl of DEPC-treated water was first prepared, and then incubated for 15 min at room temperature. To terminate the reaction, 6 µl of DNase stop solution (Promega) was added to the reaction mixture and incubated for 10 min at 65°C. To precipitate the RNA, 8 µl of sodium acetate and 6 µl of DEPC-treated water were added to the reaction mixture followed by the addition of 160 µl of 100% ethanol. The RNA was precipitated overnight at -80°C. The sample mixture was centrifuged at 12,000 X *g* for 15 min at 4°C. The pellet was washed in 1 ml of 70% ethanol, and the sample was centrifuged again at 12,000 X *g* for 10 min at 4°C. Ethanol was then removed; the pellet was air-dried at room temperature and dissolved in 50 µl of DEPC-treated water.

2.2.3 Reverse Transcription-Polymerase Chain Reaction (RT-PCR)

Reverse transcription (RT) was performed using oligo(dT) primer (10 µM; section 2.10.2). A mixture of 4 µl of total RNA and 1 µl of oligo(dT) primer was first incubated at 70°C for 5 min to completely denature the RNA, and then chilled at 4°C

for 5 min. A volume of 4 µl of 5X reaction buffer (Promega), 2.4 µl of 25 mM Magnesium Chloride ($MgCl_2$; Promega), 0.5 µl of 20 mM deoxynucleoside triphosphates (dNTPs) mixture (Promega), 0.5 µl of RNase inhibitor (40 U/µl; Promega), 1 µl of reverse transcriptase (Promega) and 6 µl of DEPC-treated water were then added to the reaction mixture. The RT reaction was performed as follows: 5 min at 25°C, 60 min at 42°C, and 15 min at 70°C.

PCR amplification from the synthesized first strand complementary DNA (cDNA) was then performed in a reaction mixture containing 1.5 µl of the cDNA template, 2.5 µl of 10X PCR reaction buffer, 1.5 µl of 25 mM $MgCl_2$ (Promega), 0.3 µl of 20 mM dNTPs (Promega), 0.5 µl of 10 µM forward primer, 0.5 µl of 10 µM reverse primer, 0.2 µl of *Thermus aquaticus (Taq)* DNA polymerase (GeneSys Limited) and 18 µl of autoclaved double distilled water. PCR conditions were as follows: 30 sec at 95°C, 30 sec at 60°C, and 45 sec at 72°C for 30 cycles. Primers used were (ExprF1) 5' CGG AAG AGA CGA GAA GC 3'; (ExprR) 5' GTG AAG GTA GCG AAC ATG 3' for *MJDtrQ78*; (ActinF) 5' ATG TGC AAG GCC GGT TTC GC 3' and (ActinR) 5' CGA CAC GCA GCT CAT TGT AG 3' for *actin*. Both RT and PCR reactions were performed on an i-Cycler thermocycler (Bio-Rad Laboratories).

2.2.4 Agarose gel electrophoresis

Electrophoresis was carried out in wide-mini-sub cell GT system (Bio-Rad Laboratories). DNA sample was mixed with 6X DNA loading dye (section 2.10.2) in volume ratio of 5:1, and run on a 1% agarose gel (w/v; section 2.10.2) in 1X Tris-Borate-EDTA (TBE) buffer (section 2.10.2) at 120 V until the dye front reached two-third of the gel or at an appropriate position. For each agarose gel, 2 µl/lane of DNA ladder (section 2.10.2) was loaded as molecular weight markers.

DNA band intensities were measured using AlphaEaseFC software (version 3.1.2; Alpha Innotech Corporation). Sample mean value and *s.e.m.* were calculated from three independent experiments. Differences in sample means were compared by two-tailed, unpaired Student's t-test (Microsoft Office Excel 2003). Statistical significance was demonstrated by *p*-value of less than 0.05.

2.3 Sodium Dodecyl Sulfate-Polyacrylamide Gel Electrophoresis (SDS-PAGE)

2.3.1 Protein extraction from adult *Drosophila* heads

Fifteen adult fly heads were homogenized in 75 µl of ice-cold 6X SDS sample buffer (section 2.10.3) with a motorized plastic pestle (Kontes). Homogenates were

either left unfiltered or filtered through an Ultrafree-MC membrane (Millipore) with pore size of 0.22 μm at 13,400 X *g* for 4 min at room temperature. Protein extracts were denatured at 99°C for 5 min, and stored at -20°C until use.

2.3.2 Preparation of SDS-polyacrylamide gel and electrophoresis

Electrophoresis was performed using the Mini-PROTEAN III electrophoresis cell (Bio-Rad Laboratories). Glass plates with 0.75 mm or 1.5 mm spacers were cleaned and vertically assembled into a gel cassette according to manufacturer's instructions. Running gel solution was prepared according to section 2.10.3 and loaded to the space between assembled glass plates. Isopropanol was then added onto the top of the running gel solution to remove any air bubbles and to keep the gel solution away from atmospheric oxygen. The running gel solution was allowed to polymerize for about 20 min at room temperature or until the gel was set. Isopropanol was removed from the running gel surface. The gel surface was rinsed with double distilled water and dried. Stacking gel solution was prepared according to section 2.10.3 and loaded to the top of the running gel. A gel comb of appropriate thickness with either 10 or 15 wells was inserted between the glass plates. Stacking gel solution was allowed to polymerize for 20 min at room temperature or until the gel was set. The gel cassette was then transferred to the electrophoresis cell. The

inner cell chamber was filled with freshly prepared 1X SDS electrophoresis buffer (section 2.10.3) while the outer cell chamber was filled with fresh or reused 1X SDS electrophoresis buffer (section 2.10.3). The gel comb was removed, and the wells were rinsed with fresh 1X SDS electrophoresis buffer (section 2.10.3) to remove any unpolymerized gel solution prior to sample loading. Protein extracts without cell debris were denatured at 99°C for 5 min, and loaded into the wells. For each gel, 5 µl/lane of broad-range pre-stained protein standard (Bio-Rad Laboratories) was also loaded as molecular weight markers. Electrophoresis was performed at constant voltage of 80 V initially, and then adjusted to 120 V after the dye front passed the stacking gel. The gel was run until the dye front reached the bottom of the running gel or at an appropriate position.

2.3.3 Western blotting

After electrophoresis, the gel was removed from the cassette of electrophoresis cell, and was first rinsed briefly with double distilled water and then equilibrated in 1X transfer buffer (section 2.10.3). Western blotting was carried out in Mini Trans-Blot electrophoretic transfer cell (Bio-Rad Laboratories). Polyvinylidene fluoride (PVDF) membrane (PALL) was first activated by analytical grade methanol for 10 sec and then equilibrated in 1X transfer buffer. Six pieces of 3-mm filter paper

(Whatman) and two fiber pads were also soaked in 1X transfer buffer. The transfer cassette was set up in the following order: a fiber pad on the cathode side of the transfer gel holder cassette (black side of the cassette), followed by a stack of three filter papers, the gel piece, the PVDF membrane, another stack of three filter papers and a fiber pad. The assembled sandwich was rolled over by a glass tube to expel any air bubbles trapped. The cassette was then placed into the buffer tank, together with a frozen Bio-Ice cooling unit. The tank was then filled up with 1X transfer buffer and Western blotting was performed at constant voltage of 80 V for 2 hr.

2.3.4 Immunodetection

After Western blotting, the PDVF membrane was removed from the transfer gel holder cassette, washed with 1X Tris-Buffered Saline (TBS; section 2.10.3) for 5 min twice, and then blocked with blocking buffer (section 2.10.3) for 2 hr at room temperature with continuous shaking. The blot was then incubated with primary antibodies diluted in blocking buffer overnight at 4°C with continuous rolling. The blot was washed with continuous shaking for four times in TBS-Tween-20 (TBS-T), each for 15 min, and followed by secondary antibody incubation in blocking buffer for 2 hr at room temperature with continuous rolling. The blot was again washed four times in TBS-T, each for 15 min. Finally, signal detection was performed using

Enhanced Chemiluminescent (ECL) Western blotting detection reagents (Amersham). A volume of 0.5 ml of ECL reagent 1 and 0.5 ml of ECL reagent 2 were first mixed, and then applied onto the blot and incubated for 1 min at room temperature. The blot was wrapped with a plastic wrap, and then used to expose an X-ray film (FUJI super RX) at desired time intervals. The film was developed by a medical X-ray film processor (Kodak). For re-probing, the blot was stripped with 20 ml of Western blot stripping buffer (Pierce) for 5 min at room temperature with continuous shaking, washed with 1X TBS for 5 min twice, and then incubated with another set of primary and secondary antibodies as described above. Primary antibodies used were rabbit anti-hemagglutinin (HA; 1:250; Zymed), rat anti-fly Hsp70 (1:500; a kind gift of Dr. Martin Feder, Department of Organismal Biology & Anatomy, The University of Chicago, Chicago) and mouse anti-β-tubulin E7 (1:2,000; Developmental Studies Hybridoma Bank, Iowa City, Iowa, with funding from the NICHD). Secondary antibodies used were affinity purified goat anti-rabbit, goat anti-rat and goat anti-mouse immunoglobulin G (IgG; H + L) horseradish peroxidase (HRP)-conjugate (1:2,000; Chemicon).

Protein band intensities were measured using AlphaEaseFC software (version 3.1.2; Alpha Innotech Corporation). Sample mean value and *s.e.m.* were calculated

from three independent experiments. Differences in sample means were compared by two-tailed, unpaired Student's t-test (Microsoft Office Excel 2003). Statistical significance was demonstrated by *p*-value of less than 0.05.

2.4 Immunoprecipitation

Aliquots of 50 µl EZview red anti-HA affinity gel beads HA-7 (Sigma) was used in the immunoprecipitation experiment. The gel beads were first equilibrated in 750 µl of lysis buffer (section 2.10.4) for 30 sec at 4°C, and then centrifuged at 8,200 X *g* for 30 sec at 4°C. The lysis buffer was carefully removed. This step was repeated once, and the beads were then stored on ice prior to use.

With a motorized plastic pestle (Kontes), 50 fly heads were homogenized in 1 ml of ice-cold lysis buffer freshly supplemented with 1 mM phenylmethanesulphonylfluoride (PMSF) and protease inhibitor cocktail (Sigma). Homogenates were centrifuged at 8,200 X *g* for 10 min at 4°C to remove cell debris. The cleared homogenates were transferred to a tube pre-loaded with 50 µl equilibrated EZview red anti-HA affinity gel beads. The sample mixture was vortexed briefly, and incubated overnight at 4°C with continuous gentle mixing. The sample mixture was then subject to centrifugation at 8,200 X *g* for 30 sec at 4°C, and

supernatant was transferred to a new tube and saved as the "flowthrough" fraction. The gel beads were washed with 750 µl of ice-cold lysis buffer, vortexed briefly, and incubated for 5 min at room temperature with continuous gentle mixing. The sample was then centrifuged at 8,200 X *g* for 30 sec, and supernatant was carefully removed. The washing step was repeated for two more times. Proteins collected in the "flowthrough" fraction were precipitated by 10% trichloroacetic acid (TCA) as described in section 2.8. To elute the immunoprecipitated proteins, 50 µl of 6X SDS sample buffer (section 2.10.3) was added to the gel beads. The sample mixture was then vortexed briefly, boiled at 99°C for 5 min, centrifuged at 8,200 X *g* for 30 sec, and stored at -20°C until use (sections 2.4.2-2.4.4).

2.5 Filter retardation assay

Ten fly heads were homogenized in 200 µl of ice-cold filter retardation sample buffer (section 2.10.5) with a motorized plastic pestle (Kontes). Homogenates were heated at 99°C for 5 min, and stored at -20°C until use. Alternatively, homogenates were first filtered through an Ultrafree-MC membrane (Millipore) with pore size of 0.22 µm at 13,400 X *g* for 4 min at room temperature prior to storage

A cellulose acetate membrane with pore size of 0.22 µm (Sartorius) was

inserted into the Slot Blot Manifold blot apparatus (Amersham Pharmacia Biotech PR 648) connected to a vacuum pump. Double distilled water, 0.01% SDS solution (w/v), and 2% SDS solution (w/v) were sequentially loaded onto each slot to wet and equilibrate the membrane. After heating at 99°C for 5 min, the homogenates without cell debris were then loaded onto the slots. Each slot was washed twice with 0.01% SDS solution (w/v). The membrane was then removed from the blot apparatus, and immunodetection was carried out as described in section 2.4.4.

2.6 Isolation and solubilization of SDS-insoluble protein

Fifty fly heads were homogenized in 250 µl of ice-cold protein extraction sample buffer (section 2.10.6) with a motorized plastic pestle (Kontes). Homogenates without cell debris were subject to ultracentrifugation at 100,000 rpm (Beckman TLX-120; TLA120.2 rotor; 434,513 X *g*) for 1 hr at 4°C. The supernatant was discarded and the pellet was solubilized in 80 µl of 100% formic acid (FA; Sigma) at 37°C for 30 min. Formic acid was then removed by SpeedVac (Savant) at a low drying rate for 1 hr at room temperature, and the pellet was dissolved in 10 µl of 6X SDS sample buffer (section 2.10.3). Hydroxide ions, in form of a volume of 10 µl of Tris-Hydrochloric acid (Tris-HCl; pH 8.8), was added to the sample to neutralize any residual FA prior to SDS-PAGE analysis (sections 2.4.2-2.4.4).

2.7 Sucrose gradient sedimentation

Two hundred fly heads were homogenized in a liquid nitrogen pre-chilled mortar and pestle. A volume of 1 ml of ice-cold sucrose gradient sample buffer (section 2.10.7) freshly supplemented with 1 mM PMSF was added to the mortar after homogenization. Protein extracts were further homogenized on ice with a 1 ml Dounce homogenizer (Wheaton) started with 20 loose strokes, and followed by 50 tight strokes. Homogenates were then subject to centrifugation at 12,000 X *g* for 5 min at 4°C twice to remove any residual cell debris. To generate a stepwise gradient, ice-cold sucrose gradient buffer containing 5 different sucrose concentrations (10%, 20%, 30%, 40% and 50%; 2.1 ml each; section 2.10.5) freshly supplemented with 1 mM PMSF were loaded in ascending order to the bottom of an ultra-clear centrifuge tube (capacity 13.2 ml; Beckman) using a thin capillary tubing connected to a 1 ml syringe. The stepwise gradient was equilibrated overnight at 4°C to generate a continuous gradient. Homogenates without cell debris were then loaded onto the 10.5 ml of 10% to 50% continuous sucrose gradient, and centrifuged at 35,000 rpm (Beckman XL-100K ultracentrifuge; SW 41 Ti rotor; 151,263 X *g*) for 16 hr at 4°C. Eleven 1 ml fractions were collected by piercing the centrifuge tube with a 25G fine needle (Terumo) attached to a 1 ml syringe. The fraction collected from the top of the tube was designated as "fraction 1".

Trichloroacetic acid (TCA; 10%; Sigma) was used to precipitate proteins in each fraction. Trichloroacetic acid-precipitated protein samples were centrifuged at 12,000 X *g* for 45 min at 4°C. Protein pellet was then washed with 300 µl of ice-cold acetone, and centrifuged at 12,000 X *g* for another 30 min at 4°C. The washing step was repeated for two more times. Protein pellet was then dissolved in 20 µl of 6X SDS sample buffer (section 2.10.3). To isolate proteins with size less than 0.22 µm, protein pellet was dissolved in 50 µl of 2% SDS solution (w/v), and a volume of 30 µl of protein samples were filtered through an Ultrafree-MC membrane (Millipore) with pore size of 0.22 µm at 13,400 X *g* for 4 min at room temperature. A volume of 20 µl of 6X SDS sample buffer (section 2.10.3) was subsequently added to 20 µl of the protein sample (either filtered or unfiltered) for SDS-PAGE (sections 2.4.2-2.4.4). The protein samples were then boiled at 99°C for 5 min, and stored at -20°C until use.

2.8 Preparation of *Drosophila* tissues for immunofluorescence analysis

2.8.1 Dissection and immunostaining of *Drosophila* larval imaginal eye discs

Imaginal eye discs of appropriate genotypes were dissected from third-instar larvae in 1X Phosphate-Buffered Saline (PBS; section 2.10.8), fixed in 3.7%

formaldehyde in 1X PBS for 15 min, and washed three times in Phosphate-Buffered Saline-Triton X-100 (PBS-T; section 2.10.8), each for 5 min. The dissected eye discs were then blocked in Phosphate-Buffered Saline-Goat Serum (PBS-GS; section 2.10.8) for 1 hr at room temperature, and incubated with rabbit anti-HA primary antibody (1:250; Zymed) in PBS-GS overnight at 4°C. The eye discs were then washed four times in PBS-GS, each for 5 min, and followed by fluorescein isothiocyanate (FITC)-conjugated goat anti-rabbit IgG (H+L) secondary antibody (1:250; Zymed) incubation in PBS-GS at room temperature for 2 hr. The eye discs were further washed four times in PBS-GS, each for 5 min, and then transferred to a glass slide loaded with a volume of 40 µl of Prolong Antifade Kit (Molecular Probes) reagent. Two cover slips were put on sides as spacers, while a third cover slip was placed on top of the eye discs and the junction was sealed with nail polish. The eye discs were then examined under a confocal microscope (Leica, TCS) equipped with a 100X/ NA 1.4 oil objective. Images of the imaginal eye discs were acquired using Leica confocal software (version 2.5; Leica). The images were optimized for their brightness and contrast on Adobe Photoshop 7.0 (Adobe) and such manipulations were applied across the entire image.

2.8.2 Cryosectioning and immunostaining of adult *Drosophila* heads

Decapitated adult fly heads were first equilibrated in a well of glass dissection plate containing Optimum Cryosectioning Temperature (O.C.T.) mounting medium (Sakura). During equilibrating, a flat O.C.T. platform with a diameter of 5 cm was made by freezing a thin layer of O.C.T. medium onto the lid of a plastic petri-dish at -80°C. The flat O.C.T. platform was then transferred to a petri-dish filled with dry ice. A blob of O.C.T. solution was then applied to the flat platform. Immediately before the O.C.T. blob solidified, a second spherical blob of O.C.T. was applied on top of the solidifying one. Fly heads were then transferred immediately from the dissection plate to the second freezing O.C.T. blobs in an orientation that ocelli facing upward and antennae facing forward. The solidified O.C.T. blobs were then submerged in liquid nitrogen for a few seconds to ensure complete freezing of O.C.T.. The double O.C.T. blobs containing fly heads would detach from the flat platform, and were then collected and stored in a 15 ml Falcon tube at -20°C. Cryosectioning was performed within a week after embedding to avoid dehydration of samples.

The embedded fly heads were sectioned with a cryostat (HM505E, Microm) and 12 μm sections were collected. Fly head sections were recovered on a glass slide pre-coated with 1% gelatin (w/v) in 1X PBS, fixed in 3.7% formaldehyde in 1X PBS

for 15 minutes at room temperature, and then washed briefly in 1X PBS for three times. The sections were blocked with PBS-GS (section 2.10.6) for 1 hr at room temperature, and then incubated with rabbit anti-HA primary antibody (1:250; Zymed) in PBS-GS overnight at 4°C. The sections were washed four times in PBS-GS, each for 5 min, followed by FITC-conjugated goat anti-rabbit IgG (H+L) secondary antibody (1:250; Zymed) incubation in PBS-GS for 2 hr at room temperature, and then 4'-6-Diamidino-2-phenylindole staining (DAPI; 1:75; Sigma) for another 2 min at room temperature. The sections were further washed four times in PBS-GS, each for 5 min. A volume of 40 µl of Prolong Antifade Kit (Molecular Probes) reagent was applied onto the sections as the mounting medium. The sections were then covered with a glass cover slip, sealed with nail polish, and examined under a fluorescence microscope (Olympus BX51) equipped with a 40X/ NA 0.75 objective. Images of the retinal sections were captured by a SPOT Insight CCD camera (Diagnostic Instruments Inc.) using SPOT Advanced software (version 4.1; Diagnostic Instruments Inc.). The images were optimized for their brightness and contrast on Adobe Photoshop 7.0 (Adobe) and such manipulations were applied across the entire image.

The number of microscopically visible polyQ protein aggregates in each retinal

section was measured by the Image Pro Plus imaging software (version 5.1; Media Cybernetics). A fluorescent polyQ protein was defined as a fluorescence object with an area ranges from 6 to 100 square units, and roundness of 0 to 1.5 units. Cell nuclei were determined by DAPI staining. Cell population with polyQ protein aggregates in each section was calculated by dividing the number of polyQ aggregates by the total number of cell nuclei counted. The depth of retina was determined by the thickness of the DAPI-stained retinal cell nuclei using the SPOT Advanced software (version 4.1; Diagnostic Instruments Inc.). Four to 30 retinal sections collected from three independent experiments were used to calculate the mean value and *s.e.m.*. Mean differences between samples were compared by two-tailed, unpaired Student's t-test (Microsoft Office Excel 2003). Statistical significance was demonstrated by p-value of less than 0.05.

Linear regression (SPSS 12.0 for Windows) was performed to determine the correlation between fluorescent polyQ protein aggregates detected by immunostaining and SDS-insoluble polyQ protein determined by filter retardation assay (section 2.5).

2.9 Atomic force microscopy

Atomic force microscopy (AFM) was used to analyze the morphology of aggregated polyQ protein species. Proteins isolated from 100 fly heads were immunoprecipitated as described in section 2.4, and eluted in 40 µl of 2% SDS solution (w/v) at room temperature for 5 min. The immunoprecipitated protein sample was filtered through an Ultrafree-MC membrane (Millipore) with pore size of 0.22 µm at 13,400 X *g* for 4 min at room temperature. A volume of 6 µl of the eluted proteins were spotted onto a silica wafer, and dried at room temperature for 4 min. The sample was then rinsed with distilled water, dried by compressed air, and imaged in air with a digital multimode Nanoscope III scanning probe microscope (Digital Instruments, Veeco Instruments Inc.) operated in a tapping mode at room temperature.

The resolution of AFM scans was at 512 X 512 pixels. Images acquired were flattened by the Nanoscope IV software (version 5.30r3.sr3; Digital Instruments, Veeco Instruments Inc.). The scan data were then exported as ASCII files, and analyzed by the OriginPro software (version 7.5 sr6 v7.5885; OriginLab Cooperation). For each 5 µm X 5 µm scan field, matrix data was plotted as a 3D Surface/Contour plot to visualize the three-dimensional distribution of peaks, and as

Profiles/Image plot to measure peak height of all particles. Profiles/Image plot was also used to measure the length of fibrillar structures. To ensure data reproducibility, three images of each sample were obtained from separate locations across the silica wafer surface. Sample mean value and *s.e.m.* were determined from three independent experiments. Mean differences were compared by two-tailed, unpaired Student's t-test (Microsoft Office Excel 2003). Statistical significance was demonstrated by *p*-value of less than 0.05.

2.10 Reagents and buffers

2.10.1 Reagents for *Drosophila* culture

Drosophila strains

Transgenic fly strains used in this study include *gmr-GAL4*, *UAS-HA-MJDtrQ27*, *UAS-HA-MJDtrQ61*, *UAS-HA-MJDtrQ78(w)*, *UAS-HA-MJDtrQ78(s)*, *UAS-EGFP*, *UAS-EGFP-Q76-FLAG*, *UAS-GFP::lacZ.nls*, *UAS-HSPA1L*, *UAS-HSC70-4.K71S*, *UAS-P35* and *tubP-GAL80^{ts}*. Detailed information of fly stocks is summarized in Table 2.

Cornmeal-yeast-glucose-agar medium

Fly culture medium was prepared by dissolving 12.5 g of agar (1.25%, w/v),

Table 2. Summary of *Drosophila* strains used.

Transgenic line	Stock Number	Genotype	Chromosomal location	Description	Reference
gmr-GAL4	LDR8	*w; gmr-GAL4*	X; 2	*glass multiple reporter* (*gmr*)-*GAL4* is a promoter-GAL4 line for ectopic GAL4 expression in all eye cells posterior to the morphological furrow	Ellis et al. (1993)
tub P-GAL80ts	7016 (Bloomington)	*P{tubP-GAL80^{ts}}9, w/FM7c*	X	*tubulin* Promoter (*tub* P)-*GAL80ts* is a promotor-GAL80 line for ectopic temperature-sensitive GAL80 expression in all cells	McGuire et al. (2004)
	7017 (Bloomington)	*w; P{tubP-GAL80^{ts}}2/TM2*	X; 2		
	7018 (Bloomington)	*w; noc^{Sco}/CyO; P{tubP-GAL80^{ts}}7*	X; 2; 3		
	7019 (Bloomington)	*w; P{tubP-GAL80^{ts}}20; TM2/TM6B, Tb^{1}*	X; 2; 3		
	7108 (Bloomington)	*w; P{tubP-GAL80^{ts}}10; TM2/TM6B, Tb^{1}*	X; 2; 3		

Transgenic line	Stock Number	Genotype	Chromosomal location	Description	Reference
gmr-GAL4 UAS-HA-MJDtrQ27	LDR3	*w; gmr-GAL4, UAS-HA-MJDtrQ27/CyO*	X; 2	for ectopic expression of hemagglutinin (HA)-tagged truncated human Machado-Joseph disease protein of 27 glutamines under *gmr-GAL4* regulation	Warrick et al. (1998)
gmr-GAL4 UAS-HA-MJDtrQ78	LDR1	*w; gmr-GAL4, UAS-HA-MJDtrQ78(s)/CyO*	X; 2	for ectopic expression of HA-tagged truncated human Machado-Joseph disease protein of 78 glutamines under *gmr*-GAL4 regulation	Warrick et al. (1998)
gmr-GAL4 UAS-HA-MJDtrQ61	MJDtrQ61	*w; gmr-GAL4, UAS-HA-MJDtrQ61/CyO*	X; 2	for ectopic expression of HA-tagged truncated human Machado-Joseph disease protein of 61 glutamine under *gmr*-GAL4 regulation and with same expression level as LDR1	Chan et al. (2000)
UAS-EGFP-Q76-FLAG	14.3	*w; UAS-EGFP-Q76-FLAG*	X; 3	for ectopic expression of expanded polyglutamine protein of 76 glutamines fused to the N-terminus of an FLAG tag and the C-terminus of EGFP	Lam and Chan, unpublished materials
UAS-EGFP	G1	*w; UAS-EGFP*	X; 2	for ectopic expression of EGFP protein	Wong et al. (2005)

Transgenic line	Stock Number	Genotype	Chromosomal location	Description	Reference
UAS-GFP::lacZ.nls	6452 (Bloomington)	*w; P{UAS-GFP::lacZ.nls}30.1*	X; 3	for ectopic expression of GFP-beta-galatosidase fusion protein with a nuclear localization signal	Shiga et al. (1996)
UAS-HSP70	7455 (Bloomington)	*w; P{UAS-Hsap\HSPA1L.W}53.1 /CyO*	X; 2	for ectopic expression of human molecular chaperone Hsp70 protein	Warrick et al. (1999)
UAS-HSC70-K71S	7453 (Bloomington)	w^{126}; *P{UAS-Hsc70-4.K71S}I*	X; 2	for ectopic expression of human molecular chaperone Hsc70 protein with a substitution mutation from lysine to alanine at 71st position	Warrick et al. (1999)
UAS-P35	5073 (Bloomington)	*w; P{UAS-p35.H}BH2*	X; 3	for ectopic expression of caspase inhibitor P35 viral protein	Mergliano and Minden (2003)

105 g of dextrose (10.5%, w/v), 105 g cornmeal (10.5%, w/v) and 21 g yeast (2.1%, w/v) in 900 ml of distilled water. The mixture was boiled for about 20 min, followed by the addition of 80 ml of 1% nipagen (methyl p-hydroxybenzoate; dissolved in ethanol; Sigma) as mold inhibitor, and the mixture was made up to 1 L by distilled water. A volume of 15 ml of fly culture medium was dispensed to a plastic culture vial.

2.10.2 Reagents for RT-PCR

Tris-Borate-EDTA (TBE)

Stock TBE buffer (5X) was prepared by mixing 54 g of Tris-base (0.45 M), 27.5 g of boric acid (0.45 M) and 20 ml of 0.5 M ethylenediaminetetraacetic acid (EDTA; 10 mM) in 1 L of double distilled water. The pH value was calibrated to 8.0. Working TBE solution (1X) was prepared by diluting the stock buffer 5-fold with double distilled water. Both stock and working solutions were kept at room temperature.

DNA loading dye

DNA loading dye (6X) was prepared by mixing 25 mg of bromophenol blue (0.25%, w/v), 25 mg of xylene cyanol FF (0.25%, w/v), 4 g of sucrose (40%, w/v) and 1.2 ml of 0.5 M EDTA (60 mM; pH 8.0) in 10 ml of autoclaved double distilled

water. Loading dye was stored as 1-ml aliquots at -20°C while the working dye solution was kept at 4°C.

Agarose gel

One percent agarose gel (w/v) was prepared by melting 0.2 g of agarose (Bio-Rad Laboratories) in 20 ml of 1X TBE by microwave for about 2 min. The mixture was cooled to hand-warm, and about 2 µl of ethidium bromide (10 mg/ml; stored in dark at room temperature) was added to the gel solution. The gel was set on a gel caster (Bio-Rad Laboratories) at room temperature.

DNA Ladder

The working solution of either 100 base-pair or 1 kilobase-pair DNA marker (Fermentus) was prepared by mixing 1 volume of the stock DNA marker, 1 volume of 6X DNA loading dye and 4 volumes of autoclaved double distilled water. Stock DNA marker was kept at -20°C while the working solution was stored at 4°C.

Primers

Oligonucleotide primers were synthesized from Invitrogen. The lyophilized primer powders were reconstituted in autoclaved double distilled water to a stock

concentration of 100 μM. Working primer solution of 10 μM was prepared by diluting the stock solution by 10-fold with autoclaved double distilled water. Both stock and working solutions were kept at -20°C.

DEPC-treated water

Diethyl pyrocarbonate (DEPC; USB) was added to double distilled water at a volume ratio of 1:1,000 to give a 0.1% DEPC (v/v) water, and stirred overnight to disperse the DEPC. The water was then autoclaved to inactivate DEPC. Autoclaved DEPC-treated water was stored at room temperature.

2.10.3 Reagents for SDS-PAGE

SDS sample buffer

SDS sample buffer (6X) was prepared by mixing 10 mg of bromophenol blue (0.02%, w/v), 5 ml of 1 M Tris-HCl; pH 6.8 (0.1 M), 10 ml of 10% SDS solution (w/v) (2%, w/v), 10 ml of glycerol (20%, v/v) and 2.5 ml of β-mercaptoethanol (5%, v/v) in 50 ml of double distilled water. The buffer was stored as 1.5-ml aliquots at -20°C.

SDS electrophoresis buffer

Stock SDS electrophoresis buffer (10X) was prepared by dissolving 30.28 g of Tris-base (0.25 M), 144.13 g of glycine (1.92 M) and 10 g of SDS (1%, w/v) in 1 L of double distilled water. Working SDS electrophoresis buffer (1X) was prepared by diluting the stock buffer 10-fold with double distilled water. Both stock and working solutions were kept at room temperature.

Running gel solution

For each 1.5 mm mini gel, running gel solution was freshly prepared by mixing 3.5 ml of 30% acrylamide (12% final, v/v), 3.255 ml of 1 M Tris-HCl; pH 8.8 (0.4 M), 1.9 ml of double distilled water, 87.5 µl of 10% SDS solution (w/v) (1%, w/v), 35 µl of 10% (w/v) ammonium persulfate (APS; 0.04%) and 4 µl of N,N,N',N'-Di-(dimethylamino)ethane (TEMED).

Stacking gel solution

For each 1.5 mm mini gel, stacking gel solution was freshly prepared by mixing 0.49 ml of 30% acrylamide (4% final, v/v), 0.966 ml of 0.1 M Tris-HCl; pH 6.8 (0.03 M), 1.96 ml of double distilled water, 35 µl of 10% SDS solution (w/v) (1%, w/v), 14 µl of 10% (w/v) APS (0.04%) and 4 µl of TEMED.

Transfer buffer

Stock transfer buffer (10X) was prepared by dissolving 30.28 g of Tris-base (0.25 M) and 144.13 g of glycine (1.92 M) in 1 L of double distilled water. Stock solution was kept at room temperature. Working transfer buffer (1X) was freshly prepared by mixing 70 ml of 10X stock transfer buffer, 70 ml of methanol and 560 ml double distilled water together.

Tris-Buffered Saline (TBS)

Stock TBS buffer (10X) was prepared by dissolving 24.22 g of Tris-base (0.2 M) and 80.06 g of Sodium Chloride (NaCl; 1.37 M) in 1 L of double distilled water with pH adjusted to 7.6. 1X working TBS buffer (1X) was prepared by diluting the stock solution 10-fold with double distilled water. Both stock and working solutions were kept at room temperature.

Tris-Buffered Saline-Tween-20 (TBS-T)

TBS-T solution was prepared by adding 0.5 ml of Tween-20 (0.05% final, v/v) to 10 ml of 1X TBS. It was kept at room temperature.

Blocking buffer

Blocking buffer was prepared by dissolving 5 g of non-fat milk powder (5% final, w/v) in 100 ml of 1X TBS. It was kept for a week at 4°C.

2.10.4 Reagents for immunoprecipitation

Lysis buffer

Lysis buffer was prepared by mixing 6.06 g of Tris-base (50 mM), 8.77 g of NaCl (0.15 M), 2 ml of 0.5 M EDTA; pH 8.0 (1 mM) and 0.2 ml of Nonidet P-40 (NP-40; 0.02%, v/v) in 1 L of double distilled water with pH adjusted to 7.6. It was kept at 4°C.

2.10.5 Reagents for filter retardation assay

Filter retardation sample buffer

Filter retardation sample buffer was prepared by dissolving 0.46 g of dithiothreitol (DTT; 50mM) in 60 ml of 2% SDS solution (w/v). The buffer was stored as 1.5-ml aliquots at -20°C.

2.10.6 Reagents for isolation and solubilization of SDS-insoluble protein

Protein extraction sample buffer

Protein extraction sample buffer was prepared by dissolving 0.46 g of DTT (50mM) in 60 ml of 2% SDS solution (w/v). The buffer was stored as 1.5-ml aliquots at -20°C.

2.10.7 Reagents for sucrose gradient sedimentation

Sample buffer

Sample buffer was prepared by dissolving 6.06 g of Tris-base (50 mM), 8.77 g of NaCl (0.15 M), 2 ml of 0.5 M EDTA; pH 8.0 (1 mM) and 100 g of sucrose (10%, w/v) in 1 L of double distilled water with pH adjusted to 7.6. It was kept at 4°C.

Sucrose gradient buffers

Sucrose gradient buffers were prepared by dissolving 6.06 g of Tris-base (50 mM), 8.77 g of NaCl (0.15 M), 2 ml of 0.5 M EDTA; pH 8.0 (1 mM) and different amount of sucrose (10%, 20%, 30%, 40%, 50%, w/v) in 1 L of double distilled water with pH adjusted to 7.6. The buffers were kept at 4°C.

2.10.8 Reagents for immunofluorescence analysis

Phosphate-Buffered Saline (PBS)

10X PBS solution was prepared by dissolving 80.06 g of NaCl (1.37 M), 2 g of Potassium Chloride (KCl; 27 mM), 26.8 g of Sodium Phosphate dibasic heptahydrate ($Na_2HPO_4 \cdot 7H_2O$; 0.1 M) and 2.4 g of Potassium Phosphate monobasic anhydrous (KH_2PO_4; 20 mM) in 1 L of double distilled water with pH adjusted to 7.4. 1X PBS solution was prepared by diluting the 10X stock PBS solution 10-fold. Both stock and working solutions were kept at 4°C.

Phosphate-Buffered Saline- Triton X-100 (PBS-T)

PBS-T solution was prepared by adding 30 µl of Triton X-100 (0.3% final, v/v) to 10 ml of 1X PBS. It was kept at 4°C.

Phosphate-Buffered Saline-Goat Serum (PBS-GS)

PBS-GS solution was freshly prepared by adding 30 µl of Triton X-100 (0.3% final, v/v) and 0.5 ml of goat serum (5% final, v/v; Sigma) to 10 ml of 1X PBS. It was kept at 4°C.

3. RESULTS

3.1 Establishment of an inducible transgenic *Drosophila* model of polyglutamine diseases

3.1.1 Introduction

Glass multiple reporter (*gmr*)-GAL4 drives UAS-transgene expression in *Drosophila* eye, starting from the third-instar larval developmental stage (Ellis et al., 1993). Constitutive expression of the truncated form of expanded human Machado-Joseph Disease (MJD)/spinocerebellar ataxia type 3 gene product (MJDtrQ61 or MJDtrQ78) under the control of *gmr*-GAL4 driver, caused microscopically visible polyQ aggregate formation in larval imaginal eye discs, and degenerative phenotypes in adult retina (Figure 7A, C, D; reviewed by Bilen and Bonini, 2005). It is however notable that the *Drosophila* eye remodels during metamorphosis (i.e. during pupal stage; Figure 6; reviewed by Bangs and White, 2000; Campos-Ortega, 1980), so it would be more appropriate to study the relationship between polyQ protein aggregation and degeneration in a single developmental stage. As it is practically difficult to monitor degenerative phenotypes in larval and pupal stages, a method to delay *MJDtrQ78* transgene expression until

adult stage is desirable in order to examine simultaneously both polyQ protein aggregation and degeneration. This strategy also allows a continuous longitudinal study of polyQ protein aggregation and degeneration.

In this study, the inducible TARGET system was used to drive *MJDtrQ61* and *MJDtrQ78* transgene expression during adult stage. To characterize of this inducible model, Western blot analysis was performed to check for protein expression; immunofluorescence analysis and filter retardation assay were employed to monitor polyQ protein aggregation; observation of external eye depigmentation and retinal morphology, and pseudopupil assay were used to examine polyQ-mediated degenerative phenotypes.

3.1.2 Results

3.1.2.1 GAL80^{ts}-mediated inducible expression of expanded polyglutamine protein in *Drosophila*

3.1.2.1.1 GAL80^{ts} controls GAL4/UAS-mediated polyQ protein expression

In the TARGET system, relative abundance of GAL4 and GAL80^{ts} proteins determines the level of UAS-transgene expression (McGuire et al., 2004). Independent GAL80^{ts} transgenic fly lines can have different levels of GAL80^{ts}

protein expression due to positional effects of transgene integration. Five independent GAL80^{ts} lines were obtained from the Bloomington *Drosophila* Stock Center, USA (Table 2); pilot experiments were performed to select appropriate GAL80^{ts} lines based on their effectiveness to repress both polyQ protein aggregation and degenerative phenotype, which are the two most characterized approaches to monitor the expanded polyQ protein expression in *Drosophila* (reviewed by Bilen and Bonini, 2005).

Expression of either MJDtrQ78 or MJDtrQ61 protein caused a substantial accumulation of microscopically visible polyQ aggregates in adult fly retina (Figure 7B); however MJDtrQ78 led to a collapse of the retinal structure while MJDtrQ61 caused only a modest disruption (Figure 7C). The effectiveness of GAL80^{ts} to repress microscopically visible protein aggregate formation was therefore assessed on a relatively intact retinal structure using MJDtrQ61-expressing, in preference to MJDtrQ78-expressing, fly eyes. At 18°C (a permissive temperature for the action of GAL80^{ts}), no aggregates were observed in flies with *gmr-GAL4*, *UAS-MJDtrQ61* and any of the five *GAL80^{ts}* transgenes (Figure 8A). Meanwhile, the expression of MJDtrQ78 protein resulted in severe depigmentation in adult fly external eyes (Figure 7A; Figure 8B). Flies bearing *gmr-GAL4*, *UAS-MJDtrQ78* and each of the

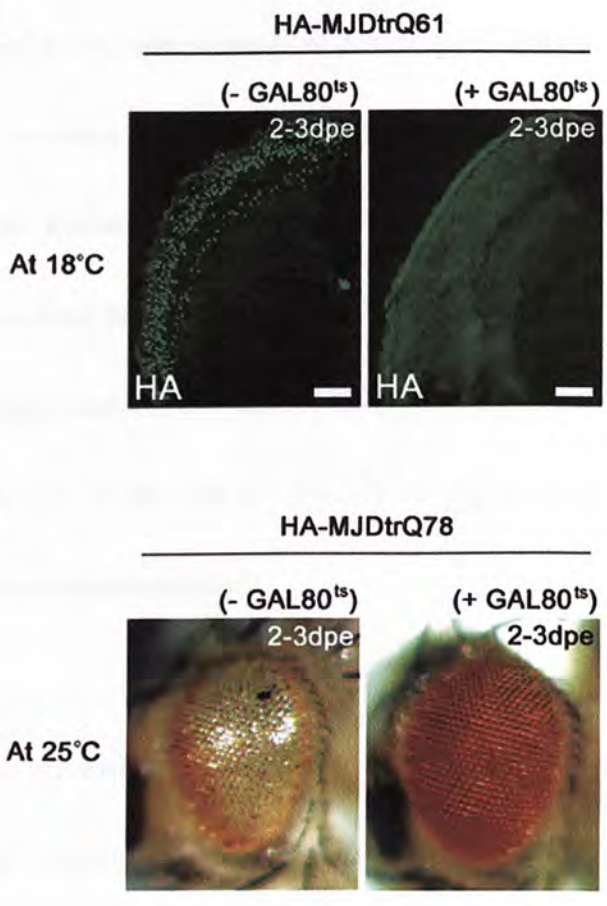

Figure 8. GAL80ts represses the polyglutamine protein expression in *Drosophila*. (**A**) Immunofluorescence analysis of the adult fly retina at 18°C (a permissive temperature for the action of GAL80ts). In the absence of GAL80ts, expression of MJDtrQ61 led to the formation of polyQ aggregates (shown in green) at 2 to 3 days post-eclosion (dpe). In the presence of GAL80ts, no polyQ aggregates were detected. Scale bars represent 50 μm. The flies were of genotypes *w*; *gmr-GAL4 UAS-MJDtrQ61*/+; +/+ and *w*; *gmr-GAL4 UAS-MJDtrQ61*/+; *tubP-GAL80ts*/+. (**B**) Observation of the adult external fly eye at 25°C (a partially permissive temperature for the action of GAL80ts). Expression of MJDtrQ78 caused eye depigmentation at 2 to 3 dpe. No external eye depigmentation phenotype was observed in MJDtrQ78 flies co-expressed with GAL80ts. The flies were of genotypes *w*; *gmr-GAL4 UAS-MJDtrQ78(s)*/+; +/+ and *w*; *gmr-GAL4 UAS-MJDtrQ78(s)*/+; *tubP-GAL80ts*/+.

five *GAL80^{ts}* transgenes did not acquire any observable eye depigmentation, even when they were raised at a partially permissive temperature for the action of GAL80^{ts} (i.e. 25°C) which increases the GAL4 to GAL80^{ts} activity ratio (Figure 8B). Altogether, these data demonstrate that all five GAL80^{ts} lines can effectively restrict the expression of expanded polyQ protein as evidenced by its effect on polyQ protein aggregation and degeneration. For the simplicity of fly stock generation for subsequent analysis, one of the GAL80^{ts} lines (Bloomington stock number: 7018) was chosen for further characterization.

3.1.2.1.2 Inducible expression of SDS-soluble expanded polyglutamine protein

Expression of *MJDtrQ78* transgene was induced when flies carrying the *gmr-GAL4*, *UAS-MJDtrQ78* and *GAL80^{ts}* transgenes were transferred from 18°C to 25°C. Western blot analysis was performed to examine the expression profile of expanded polyQ protein. SDS-soluble MJDtrQ78 protein (with a predicted molecular weight of about 35 kDa) was not detected at the running gel portion upon 25°C induction within 12 days post-induction (dpi; Figure 9A), which could be explained by the low level of MJDtrQ78 protein expression. Therefore, immunoprecipitation was performed to detect the MJDtrQ78 protein; SDS-soluble MJDtrQ78 protein was detected at the running gel portion at 4 dpi, but not at 0 dpi (Figure 9B). This

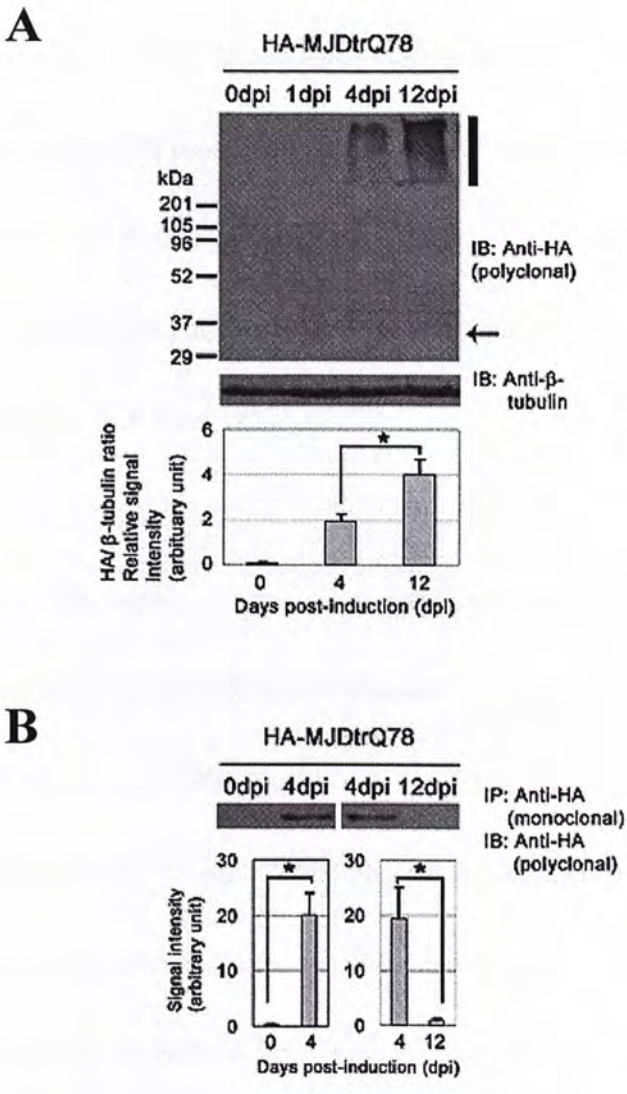

Figure 9. Induced expression of the MJDtrQ78 protein in adult flies. **(A)** Western blot analysis of the MJDtrQ78 protein extract of adult flies. A progressive accumulation of SDS-insoluble MJDtrQ78 protein was detected from 4 days post-induction (dpi) onward (stacking gel; indicated by bar). β-tubulin was used as the loading control. The significant difference in the level of SDS-insoluble MJDtrQ78 protein between 4 and 12 dpi was determined by the quantification of signal intensity ratio of MJDtrQ78 protein at stacking gel portion to β-tubulin ($*p < 0.05$; unpaired Student's t-test). No SDS-soluble monomeric MJDtrQ78 protein (of about 35 kDa; indicated by arrow) was detected. **(B)** Immunoprecipitation of the MJDtrQ78 protein extract of adult flies. A significant amount of SDS-soluble monomeric MJDtrQ78 protein (of about 35 kDa) was eluted at 4 dpi, but not at 0 or 12 dpi ($*p < 0.05$ for each comparison; unpaired Student's t-test). Error bars represent the mean ± *s.e.m.* of three independent experiments. The flies were of genotype *w*; *gmr-GAL4 UAS-MJDtrQ78(s)/+*; *tubP-GAL80ts/+*.

demonstrates the expression of SDS-soluble MJDtrQ78 protein upon induction. Since SDS-soluble MJDtrQ78 protein was only detected upon 25°C induction but not at 18°C (Figure 9B), this further confirms the effectiveness of the $GAL80^{ts}$ line to repress GAL4/UAS-mediated polyQ transgene expression, and that the repression is relieved by temperature shift from 18°C to 25°C.

3.1.2.1.3 Induced expression of expanded polyglutamine protein accumulates gradually in form of SDS-insoluble protein

As shown in Figure 9B, SDS-soluble MJDtrQ78 protein was detected at 4 dpi but its level diminished at 12 dpi. Along the same time frame of induction, a concomitant progressive accumulation of SDS-insoluble MJDtrQ78 protein was observed in the stacking gel portion from 4 dpi onwards (Figure 9A). It is possible that the expanded polyQ protein accumulates in SDS-insoluble form with time. To verify this, a filter retardation assay (Wanker et al., 1999) was performed to detect SDS-insoluble polyQ protein. In this assay, SDS-insoluble protein with size larger than the pore size of the cellulose acetate membrane (0.22 μm) would be retained on the membrane. In this inducible model, a progressive accumulation of SDS-insoluble MJDtrQ78 protein was observed from 1 to 4 dpi (Figure 10). Altogether, these data illustrate that the induction of *MJDtrQ78* transgene expression in adult flies

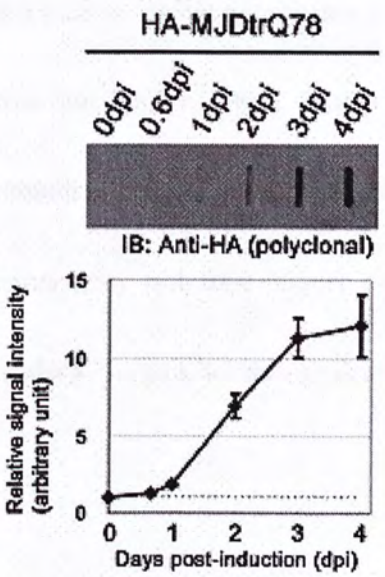

Figure 10. Induced expression of MJDtrQ78 causes progressive accumulation of SDS-insoluble protein. Detection of SDS-insoluble MJDtrQ78 protein in the adult fly protein extract using filter retardation assay. An increasing amount of SDS-insoluble MJDtrQ78 protein was retained on an 0.22-μm filter membrane from 1 to 4 days post-induction (dpi). Error bars represent the mean ± *s.e.m.* of three independent experiments. The flies were of genotype *w*; *gmr-GAL4 UAS-MJDtrQ78(s)*/+; *tubP-GAL80ts*/+.

promotes a temporal accumulation of SDS-insoluble polyQ protein.

3.1.2.1.4 Inducible expression of expanded polyglutamine protein results in progressive accumulation of microscopically visible aggregates

Formation of microscopically visible aggregates is a hallmark feature of polyQ diseases (reviewed by Ross and Poirier, 2004). In this inducible MJDtrQ78 model, polyQ-immunoreactive protein aggregates were first detected in retinal neurons at 2 dpi, and accumulated progressively with time (Figure 11). This data demonstrates the tendency of expanded polyQ protein to accumulate as microscopically visible aggregates.

3.1.2.2 Inducible expression of expanded polyglutamine protein causes late-onset progressive neuronal degeneration in *Drosophila*

3.1.2.2.1 Inducible expression of expanded polyglutamine protein leads to late-onset progressive deterioration of photoreceptor neurons

In *Drosophila*, each compound eye is comprised of about 800 repeating optical arrays called ommatidia. Each ommatidium contains a set of photoreceptor neurons in which rhabdomeres refer to the photosensitive organelles enriched with rhodopsin and other components of the phototransduction cascade (Figure 12A; Rosenbaum et

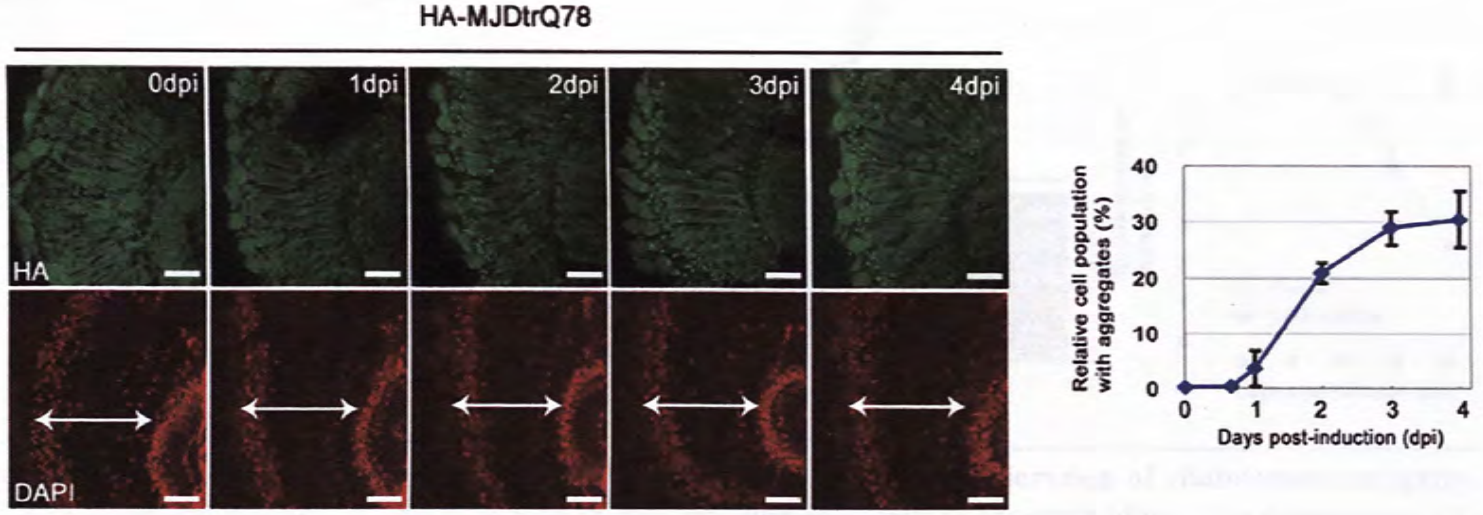

Figure 11. Induced expression of MJDtrQ78 leads to progressive accumulation of light microscopically visible protein aggregates. Detection of MJDtrQ78 protein aggregates in the adult fly retina using immunofluorescence analysis. The induction of MJDtrQ78 expression led to progressive accumulation of polyQ aggregates (shown in green) from 2 days post-induction (dpi). DAPI was used to stain the cell nuclei (shown in red). Double-headed arrows represent the depth of the retina. Scale bars represent 30 μm. The cell population with aggregates was calculated by dividing the number of aggregates by the number of DAPI-stained cell nuclei. Error bars represent the mean ± *s.e.m.* of three independent experiments. The flies were of genotype *w*; *gmr-GAL4 UAS-MJDtrQ78(s)*/+; *tubP-GAL80ts*/+.

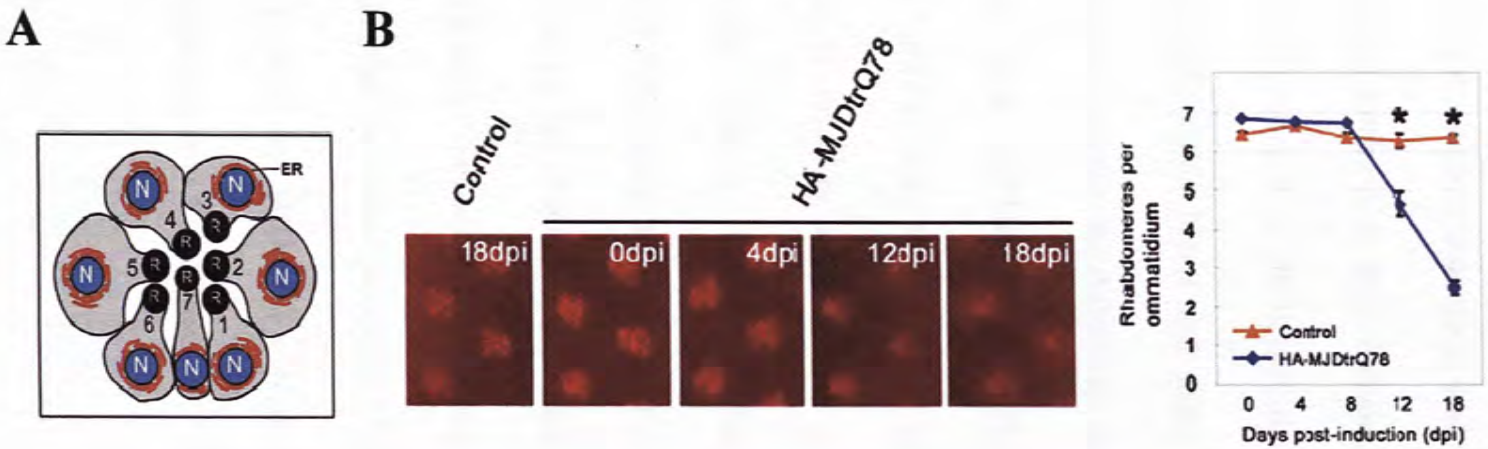

Figure 12. Induced expression of MJDtrQ78 triggers progressive deterioration of rhabdomere integrity. (**A**) A schematic diagram of a cross-section of the 7 photoreceptor cells in an ommatidium. The rhabdomeres (R, shown in black) are the photosensitive organelles comprised of the rhodopsin photopigments and the other components of the phototransduction cascade. The nuclei (N; shown in blue) and endoplasmic reticular (ER) membrane system (shown in red) of the photoreceptor cells are indicated. (Adapted from Rosenbaum et al. (2006)). (**B**) Pseudopupil assay of rhabdomeres in the adult fly eye. Control flies showed a normal average number of rhabdomeres per ommatidium count up to 18 days post-induction (dpi). The induced expression of MJDtrQ78 caused a progressive reduction in the average number of rhabdomeres per ommatidium count starting from 12 dpi (*$p < 0.05$ for each comparison between Control and MJDtrQ78 at the specified time point; Mann-Whitney U-test). Error bars represent the mean ± *s.e.m.* of three independent experiments. The flies were of genotypes *w*; *gmr-GAL4*/+; *tubP-GAL80ts*/+ (Control) and *w*; *gmr-GAL4 UAS-MJDtrQ78(s)*/+; *tubP-GAL80ts*/+.

al., 2006). Pseudopupil assay is a widely used method to assess the functional integrity of rhabdomere structure in adult fly eyes (Agrawal et al., 2005; Apostol et al., 2003; Boeddrich et al., 2006; Jackson et al., 1998; Slepko et al., 2006; Steffan et al., 2001; Wolfgang et al., 2005), and has been employed to measure polyQ-mediated cellular degeneration before cell death (Berger et al., 2005). In degenerating photoreceptor neurons, the rhabdomere structure would be disrupted and cannot be detected using pseudopupil assay. The number of visible rhabdomeres per ommatidium has an inverse correlation with the functional intactness of the retinal neurons, is therefore a quantitative measurement of neuronal degeneration. Continuous induction of *MJDtrQ78* transgene expression reduced the average number of rhabdomeres per ommatidium count at 12 dpi, and the effect became more evident at 18 dpi (Figure 12B). Control flies bearing no *MJDtrQ78* transgene retained a normal number of rhabdomeres per ommatidium up to 18 dpi (Figure 12B), suggesting that the decline brought by MJDtrQ78 expression was not due to normal aging. To sum up, MJDtrQ78 expression initiated progressive deterioration of photoreceptor neurons from 12 dpi.

3.1.2.2.2 Inducible expression of expanded polyglutamine protein neither causes external eye degenerative phenotype nor disrupts gross retinal morphology despite deterioration of photoreceptor neurons

Constitutive expression of MJDtrQ78, but not MJDtrQ27, led to depigmentation of external adult eyes (Figure 7A) and collapse of the internal retinal structure (Figure 7C) that are reliable indicators of cell death in pigment cells and photoreceptor neurons respectively. Interestingly though, neither external eye depigmentation (Figure 13A) nor significant collapse of the internal retinal structure (Figure 13B, C; indicated by the retinal depth; Boeddrich et al., 2006; Fernandez-Funez et al., 2000; Warrick et al., 2005) were observed within 12 dpi of MJDtrQ78 expression. Induction of MJDtrQ78 expression did not therefore result in significant cell death within 12 dpi, at the time when deterioration of rhabdomeric structures occurred (Figure 12).

3.1.2.3 Co-expression of caspase inhibitor P35 suppresses polyglutamine-induced neuronal degeneration

Caspase activation is associated with polyQ-mediated degeneration (reviewed by Ross, 2002). Co-expression of a caspase inhibitor protein P35 (Mergliano and Minden, 2003) significantly rescued the loss of rhabdomeres in

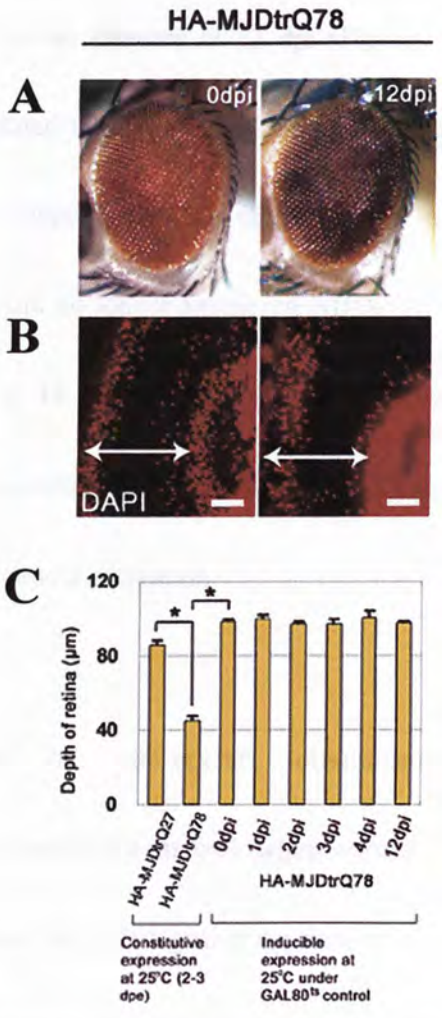

Figure 13. Induced expression of MJDtrQ78 does not cause external eye depigmentation and disruption of gross retinal morphology. **(A)** Observation of the adult external fly eye. The induction of MJDtrQ78 expression did not cause eye depigmentation at 12 days post-induction (dpi). **(B)** Monitoring of the adult fly retinal morphology under fluorescence microscopy. No alteration in the depth of the retina (indicated by double-headed arrows) was observed within 12 dpi of MJDtrQ78 expression. DAPI was used to label the cell nuclei (shown in red). This method has been commonly used to assess retinal cell death (Boeddrich et al. (2006); Fernandez-Funez et al. (2000); Warrick et al. (2005)). Scale bars represent 30 μm. The flies were of genotype *w*; *gmr-GAL4 UAS-MJDtrQ78(s)*/+; *tubP-GAL80ts*/+. **(C)** Quantification of (B), Figure 7C and Figure 11. Error bars represent the mean ± *s.e.m.* of three independent experiments. (*$p < 0.05$ for each comparison; unpaired Student's t-test).

MJDtrQ78-expressing retinal neurons at 12 dpi (Figure 14). No such rescue was observed when an unrelated GFP-lacZ fusion protein was co-expressed (Figure 14), which indicates that the suppressive effect mediated by P35 was specific. Meanwhile, co-expression of P35 could no longer ameliorate MJDtrQ78-induced deterioration of photoreceptor neurons at 18 dpi (Figure 14). These results indicate that the early stage of neuronal degeneration induced by MJDtrQ78 expression is, to a certain extent, associated with caspase activation.

3.1.2.4 Co-expression of molecular chaperone Hsp70 suppresses polyglutamine-induced neuronal degeneration

Molecular chaperone Hsp70 is a potent suppressor of polyQ-mediated neuronal degeneration (reviewed by Muchowski and Wacker, 2005). In this inducible model, co-expression of Hsp70 restored the normal number of rhabdomeres per ommatidium count in MJDtrQ78-expressing flies at 12 dpi, but not at 18 dpi (Figure 14). This is also consistent with the finding that Hsp70 delayed polyQ-mediated pigment cell degeneration in the constitutive MJDtrQ78 model (Huen and Chan, 2005), and further demonstrates that Hsp70 only delays, but not completely prevents, degeneration of neurons.

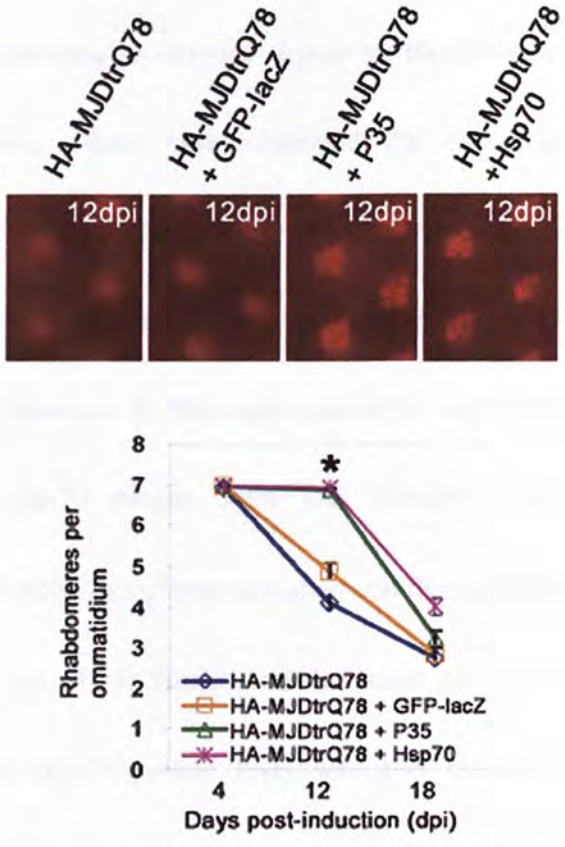

Figure 14. The effect of caspase inhibitor P35 and molecular chaperone Hsp70 on MJDtrQ78-induced deterioration of rhabdomere integrity. Assessment of rhabdomere integrity using pseudopupil assay. The induced expression of MJDtrQ78 resulted in a reduction in the average number of rhabdomeres per ommatidium count in adult fly eye at 12 days post-induction (dpi). Co-expression of the caspase inhibitor P35 and molecular chaperone Hsp70 protein, but not the control GFP-lacZ fusion protein, with MJDtrQ78 rescued the average number of rhabdomeres per ommatidium count at 12 dpi (*$p < 0.05$ for comparison between MJDtrQ78 and MJDtrQ78 + P35, as well as for comparison between MJDtrQ78 and MJDtrQ78 + Hsp70, at the specified time point; Mann-Whitney U-test). Error bars represent the mean ± *s.e.m.* of three independent experiments. The flies were of genotypes *w*; *gmr-GAL4 UAS-MJDtrQ78(s)/+*; *tubP-GAL80ts/+*, *w*; *gmr-GAL4 UAS-MJDtrQ78(s)/UAS-GFP::lacZ.nls*; *tubP-GAL80ts/+*, *w*; *gmr-GAL4 UAS-MJDtrQ78(s)/+*; *tubP-GAL80ts/UAS-P35*, and *w*; *gmr-GAL4 UAS-MJDtrQ78(s)/UAS-HSPA1L; tubP-GAL80ts/+*.

3.1.2.5 Inducible expression of expanded polyglutamine protein results in biphasic expression of molecular chaperone Hsp70 in *Drosophila*

Our laboratory and others have employed the *Drosophila* model with constitutive expression of expanded polyQ proteins to dissect polyQ-mediated pathogenic consequences (reviewed by Bilen and Bonini, 2005; Marsh and Thompson, 2006). For instance, in flies with constitutive expression of MJDtrQ78, an up-regulation of Hsp70 protein level was detected which then decline progressively due to the polyQ-mediated transcriptional dysregulation of Hsp70 gene induction (Huen and Chan, 2005). Here, in this inducible model of MJDtrQ78, such biphasic expression of Hsp70 protein level was also observed. A progressive elevation of Hsp70 protein level was found at 2 dpi (Figure 15). The induction of Hsp70 protein peaked at 3 dpi, and then started to decrease at 4 dpi and declined dramatically at 12 dpi (Figure 15). This observation shows that this inducible model recapitulates polyQ-mediated pathogenic events as previously described (Huen and Chan, 2005).

3.1.3 Discussion

To elucidate the relationship between polyQ-mediated neurodegeneration and protein aggregation in a *Drosophil*a model *in vivo*, it would be desirable to study

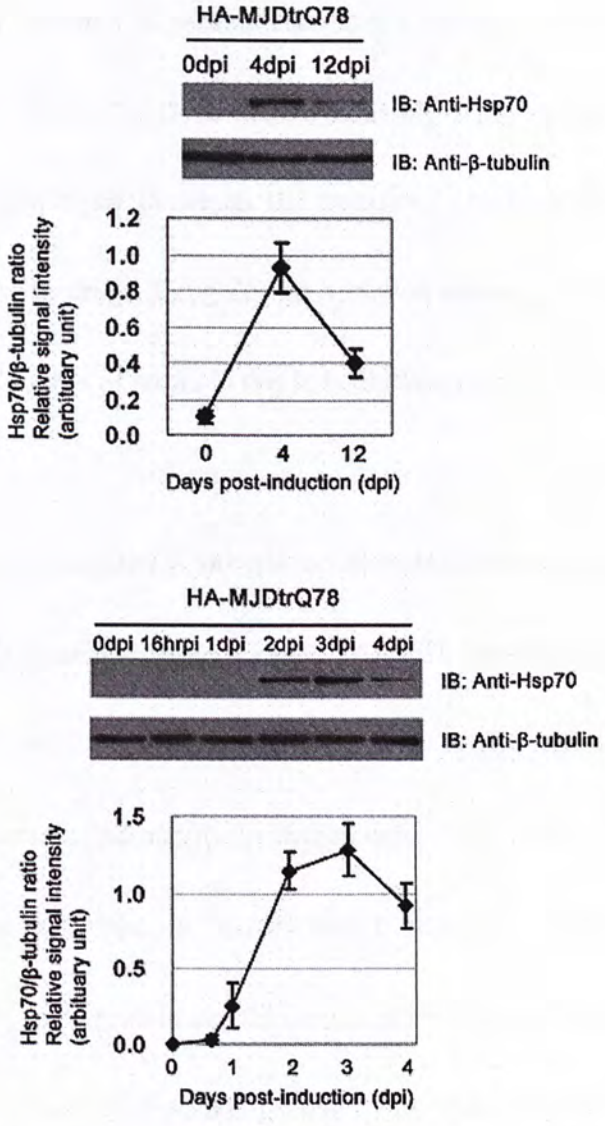

Figure 15. Induced expression of MJDtrQ78 results in biphasic expression profile of molecular chaperone Hsp70 protein. Immunoblotting analysis of the endogenous level of Hsp70 protein in MJDtrQ78-expressing flies. The induction of MJDtrQ78 expression led to an elevation of the level of Hsp70 protein at 4 days post-induction (dpi), and declined at 12 dpi. Hsp70 protein induction was further shown to start increase at 2 dpi, peak at 3 dpi, and then decrease since 4 dpi. β-tubulin was used as the loading control. Error bars represent the mean ± *s.e.m.* of three independent experiments. The flies were of genotype *w*; *gmr-GAL4 UAS-MJDtrQ78(s)/+*; *tubP-GAL80ts/+*.

these two parameters in a single developmental stage. An inducible *Drosophila* model was recently reported to recapitulate SCA 7 pathogenesis (Latouche et al., 2007). In the SCA 7 model, the Gene-Switch inducible expression system (Latouche et al., 2007) was employed in which the transgene expression was induced by feeding adult flies with drugs. Drug dosage variation among individual flies could however be a major source of errors in this inducible expression system.

In this study, an inducible *Drosophila* model of MJD was established by the use of another transgene induction strategy called TARGET (McGuire et al., 2003). One advantage of the TARGET system over the Gene-Switch system is that transgene expression can be controlled simply by temperature shift, which is devoid of the problem of dosage variation. In the TARGET expression system, ideally, the expression level of polyQ protein should remain minimal at low temperature (i.e. at 18°C in this study) when the $GAL80^{ts}$ protein binds to the GAL4 protein and thus impedes the GAL4-mediated transcriptional activation of the UAS-transgene. Apart from the repressive mechanism by $GAL80^{ts}$, GAL4/UAS expression is itself temperature-dependent (Brand et al., 1994). Only a low expression level of the UAS-transgene occurs at a low temperature. This serves as an additional mechanism to ensure the UAS-transgene expression is kept at a minimal level at 18°C. As

ascertained by Western blot analysis, MJDtrQ78 protein was not detected in flies co-expressed with MJDtrQ78 and GAL80^{ts} at 0 dpi (Figure 9A, B). This therefore confirms the practical utilization of this inducible MJDtrQ78 model. On the other hand, the leakiness of the GAL80^{ts} system at 25°C (i.e. a partially permissive temperature for the action of GAL80^{ts}; McGuire et al., 2004) makes it possible to manipulate the GAL80^{ts} to GAL4 activity ratio, and thus the inducible expression of *MJDtrQ78* transgene, to a desired level in order to monitor polyQ toxicity at a longer time period in detail.

Inducible expression of MJDtrQ78 allowed temporal analysis on the aggregation kinetics of the expanded polyQ protein. In both a filter retardation assay (Figure 10) and immunofluorescence analysis (Figure 11), a lag phase of about 1 day was observed for the initial appearance of polyQ-immunoreactive protein. Meanwhile, the accumulation of polyQ protein approached a plateau level at 4 dpi. This kinetic behavior is consistent with a nucleated polymerization reaction as described for the expanded polyQ protein *in vitro* (Chen et al., 2002; Ellisdon et al., 2006; Scherzinger et al., 1999; Slepko et al., 2006). This result therefore demonstrates that aggregation of the expanded polyQ protein is initiated by a nucleation process *in vivo*.

While the expanded polyQ protein tends to accumulate in SDS-insoluble, but not SDS-soluble form (Figures 9; Figure 10), a positive correlation between temporal accumulation of microscopically visible aggregates and SDS-insoluble polyQ protein retained by filter retardation assay was further demonstrated (Figure 16). This finding implies that aggregation of the expanded polyQ protein involves a change in protein solubility properties.

Previously shown in the fly model with constitutive expression of MJDtrQ78, microscopically visible protein aggregates were detected in larval stage and degenerative phenotypes were observed in adult stage (Warrick et al., 1998). In support of this, this inducible MJDtrQ78 model provides further evidence that these protein aggregates were formed before degenerative phenotypes were observed in neurons (Figure 11; Figure 12). Meanwhile, the neurodegenerative phenotype detected was distinct from cell death (Figure 13). MJDtrQ78-induced degeneration occurred at 12 dpi, but not later at 18 dpi, was modulated by the co-expression of molecular chaperone Hsp70 or caspase inhibitor P35 (Figure 14). This observation suggests that disturbance of cellular protein folding machineries (Figure 15; Huen et al., 2007) and caspase activation (Ross, 2002) are involved in the early stage of polyQ degeneration.

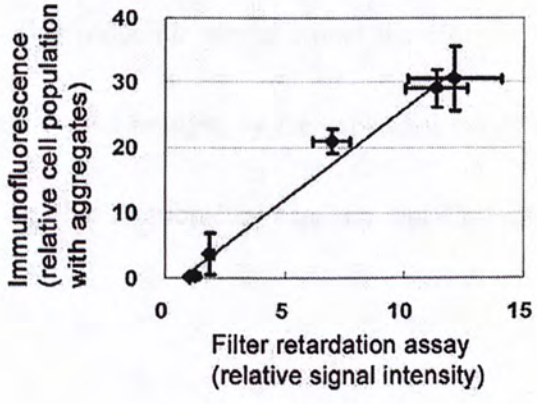

Figure 16. A linear correlation between accumulation of SDS-insoluble MJDtrQ78 protein and microscopically visible protein aggregates. An X-Y plot of data from Figure 10 and Figure 11. A linear relationship (R^2 = 0.985; p < 0.001) between the amount of SDS-insoluble MJDtrQ78 protein (i.e. detected using filter retardation assay; X-axis) and the population of cells with MJDtrQ78 aggregates (i.e. detected using immunofluorescence; Y-axis) can be observed. Error bars represent the mean ± *s.e.m.* of three independent experiments.

To conclude, results in this section demonstrate that this inducible MJDtrQ78 model recapitulates many features of polyQ-mediated pathogenic events, including accumulation of microscopically visible polyQ protein aggregates (Figure 11), progressive neurodegeneration (Figure 12), Hsp70- and P35-mediated suppression of the early stage of polyQ degeneration (Figure 14), and biphasic expression of Hsp70 protein (Figure 15). This inducible model would therefore be an invaluable tool to investigate pathogenic events brought by the expanded polyQ protein expression *in vivo*, in particular on the relationship between polyQ protein aggregation and neuronal degeneration.

3.2 Involvement of microscopically visible polyglutamine aggregates in neurodegeneration

3.2.1 Introduction

Accumulation of microscopically visible protein aggregates in neurons has long been recognized in polyQ pathogenesis (reviewed by Ross and Poirier, 2004). Current understanding of the role of microscopically visible protein aggregates in polyQ pathogenesis have been discussed in section 1.3. In this section, the role of these polyQ aggregates in neuronal degeneration was evaluated in the inducible *Drosophila* model.

3.2.2 Results

3.2.2.1 Effect of Hsc70-K71S on microscopically visible polyglutamine aggregates and neuronal degeneration

3.2.2.1.1 Co-expression of Hsc70-K71S reduces the level of microscopically visible polyglutamine aggregates

In order to examine the role of microscopically visible protein aggregates in polyQ-mediated neuronal degeneration, it is important to find out ways to manipulate the abundance of these polyQ aggregates. Hsp70 is an ATPase that plays roles in

protein folding and degradation in cells (reviewed by Bukau et al., 2006; Young et al., 2004). A substitution mutation (K71S; lysine to serine residue at position 71) in the ATPase domain of Hsp70 has previously been shown to impair its protein folding activity, but not its protein degradation function (Klucken et al., 2004). It has also been found that an ATPase domain deletion mutant of Heat shock cognate 70 (Hsc70; a constitutively expressed form of Hsp70) interacts with the expanded polyQ protein and suppressed its aggregation *in vitro* (Jana et al., 2000). When MJDtrQ78 and Hsc70-K71S mutant proteins were co-expressed in the adult retina under the control of $GAL80^{ts}$, a significant reduction in the number of polyQ aggregate-containing cells was observed (Figure 17). This demonstrates that co-expression of Hsc70-K71S is capable of restricting the level of microscopically visible MJDtrQ78 aggregates.

3.2.2.1.2 Co-expression of Hsc70-K71S does not alter polyglutamine transgene expression

Manipulations that alter *MJDtrQ78* transgene expression would inevitably modify the level of MJDtrQ78 protein aggregates. Using RT-PCR, comparable level of *MJDtrQ78* messenger RNA was detected in MJDtrQ78-expressing and MJDtrQ78/Hsc70-K71S-expressing flies (Figure 18). This indicates that the action of Hsc70-K71S on microscopically visible MJDtrQ78 aggregates is not due to the

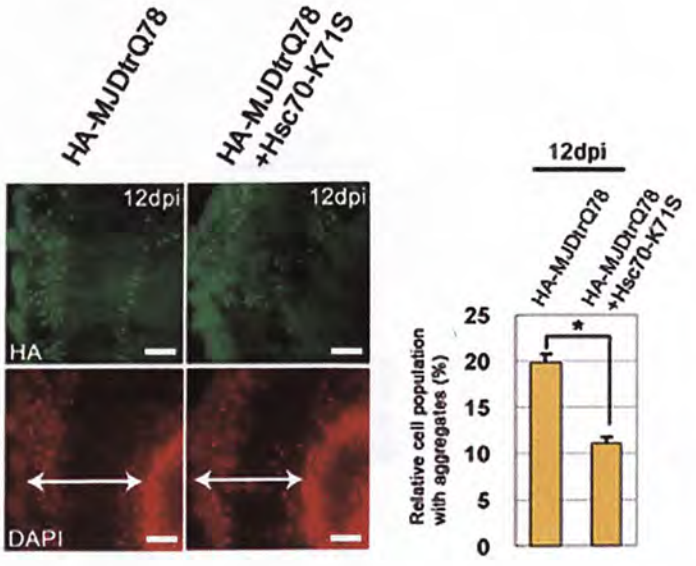

Figure 17. Co-expression of mutant Hsc70-K71S molecular chaperone reduces the number of microscopically visible MJDtrQ78 protein aggregates. Immunofluorescence analysis of the adult fly retinal section. The induced expression of MJDtrQ78 resulted in aggregate formation at 12 days post-induction (dpi). The co-expression of Hsc70-K71S with MJDtrQ78 significantly reduced the percentage of cells with aggregates (shown in green) at 12 dpi ($*p < 0.05$; unpaired Student t-test). DAPI was used to label the cell nuclei (shown in red). Double-headed arrows represent the depth of the retina. Scale bars represent 30 μm. The cell population with aggregates was calculated by dividing the number of aggregates by the number of DAPI-stained cell nuclei. Error bars represent the mean ± *s.e.m.* of three independent experiments. The flies were of genotypes *w*; *gmr-GAL4 UAS-MJDtrQ78(s)/+*; *tubP-GAL80ts/+*, and *w*; *gmr-GAL4 UAS-MJDtrQ78(s)/UAS-Hsc70-4.K71S*; *tubP-GAL80ts/+*.

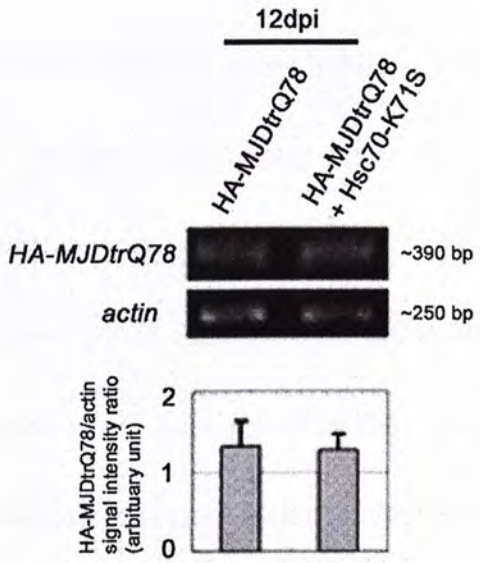

Figure 18. Co-expression of mutant Hsc70-K71S molecular chaperone does not alter *MJDtrQ78* transgene expression. Semi-quantitative RT-PCR analysis of extracted RNA of adult flies. A comparable level of expression of *MJDtrQ78* messenger RNA was detected in MJDtrQ78 flies at 12 days post-induction (dpi) with and without the co-expression of Hsc70-K71S. *actin* messenger RNA was used as the loading control. The band signal intensity ratio (*HA-MJDtrQ78/actin*) was quantified. Error bars represent the mean ± *s.e.m.* of three independent experiments. The flies were of genotypes *w*; *gmr-GAL4 UAS-MJDtrQ78(s)/+*; *tubP-GAL80ts/+* and *w*; *gmr-GAL4 UAS-MJDtrQ78(s)/UAS-Hsc70-4.K71S*; *tubP-GAL80ts/+*.

alteration of *MJDtrQ78* transgene expression.

3.2.2.1.3 Co-expression of Hsc70-K71S does not modify polyglutamine-induced neuronal degeneration

To determine the effect of microscopically visible protein aggregates on polyQ-expressing cells, pseudopupil assay was performed to assess the degree of neuronal degeneration in MJDtrQ78/Hsc70-K71S-expressing flies. If microscopically visible polyQ aggregates are neuroprotective, an enhancement of neuronal degeneration would be expected in these flies. On the contrary, if these aggregates are neurotoxic, neuronal degeneration would be attenuated or delayed. Unexpectedly, no significant difference in the average number of rhabdomeres per ommatidium count was observed between MJDtrQ78-expressing and MJDtrQ78/Hsc70-K71S-expressing flies at all time points examined (Figure 19). Besides, no difference of the gross retinal structure was observed in MJDtrQ78 flies with and without the co-expression of Hsc70-K71S (Figure 20). All these data indicate that microscopically visible polyQ aggregates do not promote or delay MJDtrQ78-induced neuronal degeneration and cell death.

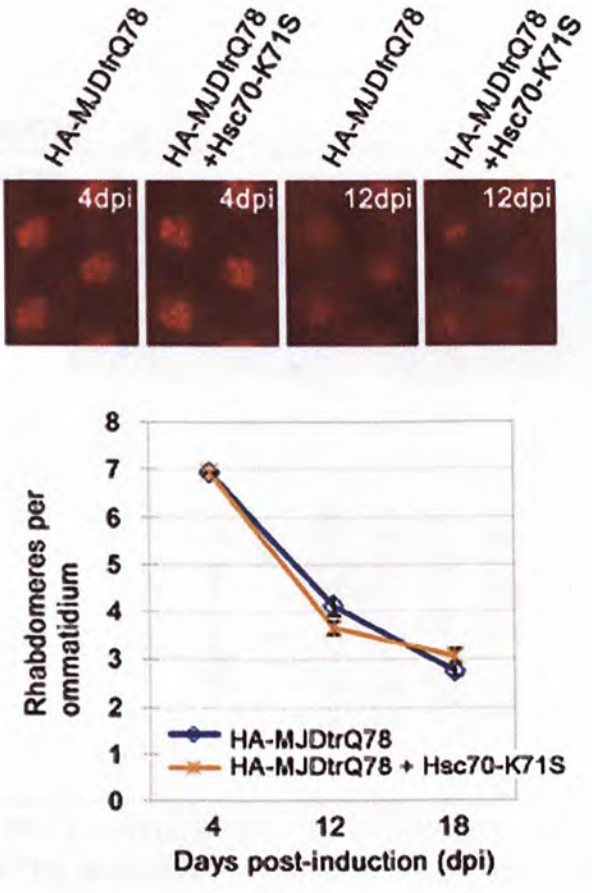

Figure 19. Co-expression of mutant Hsc70-K71S molecular chaperone does not modify MJDtrQ78-induced deterioration of rhabdomere integrity. Pseudopupil assay of rhabdomere integrity in the adult fly eye. The induced expression of MJDtrQ78 caused a progressive reduction in the average number of rhabdomeres per ommatidium count starting from 12 days post-induction (dpi). Co-expression of Hsc70-K71S with MJDtrQ78 resulted in the similar average number of rhabdomeres per ommatidium count as in MJDtrQ78 at all time points examined. Error bars represent the mean ± *s.e.m.* of three independent experiments. The flies were of genotypes *w*; *gmr-GAL4 UAS-MJDtrQ78(s)/+*; *tubP-GAL80ts/+* and *w*; *gmr-GAL4 UAS-MJDtrQ78(s)/UAS-Hsc70-4.K71S*; *tubP-GAL80ts/+*.

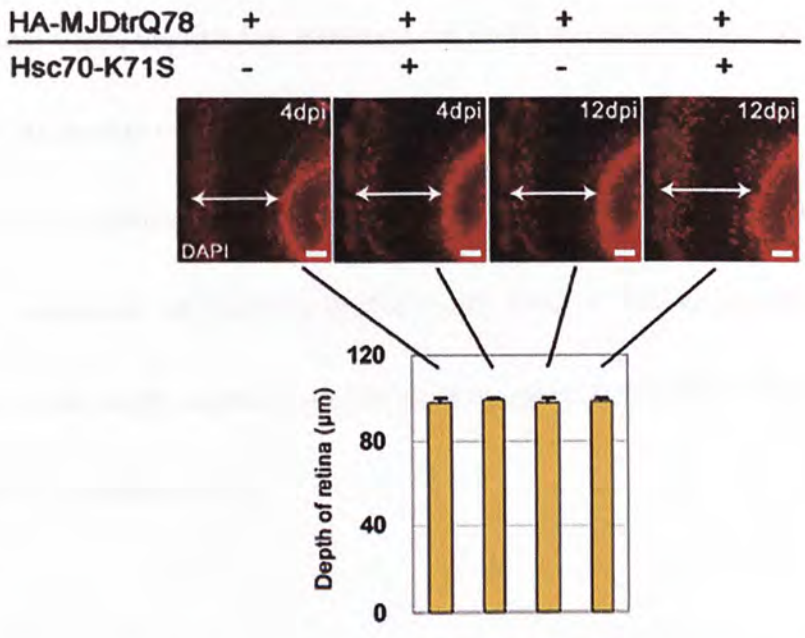

Figure 20. Co-expression of MJDtrQ78 with mutant Hsc70-K71S molecular chaperone does not affect gross retinal morphology. Monitoring of retinal morphology of the adult fly eye under fluorescence microscopy. At both 4 days post-induction (dpi) and 12 dpi, no significant alteration in the depth of the retina (indicated by double-headed arrows) was observed between MJDtrQ78-expressing and MJDtrQ78/Hsc70-K71S-expressing flies. DAPI was used to label the cell nuclei (shown in red). This method has been commonly used to assess retinal cell death (Boeddrich et al. (2006); Fernandez-Funez et al. (2000); Warrick et al. (2005)). Scale bars represent 30 μm. Error bars represent the mean ± *s.e.m.* of three independent experiments. The flies were of genotypes *w*; *gmr-GAL4 UAS-MJDtrQ78(s)/+*; *tubP-GAL80ts/+* and *w*; *gmr-GAL4 UAS-MJDtrQ78(s)/UAS-Hsc70-4.K71S*; *tubP-GAL80ts/+*.

3.2.2.2 Microscopically visible polyglutamine aggregates do not correlate with neuronal degeneration

Our group had previously established an EGFP-polyQ76-FLAG transgenic fly model (Lam and Chan, unpublished materials), in which an expanded polyQ protein containing 76 glutamine repeats was fused with the N-terminus of a FLAG tag and the C-terminus of enhanced green fluorescent protein (EGFP). Similar to MJDtrQ78, constitutive expression of EGFP-polyQ76-FLAG protein led to external eye depigmentation and microscopically visible protein aggregate formation (Figure 21; Lam and Chan, unpublished data).

To further address the correlation between microscopically visible polyQ aggregates and neuronal degeneration, the possibility to simultaneously visualize both GFP-positive polyQ aggregates and rhabdomere integrity in the same EGFP-polyQ76-FLAG-expressing fly eye was explored. Under the regulation of $GAL80^{ts}$, diffuse green fluorescent signals were observed in control EGFP-expressing flies at 4 dpi but not 0 dpi (Figure 22). Discrete nuclear green fluorescent signals were also observed when the expression of a GFP-lacZ fusion protein tagged with a nuclear localization signal was induced for 8 days (Figure 22). In EGFP-polyQ76-FLAG-expressing flies, both diffuse and distinct green fluorescent

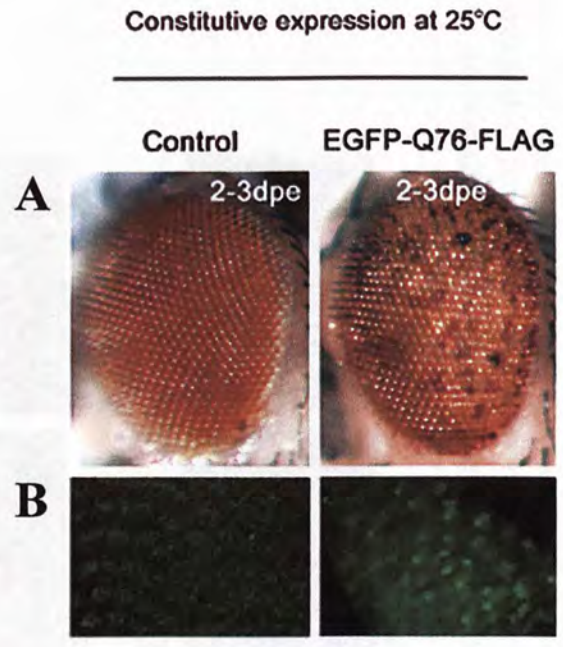

Figure 21. Characterization of EGFP-polyQ76-FLAG transgenic *Drosophila* model. (**A**) Observation of the external eye of adult flies. Constitutive expression of EGFP-polyQ76-FLAG caused external eye depigmentation at 2 to 3 days post-eclosion (dpe), but not in the Control. (**B**) Detection of EGFP-polyQ76-FLAG aggregates in the larval imaginal eye disc under fluorescence microscopy. Constitutive expression of EGFP-polyQ76-FLAG led to the formation of GFP-positive aggregates (shown in green). The larva and flies were of genotypes *w*; *gmr-GAL4*/+; +/+ (Control) and *w*; *gmr-GAL4*/+; *UAS-EGFP-Q76-FLAG*/+. (Lam and Chan, unpublished data).

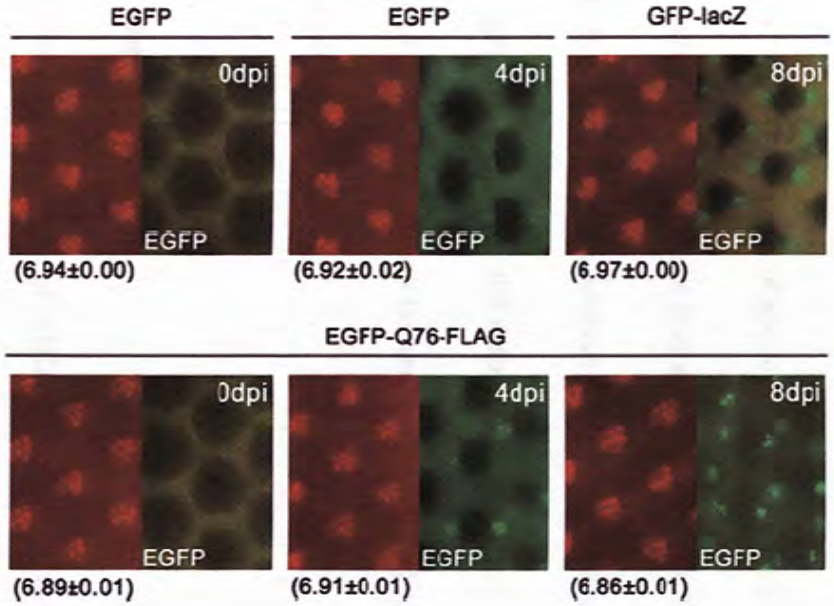

Figure 22. Simultaneous monitoring of rhabdomere integrity and polyQ protein aggregation in EGFP-polyQ76-FLAG flies. Detection of the GFP-tagged protein under fluorescence microscopy and rhabdomere integrity using pseudopupil assay in the same adult fly eye. Inducible expression of EGFP at 4 days post-induction (dpi), and GFP-lacZ fusion protein at 8 dpi showed cytoplasmic and nuclear GFP signals respectively. Induction of EGFP-polyQ76-FLAG protein expression led to progressive accumulation of GFP-positive aggregates starting from 4 dpi. Rhabdomere integrity was simultaneously monitored using pseudopupil assay, and the average number of rhabdomeres per ommatidium count is shown as mean ± *s.e.m.*. The flies were of genotypes: *w*; *gmr-GAL4/UAS-EGFP*; *tubP-GAL80ts/+*, *w*; *gmr-GAL4/UAS-GFP::lacZ.nls*; *tubP-GAL80ts/+* and *w*; *gmr-GAL4/+*; *tubP-GAL80ts/UAS-EGFP-Q76-FLAG*.

signals were detected at 4 and 8 dpi (Figure 22). The distinct, rather than diffuse, green fluorescent signal would probably represent EGFP-polyQ76-FLAG aggregates. Simultaneous to the green fluorescent signal detection, the rhabdomere integrity was monitored in these flies and with the average number of rhabdomeres per ommatidium count determined (Figure 22). Collectively, these results demonstrate the practicability to simultaneously monitor both GFP-tagged protein and rhabdomeres in the fly eye. In flies expressed with EGFP-polyQ76-FLAG, statistical analysis revealed neither a positive nor negative correlation between GFP-positive polyQ aggregate formation and rhabdomere integrity (Figure 23). This data therefore supports a lack of association between microscopically visible polyQ aggregates and neuronal degeneration.

3.2.3 Discussion

Inducible expression of MJDtrQ78 protein formed microscopically visible protein aggregates (Figure 11), and its sustained expression (12 dpi and onwards) resulted in neuronal degeneration (Figure 12). When the number of microscopically visible polyQ aggregate-containing cells was reduced by the co-expression of an ATPase-defective mutant Hsc70 molecular chaperone protein (Figure 17), no modification of neuronal degeneration was observed (Figure 19; Figure 20). It was

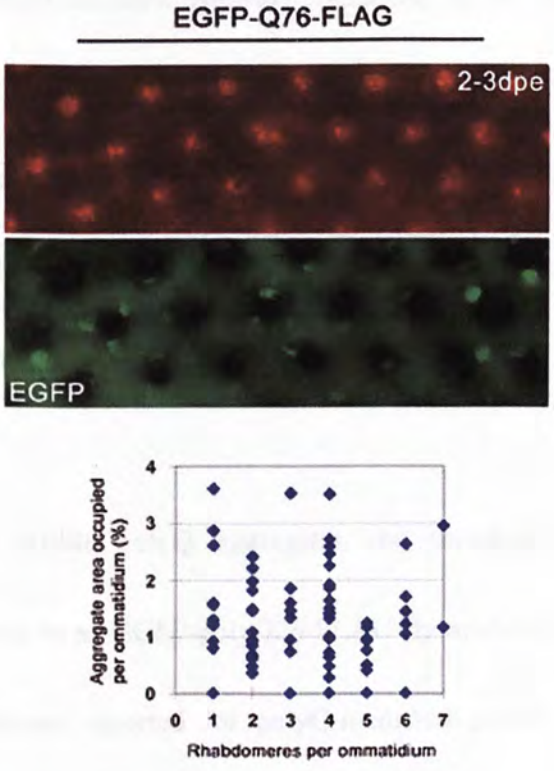

Figure 23. Accumulation of polyQ aggregates is not correlated with deterioration of rhabdomere integrity in the EGFP-polyQ76-FLAG model. Detection of EGFP-polyQ76-FLAG aggregates under fluorescence microscopy and rhabdomere integrity using pseudopupil assay in the same adult fly eye. No linear correlation was observed between the area occupied by GFP-positive aggregates (defined as the total area of green fluorescence signals over the area of a single ommatidium) and the average number of rhabdomeres per ommatidium count (R^2 = 0.001; p = 0.752) in EGFP-polyQ76-FLAG-expressing flies of 2 to 3 days post-eclosion (dpe). The flies were of genotype *w*; *gmr-GAL4*/+; *tubP-GAL80ts*/*UAS-EGFP-Q76-FLAG*.

previously reported that the K71S mutation promotes degradation of α-synuclein, an aggregation-prone disease protein involved in Parkinson's disease, through a non-proteasome inhibitor-sensitive pathway (Klucken et al. 2004). The exact mechanism by which Hsc70-K71S attenuated the accumulation of microscopically visible polyQ aggregates requires further investigation. Nevertheless, these MJDtrQ78 aggregates appear to play neither a neurotoxic nor protective role in triggering polyQ-induced neuronal degeneration.

Microscopically visible polyQ aggregates and rhabdomere integrity were assessed simultaneously in an EGFP-polyQ76-FLAG fly model. Of note, this model reiterates several features reported for polyQ-mediated protein aggregation and neurodegeneration. First, both diffuse and distinct green fluorescent signals of EGFP-polyQ76-FLAG protein were detected at 4 dpi, with the latter signal being predominant at 8 dpi (Figure 22). In the view that the distinct green fluorescent signal corresponds to EGFP-polyQ76-FLAG aggregates, this is consistent with the real-time observation in a cell culture model of HD that microscopically visible polyQ aggregates grow by incorporation of the diffuse expanded polyQ protein (Schiffer et al., 2007). Second, accumulation of EGFP-polyQ76-FLAG aggregates was observed at 8 dpi, but the average number of rhabdomeres per ommatidium at 8

dpi remains comparable to that at 0 dpi (Figure 22). This is again in agreement with that no neurodegenerative phenotype was detected despite widespread occurrence of microscopically visible polyQ aggregates in the inducible MJD fly model (Figure 11; Figure 12) and in a previously reported transgenic mouse model of HD (Slow et al., 2005). Third, further expression of EGFP-polyQ76-FLAG protein resulted in degenerative phenotypes (Figure 21A; Figure 23). All these provide further basis on the use of this EGFP-polyQ76-FLAG model to study polyQ protein aggregation and neurodegeneration. Using this model, no linear correlation between the number of EGFP-polyQ76-FLAG aggregates formed and neuronal degeneration was found (Figure 23).

Summarizing data from the two independent fly models, proteins with expanded polyQ tracts form microscopically visible aggregates which do not associate with polyQ-induced neuronal degeneration *in vivo*. These findings are in line with the lack of correlation between neurodegeneration and microscopically visible protein aggregates recently described in MJD patient brain tissues (Rub et al., 2006).

3.3 Detection of small SDS-insoluble expanded polyglutamine protein species and its association with neurodegeneration

3.3.1 Introduction

Disease protein with an expanded polyQ tract exists in various forms (section 1.4) which display distinct biochemical solubility properties when extracted by solvents such as sodium dodecyl sulfate (SDS) and formic acid (FA). Previous studies have established a connection between solubility properties of expanded polyQ protein and neurodegeneration. For example, it was found that molecular chaperones increased the level of SDS-soluble expanded polyQ disease protein and ameliorated polyQ-mediated toxicity in both transgenic *Drosophila* models of MJD (Chan et al., 2000) and SBMA (Chan et al., 2002), whereas compromised proteasome activity in the cell reduced the level of SDS-soluble expanded polyQ disease protein and enhanced polyQ-mediated degeneration in the transgenic *Drosophila* model of SBMA (Chan et al., 2002). In a knock-in mouse model of SCA 1, SDS-solubility properties of expanded polyQ disease protein decreased with the disease progression (Watase et al., 2002). In brain tissues of HD patients, FA-insoluble polyQ disease protein was isolated in cerebral cortex, which is one of the brain regions most vulnerable to degeneration in HD (Table 1), but not in

unaffected regions such as cerebellum (Iuchi et al., 2003). Altogether, these observations highlight an association between disease protein solubility and neurodegeneration in polyQ pathogenesis. In this section, the relationship between solubility properties of the expanded polyQ protein and neuronal degeneration was studied in the inducible *Drosophila* model.

3.3.2 Results

3.3.2.1 Accumulation of SDS-soluble expanded polyglutamine protein does not correlate with neuronal degeneration

SDS-soluble forms of the expanded polyQ protein have been widely described both *in vitro* (Behrends et al., 2006; Chai et al., 2001; Cong et al., 2006; Dehay and Bertolotti, 2006; Gales et al., 2005; Nagai et al., 2007; Schaffar et al., 2004) and *in vivo* (Chan et al., 2002; Chan et al., 2000; Hay et al., 2004; Lam et al., 2006; Li et al., 2006). In the inducible fly model, monomeric SDS-soluble MJDtrQ78 protein was detected at 4 dpi, but not 12 dpi (Figure 9) when neuronal degeneration became prominent (Figure 12). This indicates that degeneration of neurons is not mediated by the accumulation of monomeric SDS-soluble expanded polyQ protein.

3.3.2.2 Identification of small SDS-insoluble expanded polyglutamine protein species

3.3.2.2.1 Accumulation of SDS-insoluble expanded polyglutamine protein positively correlates with progressive neuronal degeneration

Expanded polyQ protein shows a tendency to accumulate in SDS-insoluble form (section 3.1.2.1.3); a temporal accumulation of SDS-insoluble MJDtrQ78 protein was detected in the stacking gel portion from 4 to 12 dpi (Figure 9; Figure 25A). To confirm this, FA extraction of SDS-insoluble polyQ protein (Hazeki et al., 2000; Hoffner et al., 2005; Iuchi et al., 2003) in MJDtrQ78-expressing flies was performed. 100% FA dissolves most SDS-insoluble MJDtrQ78 proteins in flies (Figure 24; Lam and Chan, unpublished data). Using this method, a temporal accumulation of SDS-insoluble (FA-extractable) MJDtrQ78 protein was again observed from 4 to 12 dpi (Figure 25B). These results demonstrate a concomitant buildup of SDS-insoluble expanded polyQ protein (Figure 9; Figure 25) with neuronal degeneration (Figure 12).

3.3.2.2.2 Accumulation of large SDS-insoluble expanded polyglutamine protein does not correlate with neuronal degeneration

Filter retardation assay (Wanker et al., 1999) was employed as an alternative

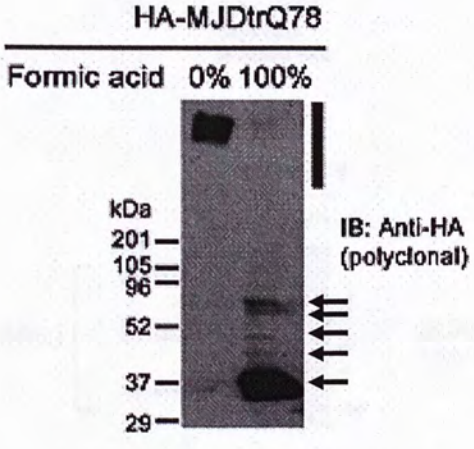

Figure 24. Formic acid dissolves SDS-insoluble MJDtrQ78 protein. Formic acid treatment of the SDS-insoluble MJDtrQ78 protein extract of adult flies. Without formic acid treatment, SDS-insoluble MJDtrQ78 protein was detected in the stacking gel portion (indicated by bar) using Western blot analysis. The MJDtrQ78 protein was found in the running gel portion (indicated by arrows) upon treatment with 100 percent (%) formic acid. The flies were of genotype *w*; *gmr-GAL4 UAS-MJDtrQ78(s)*/+; +/+. (Lam and Chan, unpublished data).

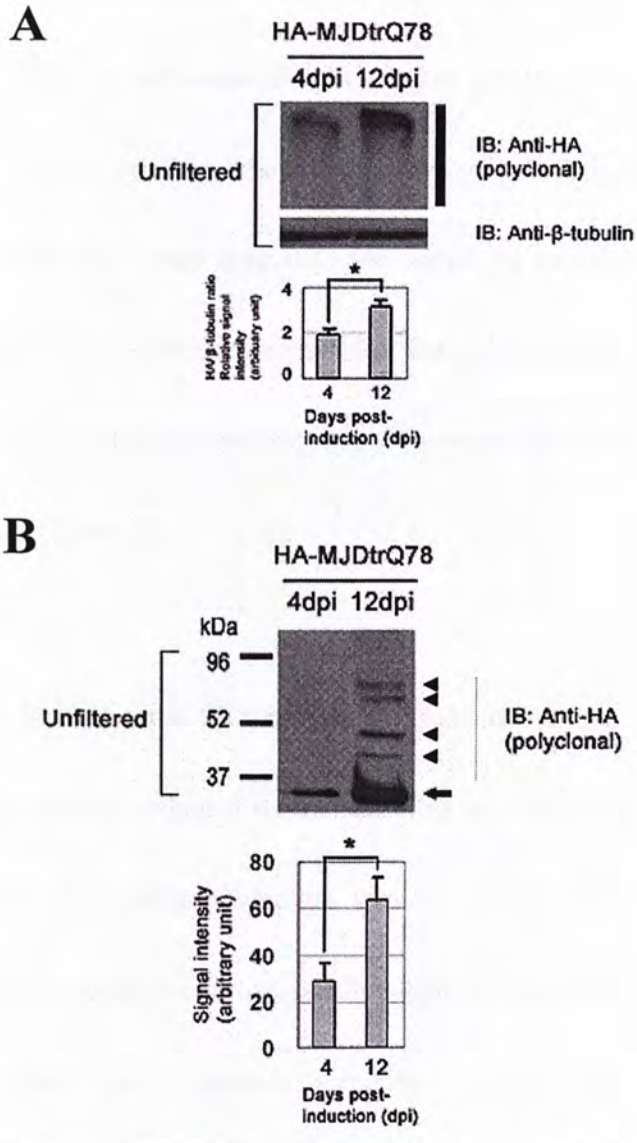

Figure 25. Temporal accumulation of SDS-insoluble MJDtrQ78 protein. (A) Western blot analysis of the MJDtrQ78 protein extract of adult flies. An increase in the level of SDS-insoluble MJDtrQ78 protein was detected from 4 days post-induction (dpi) to 12 dpi (stacking gel; indicated by bar). β-tubulin was used as the loading control ($*p < 0.05$; unpaired Student's t-test). **(B)** Detection of SDS-insoluble MJDtrQ78 protein of adult flies after formic acid (100 percent) treatment. The level of SDS-insoluble formic acid-extractable MJDtrQ78 protein (of monomeric size of about 35 kDa; indicated by arrow) increased from 4 to 12 dpi ($*p < 0.05$; unpaired Student's t-test). High-molecular-weight MJDtrQ78 protein species (indicated by arrowheads) were detected at 12, but not 4 dpi. Error bars represent the mean ± *s.e.m.* of three independent experiments. The flies were of genotype *w*; *gmr-GAL4 UAS-MJDtrQ78(s)*/+; *tubP-GAL80ts*/+.

approach to study the temporal accumulation of polyQ protein; interestingly though, no significant buildup of SDS-insoluble MJDtrQ78 protein from 4 to 12 dpi was detected (Figure 26A). In filter retardation assay, only SDS-insoluble MJDtrQ78 protein species with size larger than 0.22 μm would be retained on the cellulose acetate membrane. This observation argues that the accumulation of "large" (> 0.22 μm) SDS-insoluble MJDtrQ78 protein does not increase with neuronal degeneration as demonstrated in Figure 12.

The involvement of large SDS-insoluble expanded polyQ protein in neuronal degeneration was further evaluated by manipulating its abundance in the inducible MJDtrQ78 model. The ATPase-defective form of Hsc70 (Hsc70-K71S; section 3.2.2.1.1) reduced the level of microscopically visible MJDtrQ78 protein aggregates, and meanwhile there was a positive correlation between the accumulation of microscopically visible aggregates and large SDS-insoluble polyQ protein (Figure 16). The effect of Hsc70-K71S on large SDS-insoluble MJDtrQ78 protein was therefore tested. In MJDtrQ78 flies co-expressed with Hsc70-K71S, the level of large SDS-insoluble MJDtrQ78 protein was reduced at both 4 and 12 dpi (Figure 26A). Meanwhile, using immunoprecipitation, co-expression of Hsc70-K71S did not alter the level of SDS-soluble MJDtrQ78 protein (Figure 26B). These results demonstrate

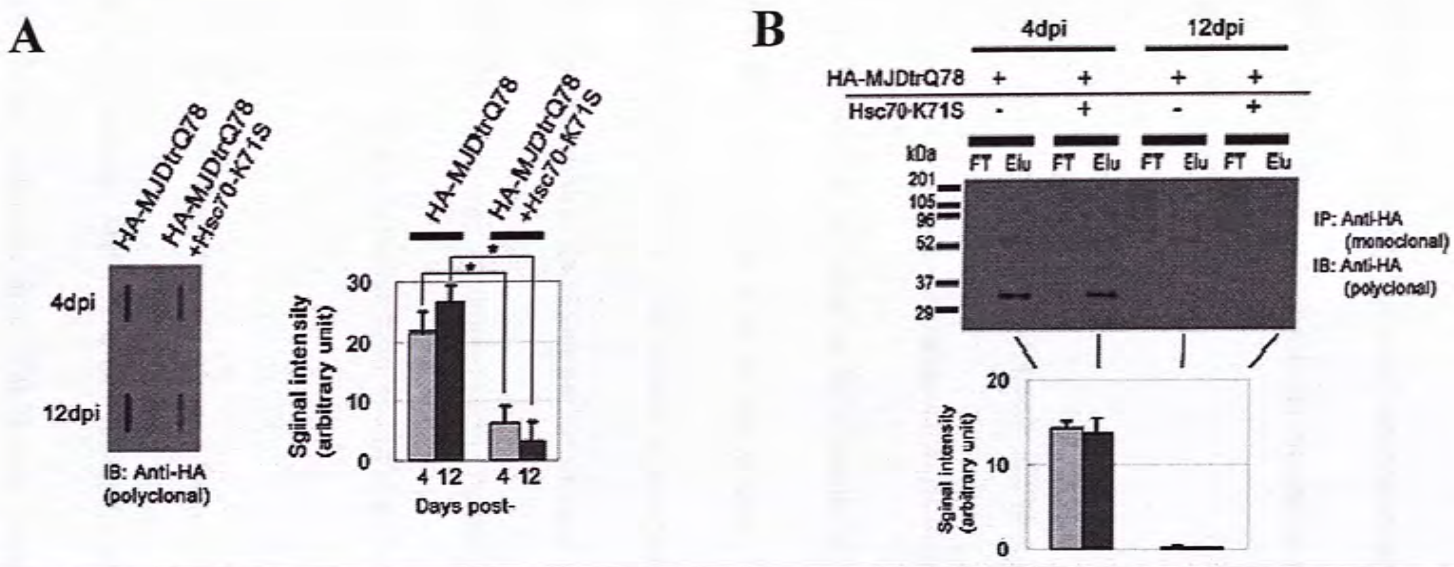

Figure 26. Large SDS-insoluble MJDtrQ78 protein does not accumulate temporally and its level is selectively reduced by the co-expression of mutant Hsc70-K71S molecular chaperone. (**A**) Detection of SDS-insoluble MJDtrQ78 protein of adult flies using filter retardation assay. Comparable amount of SDS-insoluble MJDtrQ78 protein was retained on an 0.22- μm filter membrane after 4 days post-induction (dpi) and 12 dpi of MJDtrQ78 expression. Co-expression of Hsc70-K71S significantly reduced the amount of SDS-insoluble MJDtrQ78 protein that was retained on the filter membrane at both 4 and 12 dpi (*$p < 0.05$ for each comparison; unpaired Student's t-test). (**B**) Immunoprecipitation of the MJDtrQ78 protein extract of adult flies. SDS-soluble monomeric MJDtrQ78 protein (of about 35 kDa) was found in the eluent (Elu) fractions at 4, but not 12 dpi. Similar level of SDS-soluble MJDtrQ78 protein was detected between MJDtrQ78-expressing and MJDtrQ78/Hsc70-K71S-expressing flies at 4 dpi. No MJDtrQ78 protein was found in the flowthrough (FT) fractions. Error bars represent the mean ± *s.e.m.* of three independent experiments. The flies were of genotypes *w*; *gmr-GAL4 UAS-MJDtrQ78(s)/+*; *tubP-GAL80ts/+* and *w*; *gmr-GAL4 UAS-MJDtrQ78(s)/UAS-Hsc70-4.K71S*; *tubP-GAL80ts/+*.

that Hsc70-K71S selectively acts on large SDS-insoluble expanded polyQ protein species. As Hsc70-K71S co-expression exerted neither suppression nor enhancement of MJDtrQ78-induced neuronal degeneration (Figure 19), this further indicates that the level of large SDS-insoluble expanded polyQ protein does not associate with neuronal degeneration.

3.3.2.2.3 Accumulation of small SDS-insoluble expanded polyglutamine protein correlates with neuronal degeneration

A temporal accretion of SDS-insoluble MJDtrQ78 protein was observed in this inducible model from 4 to 12 dpi (Figure 9; Figure 25). Conversely, the level of SDS-insoluble MJDtrQ78 protein retained on the filter membrane did not appear to accumulate within the same period of time (Figure 26A). This therefore favors an idea that there was a temporal accumulation (from 4 to 12 dpi) of MJDtrQ78 protein species that are SDS-insoluble and of size less than 0.22 μm.

To show the presence of such "small" (< 0.22 μm) SDS-insoluble MJDtrQ78 protein species, MJDtrQ78-expressing fly protein extracts were filtered through a membrane with pore size of 0.22 μm. Using filter retardation assay, no detectable amount of SDS-insoluble MJDtrQ78 protein was found after filtration (Figure 27A).

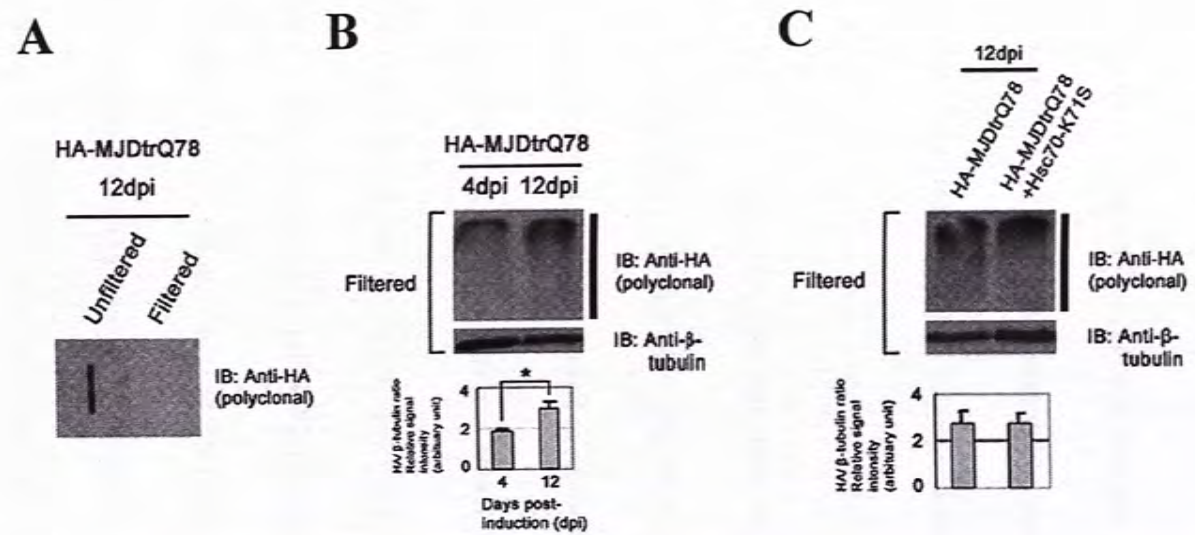

Figure 27. Small SDS-insoluble MJDtrQ78 protein accumulates temporally and its level is not affected by the co-expression of mutant Hsc70-K71S molecular chaperone. (**A**) Detection of SDS-insoluble MJDtrQ78 protein in the adult fly protein extract using filter retardation assay. SDS-insoluble MJDtrQ78 protein was detected at 12 days post-induction (dpi) of MJDtrQ78 expression. No SDS-insoluble MJDtrQ78 protein was detected when the protein extract was filtered through a membrane with pore size of 0.22 μm prior to the filter retardation assay. (**B-C**) Western blot analysis of the MJDtrQ78 protein in filtered (i.e. 0.22 μm) protein extract of adult flies. SDS-insoluble MJDtrQ78 protein (stacking gel, indicated by bar) was found to increase from 4 to 12 dpi (B; $*p < 0.05$; unpaired Student's t-test). Similar level of SDS-insoluble MJDtrQ78 protein (stacking gel, indicated by bar) was detected in MJDtrQ78-expressing and MJDtrQ78/Hsc70-K71S-expressing flies at 12 dpi (C). β-tubulin was used as the loading control (B, C). Error bars represent the mean ± *s.e.m.* of three independent experiments. The flies were of genotypes *w; gmr-GAL4 UAS-MJDtrQ78(s)/+; tubP-GAL80ts/+* and *w; gmr-GAL4 UAS-MJDtrQ78(s)/UAS-Hsc70-4.K71S; tubP-GAL80ts/+*.

This indicates that the filtration process effectively removes large SDS-insoluble MJDtrQ78 protein. Notably, after filtration, an increased amount of SDS-insoluble polyQ protein was detected at the stacking gel portion in MJDtrQ78-expressing flies from 4 to 12 dpi (Figure 27B). Together with the data showing that neuronal degeneration occurred at 12 dpi but not 4 dpi (Figure 12), a contemporaneous accumulation of small SDS-insoluble polyQ protein species (Figure 27B) and neuronal degeneration (Figure 12) was therefore clearly demonstrated.

To further examine the link between small SDS-insoluble expanded polyQ protein species and neuronal degeneration, the level of small SDS-insoluble MJDtrQ78 protein was monitored in MJDtrQ78 flies co-expressed with Hsc70-K71S. Co-expression of Hsc70-K71S was shown to have no effect on MJDtrQ78-induced degeneration (Figure 19). At the time when degeneration occurred (i.e. 12 dpi; Figure 19), the accumulation of small SDS-insoluble MJDtrQ78 protein was observed in the stacking gel portion in MJDtrQ78/Hsc70-K71S-expressing flies, as in MJDtrQ78-expressing flies (Figure 27C). These results therefore demonstrate the association between small SDS-insoluble MJDtrQ78 protein species and neuronal degeneration. Altogether, these findings indicate that small SDS-insoluble expanded polyQ protein species exerts a neurotoxic role.

3.3.3 Discussion

Several types of expanded polyQ protein species were identified in this inducible *Drosophila* model, and they include monomeric SDS-soluble (Figure 9), "large" SDS-insoluble (Figure 10; Figure 26A) and "small" SDS-insoluble (Figure 27) expanded polyQ protein species. Contribution of these expanded polyQ protein species to neuronal degeneration was assessed in this inducible model. Temporal analyses demonstrated that MJDtrQ78-induced neuronal degeneration (Figure 12) was tied with the accumulation of small SDS-insoluble (Figure 27B), but not monomeric SDS-soluble (Figure 9) and large SDS-insoluble (Figure 26A), expanded polyQ protein species. At the time when degeneration occurred, the level of small (Figure 27C), but not large (Figure 26A), SDS-insoluble MJDtrQ78 protein species remained unaffected by action of Hsc70-K71S, which also did not either modulate neuronal degeneration (Figure 19). Despite the mechanism governing the selective action of Hsc70-K71S on distinct type of the expanded polyQ protein being currently unknown, these results altogether provide evidence that small SDS-insoluble expanded polyQ protein species is associated with neuronal degeneration.

High-molecular-weight SDS-soluble expanded polyQ protein species have been detected in yeast models of HD (Behrends et al., 2006; Schaffar et al., 2004) and a

transgenic mouse model of SBMA (Li et al., 2006), and that which were shown to associate with degenerative phenotypes. Similar protein species were not detected in this inducible transgenic fly model of MJD, which may be due to the difference in expression levels of the polyQ protein and/or the disease protein used between these investigations. Summing up the data from this inducible fly model, the involvement of small SDS-insoluble expanded polyQ protein species in neuronal degeneration is strongly suggested.

3.4 Biophysical characterization of small SDS-insoluble expanded polyglutamine protein species

3.4.1 Introduction

Expanded polyQ disease proteins exist in a number of biophysical conformations (section 1.4) that exhibit distinct biochemical solubility properties. For instance, expanded polyQ protein monomers of native or β-sheet conformation (Nagai et al., 2007) and amorphous aggregates (Muchowski et al., 2000) were found to be SDS soluble, whereas spherical oligomers (Wacker et al., 2004), annular oligomers (Wacker et al., 2004) and fibrils (Muchowski et al., 2000; Poirier et al., 2002) were demonstrated to be SDS insoluble. In the previous section 3.3, biochemical and filtration analyses identified small SDS-insoluble expanded polyQ protein as a strong candidate to be a neurotoxic species in polyQ pathogenesis. However, it is not known if such protein species comprise a distinct type of polyQ protein conformers. To address this issue, sucrose gradient sedimentation and atomic force microscopy (AFM) were employed as parallel approaches to characterize the biophysical properties of such toxic species.

3.4.2 Results

3.4.2.1 Separation of expanded polyglutamine protein species by sucrose gradient sedimentation

Protein conformers can be separated by means of sucrose gradient sedimentation based on their sedimentation coefficients (Dehay and Bertolotti, 2006; Schrodel and de Marco, 2005). In previous cell culture studies, expanded polyQ proteins were found to sediment broadly across fractions of different sucrose densities (Chai et al., 2001; Dehay and Bertolotti, 2006), and the expanded polyQ proteins of different conformations sedimented at dissimilar rates in a sucrose gradient (Dehay and Bertolotti, 2006). These observations concur with the idea that the expanded polyQ protein exhibits different conformations in the cell. Here, sucrose gradient sedimentation was performed to review the sedimentation profile of MJDtrQ78 protein in *Drosophila*. In brief, a continuous sucrose density gradient (10% to 50%) was generated, and protein extracts from MJDtrQ78-expressing flies were centrifuged through the gradient. After the separation, 11 fractions (each of 1 ml) were collected and subject to Western blot analysis. As expected, SDS-soluble MJDtrQ78 protein was isolated only from fraction of low sucrose density (i.e. fraction 2) while SDS-insoluble MJDtrQ78 protein was sedimented across a broad range of fractions of high sucrose density (i.e. fractions 7 to 10; Figure 28). This

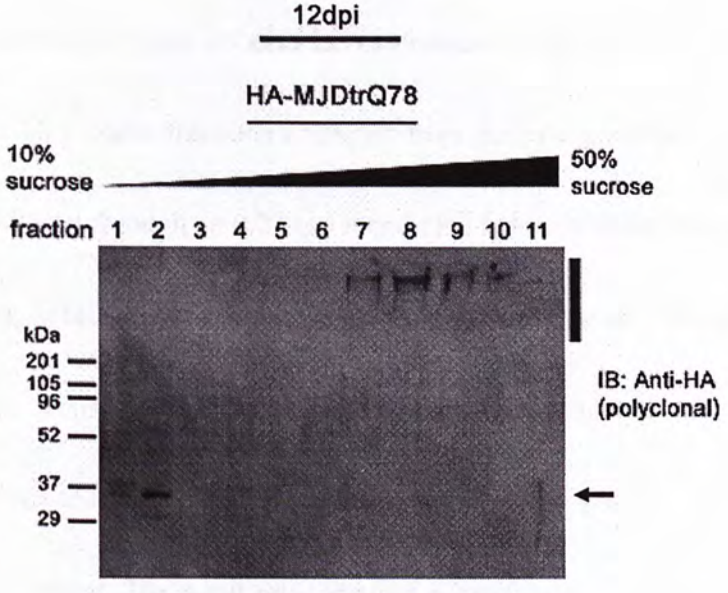

Figure 28. Sucrose gradient sedimentation analysis on MJDtrQ78 protein. Separation of the MJDtrQ78 protein using a continuous 10 to 50 percent sucrose density gradient. At 12 days of post-induction (dpi) of MJDtrQ78 expression, SDS-soluble monomeric MJDtrQ78 protein (of about 35 kDa; indicated by arrow) was detected at fraction 2. SDS-insoluble MJDtrQ78 protein sedimented broadly across fractions 7 to 10 in the stacking gel portion (indicated by bar). Similar results were observed in three independent experiments. The flies were of genotype *w*; *gmr-GAL4 UAS-MJDtrQ78(s)*/+; *tubP-GAL80ts*/+.

result therefore indicates that the expanded MJDtrQ78 protein exists in different conformations *in vivo*.

To check whether the small SDS-insoluble MJDtrQ78 protein fraction comprises a particular type of protein conformers with distinct sedimentation coefficient, the 11 protein fractions collected from sucrose gradient sedimentation analysis were filtered through an 0.22-μm membrane before Western blot analysis. In one experiment, small SDS-insoluble MJDtrQ78 protein species was identified in several sucrose density fractions collected. However, such species were not reproducibly detected in three other independent sucrose gradient sedimentation experiments performed. The result was therefore inconclusive.

3.4.2.2 Morphological studies of small SDS-insoluble expanded polyglutamine protein species by atomic force microscopy

Atomic force microscopy (AFM) has been commonly used to investigate the morphology of proteins (reviewed by Engel and Muller, 2000; Lyubchenko et al., 2006), including the polyQ protein (Dahlgren et al., 2005; Diaz-Hernandez et al., 2004; Ehrnhoefer et al., 2006; Li et al., 2006; Mukai et al., 2005; Poirier et al., 2002; Wacker et al., 2004). The possibility to utilize AFM to study the morphological

appearance of the small SDS-insoluble polyQ protein species was explored. SDS-insoluble MJDtrQ78 protein was isolated by immunoprecipitation (Figure 29), filtered through membrane with pore size of 0.22 μm, and visualized directly under AFM. A population of round-shaped particles was detected at 12 dpi of MJDtrQ78 expression, but not at 0 dpi which serves as the negative control (Figure 30A). These round-shaped particles were estimated to have their size (height) ranging from 5 to 60 nm (Figure 30B), and over 90 percent of them were within the size (height) range of 5 to 20 nm (i.e. 964 out of 1022 round-shaped particles; Figure 30B). Meanwhile, the overall density (particles/field) of these round-shaped particles (i.e. 5 to 20 nm) significantly increased from 4 to 12 dpi (Figure 30B), which is in line with the temporal accumulation of small SDS-insoluble MJDtrQ78 protein species observed in the biochemical and filtration analyses (Figure 27). These results collectively indicate that small SDS-insoluble MJDtrQ78 protein species encompasses a population of round-shaped particles.

Ordered arrays of round-shaped particles (Figure 30A) and fibril-like structures (Figure 31) were also observed in the sample of small SDS-insoluble MJDtrQ78 protein species. These structures were of length varied from 45 to 275 nm, and height ranging from 5 to 10 nm (Figure 31). Meanwhile, no remarkable change in the

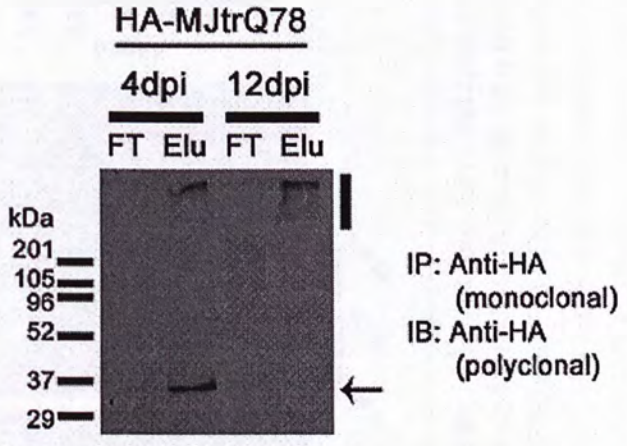

Figure 29. Immunoprecipitation of SDS-insoluble MJDtrQ78 protein. Western blot analysis of immunoprecipitated MJDtrQ78 protein of adult flies. SDS-soluble monomeric MJDtrQ78 protein (of about 35 kDa; indicated by arrow) was detected in the eluent (Elu) fraction at 4, but not 12 days post-induction (dpi). SDS-insoluble MJDtrQ78 protein was detected in the stacking gel portion (indicated by bar) of the Elu fraction at both 4 and 12 dpi. No MJDtrQ78 protein was found in the flowthrough (FT) fraction. Similar results were observed in three independent experiments. The flies were of genotype *w*; *gmr-GAL4 UAS-MJDtrQ78(s)*/+; *tubP-GAL80ts*/+.

A

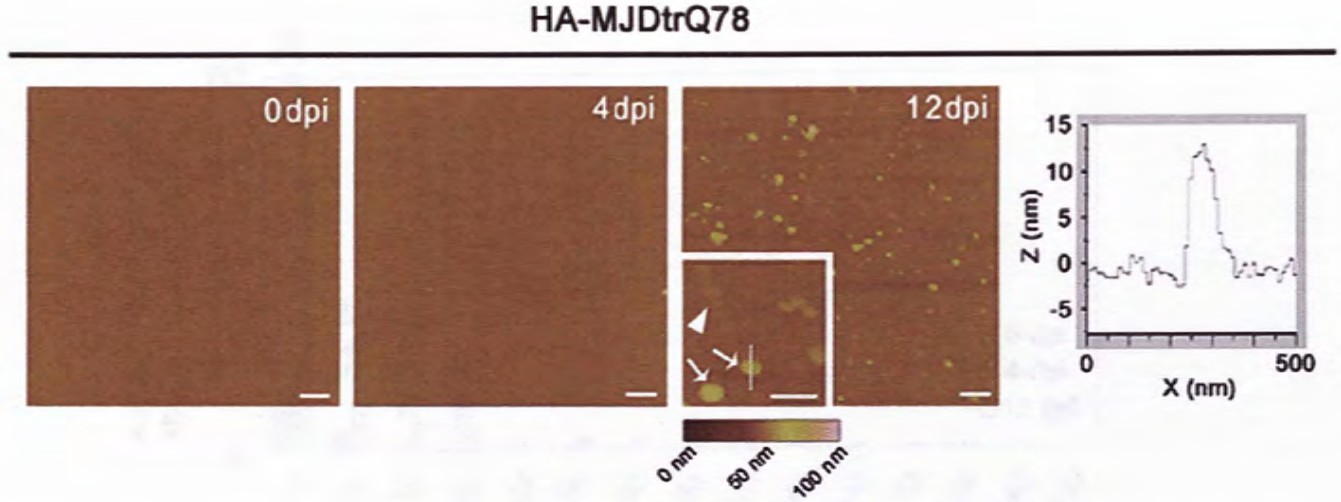

Figure 30. Detection of spherical MJDtrQ78 oligomers. (A) Atomic force microscopy (AFM) analysis of small SDS-insoluble MJDtrQ78 protein. The immunoprecipitated MJDtrQ78 protein of adult flies was filtered through a membrane with pore size of 0.22 μm and subject to AFM analysis. The higher magnification highlights the round-shaped particles (indicated by arrows) that were observed at 12 dpi. Ordered arrays of round-shaped particles were also occasionally detected (indicated by arrowhead). Scale bars represent 500 nm. The height (Z-scale), rather than diameter (X-scale), is a more accurate measure of particle size. Height scan across a round-shaped particle (indicated by line) showed its size to be about 12 nm. The flies were of genotype *w*; *gmr-GAL4 UAS-MJDtrQ78(s)*/+; *tubP-GAL80ts*/+.

B

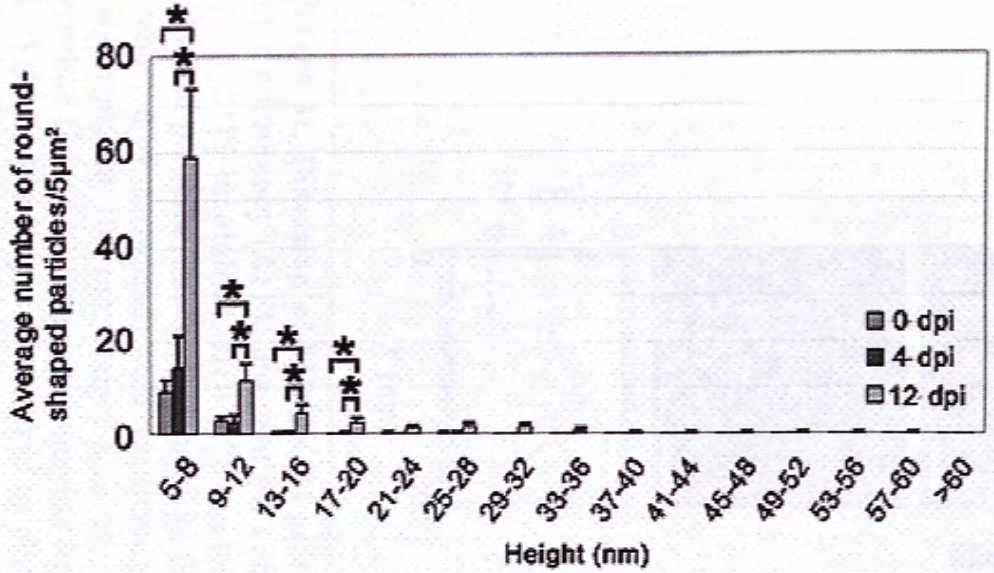

Figure 30 (continued). (B) Quantification of (A). An increased average number of round-shaped particles was detected at 12 days post-induction (dpi) of MJDtrQ78 expression when compared to 0 and 4 dpi (*$p < 0.05$ for each comparison; unpaired Student's t-test). Error bars represent the mean ± *s.e.m.* of three independent experiments.

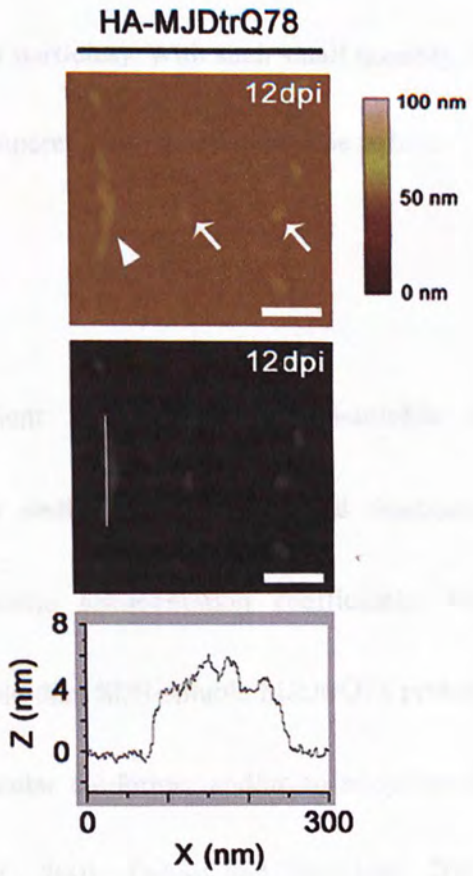

Figure 31. Detection of MJDtrQ78 protofibrils. Atomic force microscopy (AFM) image of the immunoprecipitated small SDS-insoluble MJDtrQ78 protein. Apart from spherical particles (indicated by arrows), fibrillar structures (indicated by arrowhead) were occasionally detected. Scale bars represent 100 nm. Height scan across of a fibrillar structure (i.e. at 12 days post-induction (dpi); indicated by line) showed its height (Z-scale) to be about 5 nm, and its length (X-scale) to be approximately 150 nm. The flies were of genotype *w*; *gmr-GAL4 UAS-MJDtrQ78(s)*/+; *tubP-GAL80ts*/+.

overall height was detected along these structures (Figure 31). These structures however contributed only to less than 4 percent of the detected population of particles (i.e. 41 out of 1063 particles). With such small quantity, their overall density (particles/field) was not compared among different time points.

3.4.3 Discussion

After sucrose gradient sedimentation, SDS-soluble and SDS-insoluble MJDtrQ78 proteins were sedimented in separated fractions (Figure 28), this demonstrates their inimitable sedimentation coefficients. Higher sedimentation coefficient of SDS-insoluble than SDS-soluble MJDtrQ78 protein is indicative of the presence of a macromolecular conformer and/or an adoption of a dense misfolded conformation (Chai et al., 2001; Dehay and Bertolotti, 2006). Likewise, small SDS-insoluble MJDtrQ78 protein species perhaps exists in a conformation of sedimentation coefficient distinct from large SDS-insoluble protein species. Unfortunately, small SDS-insoluble MJDtrQ78 protein was not reproducibly detected in sucrose gradient sedimentation experiments, which may be due to the considerable protein loss after numerous steps of isolation and extraction procedures.

Expanded polyQ protein exists in several biophysical conformations such as

spherical oligomers, annular oligomers, amorphous aggregates, protofibrils and fibrils (section 1.4). These polyQ conformers were reported to have dissimilar morphological appearance (Table 3; Figure 32) under AFM analysis. One limitation of AFM is, however, on the size determination of a particle. The diameter of a particle imaged is often perturbed by the size of the AFM tip, which is referred to as AFM tip convolution (Bustamante and Keller, 1995). The error would be more significant when a small particle size is measured. Despite the additional height errors introduced by tip compression and surface adsorption forces, the height value, rather than the diameter, is a more accurate measure of the particle size. With AFM, the particle size is often therefore defined as the maximum height of the particle. Size ranges reported for various polyQ conformers under AFM were summarized in Table 3 for references.

To characterize the biophysical conformation of small SDS-insoluble expanded polyQ protein species identified in this inducible fly model (section 3.3), SDS-insoluble MJDtrQ78 protein was isolated by immunoprecipitation (Figure 29), filtered through a membrane with pore size of 0.22 μm, and subject to AFM analysis. The predominant structures observed were particles that are round-shaped (Figure 30A) and have a size range of 5 to 60 nm (Figure 30B). The morphology and size of

Table 3. Morphology and size range of expanded polyQ conformers under atomic force microscopy.

Expanded polyQ conformer	Description	Reference
Spherical oligomers	composed of about 3-50 monomers; with a globular appearance; typically of 5-20 nm in size but can exist as large as 80 nm	Ehrnhoefer et al. (2006); Mukai et al. (2005); Wacker et al. (2004)
Annular oligomers	composed of a discontinuous ring of short and elongated structures inclusive of spherical subunits; with an average diameter of about 105 nm	Wacker et al. (2004)
Protofibrils	composed of a fibril-like chain of spherical subunits; thinner and shorter than mature fibrils; typically of about 4-10 nm in height but varies in length	Li et al. (2006); Diaz-Hernandez et al. (2004); Poirier et al. (2002)
Fibrils	composed of protofibrils; structurally organized protein aggregates; typically of about 10-20 nm in height but varies in length	Dahlgren et al. (2005); Muchowski et al. (2000); Poirier et al. (2002); Scherzinger et al. (1999); Wacker et al. (2004)
Amorphous aggregates	unstructured protein aggregates; with an average diameter of about 60-125 nm	Wacker et al. (2004); Muchowski et al. (2000)

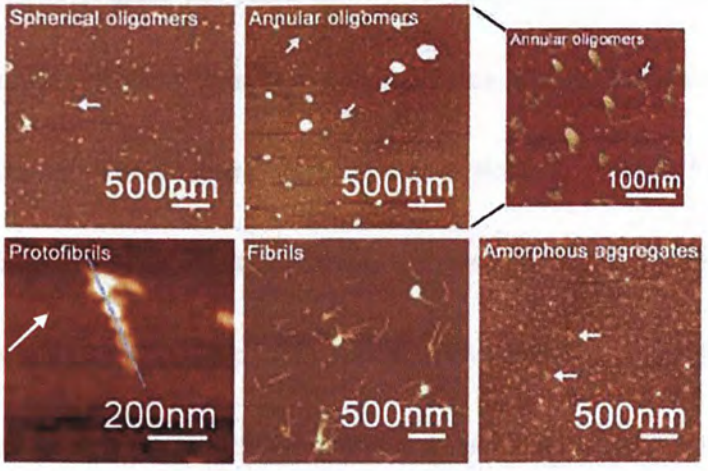

Figure 32. Morphological appearance of expanded polyQ protein conformers under atomic force microscopy. Atomic force microscopy (AFM) images of expanded polyQ protein conformers, which include spherical oligomers, annular oligomers, protofibrils, fibrils, and amorphous aggregates. The polyQ conformer was highlighted by arrow(s) and with scale bar specified in each image. (Modified from Wacker et al. (2004) and Li et al. (2006)).

these particles resembled those described previously for spherical polyQ oligomers (Table 3; Figure 32; Ehrnhoefer et al., 2006; Mukai et al., 2005; Wacker et al., 2004). Small SDS-insoluble MJDtrQ78 protein species therefore existed mostly in form of spherical oligomers. Ordered arrays of round-shaped particles (Figure 30A) and fibril-like structures (Figure 31) were also occasionally observed in the sample of small SDS-insoluble MJDtrQ78 protein species. These structures had morphological feature and size similar to those reported for protofibrils (Table 3; Figure 32; Diaz-Hernandez et al., 2004; Li et al., 2006; Poirier et al., 2002). A minor portion of small SDS-insoluble MJDtrQ78 protein species thus existed in form of protofibrils. In AFM studies on the polyQ protein, protofibrils were shown to comprise units of spherical oligomers (Diaz-Hernandez et al., 2004; Li et al., 2006; Poirier et al., 2002), which indicates that protofibrils are indeed assemblies of spherical oligomers. Taken together, results indicate that small SDS-insoluble MJDtrQ78 protein species exist principally in form of spherical oligomers.

Neuronal degeneration occurred with a temporal accumulation of small SDS-insoluble MJDtrQ78 protein species (i.e. from 4 to 12 dpi; section 3.3). Concomitantly, a significant buildup of spherical MJDtrQ78 protein oligomers (of size ranging from 5-20 nm; encompass over 90 percent of total small SDS-insoluble

MJDtrQ78 protein species) was detected (Figure 30B). These results therefore suggest the neurotoxic property of such spherical polyQ oligomers.

4. GENERAL DISCUSSION

Aggregation of disease protein is a common trait of various neurodegenerative disorders (section 1.1) including polyQ diseases (section 1.2). For over a decade, the mechanism and role of protein aggregation are topical areas of research (section 1.3; section 1.4). Disease-causing proteins are known to exist in a number of aggregated forms with distinct biophysical conformation (section 1.4) and biochemical solubility properties (section 3.4.1). A major challenge has been to identify the distinct form of disease protein species which is decisive for pathogenesis (reviewed by Caughey and Lansbury, 2003).

The relationship between protein aggregates and neurodegeneration cannot be however readily assessed in human beings due to ethical issues and also the naturally long pre-symptomatic period (section 1.1). Clinically characterized tissues are likely to represent only the advanced stage of the disease progression. To compare the course of protein aggregation and neurodegeneration, researchers have shifted to animal modeling studies (reviewed by Caughey and Lansbury, 2003; Zoghbi and Orr, 2000). Nowadays, *Drosophila* emerges as one of the most employed models to examine pathogenic mechanisms in neurodegenerative disorders such as polyQ

diseases (section 1.5).

In this work, an inducible fly model was established to look into the link between polyQ protein aggregates and neurodegeneration and, with an ultimate goal, to uncover the identity of the toxic polyQ protein species (section 3.1). This inducible model recapitulates early pathogenic features of polyQ diseases, including neuronal degeneration without cell death (section 3.1.2.2.1; section 3.1.2.2.2), and formation of protein aggregates (section 3.1.2.1.4). This model would hence facilitate the investigation on polyQ protein aggregation during the early stage of neuronal degeneration.

To look for distinct polyQ protein species that are toxic in nature, a prerequisite criterion to be considered would be its association with neuronal degeneration. In this inducible fly model, microscopically visible polyQ aggregates appear to exert neither a neurotoxic nor protective role in triggering polyQ-mediated neuronal degeneration (section 3.2.2.1). Further, cellular load of these polyQ aggregates also does not have a direct implication in neuronal degeneration (section 3.2.2.2.). Expanded polyQ protein species that appear diffuse, rather than distinct, under light microscopy may indeed be toxic (Arrasate et al., 2004; Taylor et al., 2003a); however, it is not known

in which form(s) of this small diffuse disease protein species would trigger detrimental effects in the cell. Notably, my biochemical and filtration analyses identified a toxic, small-sized, SDS-insoluble expanded polyQ protein species (section 3.3), and such polyQ protein species was further demonstrated to be in form of spherical oligomers (section 3.4.2.2; section 3.4.3). These results provide evidence that spherical polyQ oligomers exist *in vivo* and underlie neuronal degeneration.

In this study, the involvement of polyQ disease protein species in the early stage of neuronal degeneration was evaluated. The contributions of other polyQ species to long-term neurotoxicity, for example when cell death occurs, were not inevitably ruled out. Remarkably though, the identification of spherical oligomers as pathogenic polyQ protein species is in line with the detection of toxic oligomers described in other neurodegenerative disorders (reviewed by Caughey and Lansbury, 2003) including amyloid β oligomers in Alzheimer's disease (Walsh et al., 2002) and α-synuclein spherical oligomers in Parkinson's disease (Conway et al., 1998). This highlights that various neurodegenerative disorders may share a common pathogenic mechanism.

5. CONCLUSION

This project aims to address two important questions in polyQ pathogenesis, which are 1) the role of protein aggregates in neurodegeneration, and 2) the toxic form of polyQ protein species. An inducible *Drosophila* model was established to monitor both polyQ disease protein aggregation and neuronal degeneration *in vivo*. Progressive degeneration of neurons was observed in this model; results further indicate that the early stage of degeneration involve mechanisms such as alteration of endogenous Hsp70 molecular chaperone protein level. Accumulation of microscopically visible protein aggregates is a hallmark feature of polyQ diseases; such accretion was also detected in the inducible model. However, these aggregates did not exert a protective or detrimental role in neuronal degeneration. Indeed, a biochemically-characterized form of small-sized SDS-insoluble polyQ protein species was associated tightly with neuronal degeneration. Such neurotoxic polyQ species was further demonstrated to exist in a conformation of spherical oligomers. The present study directly demonstrates that spherical polyQ oligomers are involved in neuronal degeneration *in vivo*.

To learn how these spherical polyQ oligomers underlie neuronal degeneration, a

few more issues are to be addressed. For example, to find out the mechanism by which these polyQ oligomers formed, to uncover the composition of these polyQ oligomers, and to identify cellular interacting partners of these polyQ oligomers. Learning all these would give a better understanding of the involvement of spherical polyQ oligomers in neurodegeneration.

6. REFERENCES

Adachi, H., Kume, A., Li, M., Nakagomi, Y., Niwa, H., Do, J., Sang, C., Kobayashi, Y., Doyu, M. and Sobue, G. (2001) Transgenic mice with an expanded CAG repeat controlled by the human AR promoter show polyglutamine nuclear inclusions and neuronal dysfunction without neuronal cell death. *Hum Mol Genet*, **10**, 1039-1048.

Agrawal, N., Pallos, J., Slepko, N., Apostol, B.L., Bodai, L., Chang, L.W., Chiang, A.S., Thompson, L.M. and Marsh, J.L. (2005) Identification of combinatorial drug regimens for treatment of Huntington's disease using Drosophila. *Proc Natl Acad Sci U S A*, **102**, 3777-3781.

Apostol, B.L., Kazantsev, A., Raffioni, S., Illes, K., Pallos, J., Bodai, L., Slepko, N., Bear, J.E., Gertler, F.B., Hersch, S., Housman, D.E., Marsh, J.L. and Thompson, L.M. (2003) A cell-based assay for aggregation inhibitors as therapeutics of polyglutamine-repeat disease and validation in Drosophila. *Proc Natl Acad Sci U S A*, **100**, 5950-5955.

Arbouzova, N.I. and Zeidler, M.P. (2006) JAK/STAT signalling in Drosophila: insights into conserved regulatory and cellular functions. *Development*, **133**, 2605-2616.

Arrasate, M., Mitra, S., Schweitzer, E.S., Segal, M.R. and Finkbeiner, S. (2004) Inclusion body formation reduces levels of mutant huntingtin and the risk of neuronal death. *Nature*, **431**, 805-810.

Bangs, P. and White, K. (2000) Regulation and execution of apoptosis during Drosophila development. *Dev Dyn*, **218**, 68-79.

Behrends, C., Langer, C.A., Boteva, R., Bottcher, U.M., Stemp, M.J., Schaffar, G., Rao, B.V., Giese, A., Kretzschmar, H., Siegers, K. and Hartl, F.U. (2006) Chaperonin TRiC promotes the assembly of polyQ expansion proteins into nontoxic oligomers. *Mol Cell*, **23**, 887-897.

Bence, N.F., Sampat, R.M. and Kopito, R.R. (2001) Impairment of the ubiquitin-proteasome system by protein aggregation. *Science*, **292**, 1552-1555.

Bennett, E.J., Bence, N.F., Jayakumar, R. and Kopito, R.R. (2005) Global impairment of the ubiquitin-proteasome system by nuclear or cytoplasmic protein aggregates precedes inclusion body formation. *Mol Cell*, **17**, 351-365.

Berger, Z., Ttofi, E.K., Michel, C.H., Pasco, M.Y., Tenant, S., Rubinsztein, D.C. and O'Kane, C.J. (2005) Lithium rescues toxicity of aggregate-prone proteins in Drosophila by perturbing Wnt pathway. *Hum Mol Genet*, **14**, 3003-3011.

Bier, E. and Bodmer, R. (2004) Drosophila, an emerging model for cardiac disease. *Gene*, **342**, 1-11.

Bilen, J. and Bonini, N.M. (2005) Drosophila as a model for human neurodegenerative disease. *Annu Rev Genet*, **39**, 153-171.

Bilen, J., Liu, N., Burnett, B.G., Pittman, R.N. and Bonini, N.M. (2006) MicroRNA pathways modulate polyglutamine-induced neurodegeneration. *Mol Cell*, **24**, 157-163.

Boeddrich, A., Gaumer, S., Haacke, A., Tzvetkov, N., Albrecht, M., Evert, B.O., Muller, E.C., Lurz, R., Breuer, P., Schugardt, N., Plassmann, S., Xu, K., Warrick, J.M., Suopanki, J., Wullner, U., Frank, R., Hartl, U.F., Bonini, N.M. and Wanker, E.E. (2006) An arginine/lysine-rich motif is crucial for VCP/p97-mediated modulation of ataxin-3 fibrillogenesis. *Embo J*, **25**, 1547-1558.

Brand, A.H. and Perrimon, N. (1993) Targeted gene expression as a means of altering cell fates and generating dominant phenotypes. *Development*, **118**, 401-415.

Brand, A.H., Manoukian, A.S. and Perrimon, N. (1994) Ectopic expression in Drosophila. *Methods Cell Biol*, **44**, 635-654.

Bredesen, D.E., Rao, R.V. and Mehlen, P. (2006) Cell death in the nervous system. *Nature*, **443**, 796-802.

Brignull, H.R., Morley, J.F. and Morimoto, R.I. (2007) The stress of misfolded proteins: C. elegans models for neurodegenerative disease and aging. *Adv Exp Med Biol*, **594**, 167-189.

Bukau, B., Weissman, J. and Horwich, A. (2006) Molecular chaperones and protein quality control. *Cell*, **125**, 443-451.

Bustamante, C. and Keller, D. (1995) Scanning force microscopy in biology. *Phys Today*, **48**, 32-39.

Butler, R. and Bates, G.P. (2006) Histone deacetylase inhibitors as therapeutics for polyglutamine disorders. *Nat Rev Neurosci*, **7**, 784-796.

Campos-Ortega, J.A. (1980) On compound eye development in Drosophila melanogaster. *Curr Top Dev Biol*, **15 Pt 1**, 347-371.

Casanova, J. (2007) The emergence of shape: notions from the study of the Drosophila tracheal system. *EMBO Rep*, **8**, 335-339.

Cattaneo, E., Rigamonti, D., Goffredo, D., Zuccato, C., Squitieri, F. and Sipione, S. (2001) Loss of normal huntingtin function: new developments in Huntington's disease research. *Trends Neurosci*, **24**, 182-188.

Caughey, B. and Lansbury, P.T. (2003) Protofibrils, pores, fibrils, and neurodegeneration: separating the responsible protein aggregates from the innocent bystanders. *Annu Rev Neurosci*, **26**, 267-298.

Chai, Y., Wu, L., Griffin, J.D. and Paulson, H.L. (2001) The role of protein

composition in specifying nuclear inclusion formation in polyglutamine disease. *J Biol Chem*, **276**, 44889-44897.

Chan, H.Y., Warrick, J.M., Andriola, I., Merry, D. and Bonini, N.M. (2002) Genetic modulation of polyglutamine toxicity by protein conjugation pathways in Drosophila. *Hum Mol Genet*, **11**, 2895-2904.

Chan, H.Y., Warrick, J.M., Gray-Board, G.L., Paulson, H.L. and Bonini, N.M. (2000) Mechanisms of chaperone suppression of polyglutamine disease: selectivity, synergy and modulation of protein solubility in Drosophila. *Hum Mol Genet*, **9**, 2811-2820.

Chang, W.H., Cemal, C.K., Hsu, Y.H., Kuo, C.L., Nukina, N., Chang, M.H., Hu, H.T., Li, C. and Hsieh, M. (2005) Dynamic expression of Hsp27 in the presence of mutant ataxin-3. *Biochem Biophys Res Commun*, **336**, 258-267.

Charroux, B., Freeman, M., Kerridge, S. and Baonza, A. (2006) Atrophin contributes to the negative regulation of epidermal growth factor receptor signaling in Drosophila. *Dev Biol*, **291**, 278-290.

Chen, H.K., Fernandez-Funez, P., Acevedo, S.F., Lam, Y.C., Kaytor, M.D., Fernandez, M.H., Aitken, A., Skoulakis, E.M., Orr, H.T., Botas, J. and Zoghbi, H.Y. (2003) Interaction of Akt-phosphorylated ataxin-1 with 14-3-3 mediates neurodegeneration in spinocerebellar ataxia type 1. *Cell*, **113**, 457-468.

Chen, S., Ferrone, F.A. and Wetzel, R. (2002) Huntington's disease age-of-onset linked to polyglutamine aggregation nucleation. *Proc Natl Acad Sci U S A*, **99**, 11884-11889.

Cong, S.Y., Pepers, B.A., Roos, R.A., van Ommen, G.J. and Dorsman, J.C. (2006) Small N-terminal mutant huntingtin fragments, but not wild type, are mainly present in monomeric form: Implications for pathogenesis. *Exp Neurol*, **199**, 257-264.

Conway, K.A., Harper, J.D. and Lansbury, P.T. (1998) Accelerated in vitro fibril formation by a mutant alpha-synuclein linked to early-onset Parkinson disease. *Nat Med*, **4**, 1318-1320.

Cummings, C.J., Sun, Y., Opal, P., Antalffy, B., Mestril, R., Orr, H.T., Dillmann, W.H. and Zoghbi, H.Y. (2001) Over-expression of inducible HSP70 chaperone suppresses neuropathology and improves motor function in SCA1 mice. *Hum Mol Genet*, **10**, 1511-1518.

Dahlgren, P.R., Karymov, M.A., Bankston, J., Holden, T., Thumfort, P., Ingram, V.M. and Lyubchenko, Y.L. (2005) Atomic force microscopy analysis of the Huntington protein nanofibril formation. *Nanomedicine*, **1**, 52-57.

Dehay, B. and Bertolotti, A. (2006) Critical role of the proline-rich region in Huntingtin for aggregation and cytotoxicity in yeast. *J Biol Chem*, **281**, 35608-35615.

Di Prospero, N.A. and Fischbeck, K.H. (2005) Therapeutics development for triplet repeat expansion diseases. *Nat Rev Genet*, **6**, 756-765.

Diaz-Hernandez, M., Moreno-Herrero, F., Gomez-Ramos, P., Moran, M.A., Ferrer, I., Baro, A.M., Avila, J., Hernandez, F. and Lucas, J.J. (2004) Biochemical, ultrastructural, and reversibility studies on huntingtin filaments isolated from mouse and human brain. *J Neurosci*, **24**, 9361-9371.

Doble, A. (1999) The role of excitotoxicity in neurodegenerative disease: implications for therapy. *Pharmacol Ther*, **81**, 163-221.

Doi, H., Mitsui, K., Kurosawa, M., Machida, Y., Kuroiwa, Y. and Nukina, N. (2004) Identification of ubiquitin-interacting proteins in purified polyglutamine aggregates. *FEBS Lett*, **571**, 171-176.

Ehrnhoefer, D.E., Duennwald, M., Markovic, P., Wacker, J.L., Engemann, S., Roark, M., Legleiter, J., Marsh, J.L., Thompson, L.M., Lindquist, S., Muchowski, P.J. and Wanker, E.E. (2006) Green tea (-)-epigallocatechin-gallate modulates early events in huntingtin misfolding and reduces toxicity in Huntington's disease models. *Hum Mol Genet*, **15**, 2743-2751.

Ellis, M.C., O'Neill, E.M. and Rubin, G.M. (1993) Expression of Drosophila glass protein and evidence for negative regulation of its activity in non-neuronal cells by another DNA-binding protein. *Development*, **119**, 855-865.

Ellisdon, A.M., Thomas, B. and Bottomley, S.P. (2006) The two-stage pathway of ataxin-3 fibrillogenesis involves a polyglutamine-independent step. *J Biol Chem*, **281**, 16888-16896.

Engel, A. and Muller, D.J. (2000) Observing single biomolecules at work with the atomic force microscope. *Nat Struct Biol*, **7**, 715-718.

Fernandez-Funez, P., Nino-Rosales, M.L., de Gouyon, B., She, W.C., Luchak, J.M., Martinez, P., Turiegano, E., Benito, J., Capovilla, M., Skinner, P.J., McCall, A., Canal, I., Orr, H.T., Zoghbi, H.Y. and Botas, J. (2000) Identification of genes that modify ataxin-1-induced neurodegeneration. *Nature*, **408**, 101-106.

Frid, P., Anisimov, S.V. and Popovic, N. (2007) Congo red and protein aggregation in neurodegenerative diseases. *Brain Res Rev*, **53**, 135-160.

Gales, L., Cortes, L., Almeida, C., Melo, C.V., do Carmo Costa, M., Maciel, P., Clarke, D.T., Damas, A.M. and Macedo-Ribeiro, S. (2005) Towards a structural understanding of the fibrillization pathway in Machado-Joseph's disease: trapping early oligomers of non-expanded ataxin-3. *J Mol Biol*, **353**, 642-654.

Garesse, R. and Kaguni, L.S. (2005) A Drosophila model of mitochondrial DNA replication: proteins, genes and regulation. *IUBMB Life*, **57**, 555-561.

Gatchel, J.R. and Zoghbi, H.Y. (2005) Diseases of unstable repeat expansion: mechanisms and common principles. *Nat Rev Genet*, **6**, 743-755.

Han, D.D., Stein, D. and Stevens, L.M. (2000) Investigating the function of follicular subpopulations during Drosophila oogenesis through hormone-dependent enhancer-targeted cell ablation. *Development*, **127**, 573-583.

Hardy, J. and Gwinn-Hardy, K. (1998) Genetic classification of primary neurodegenerative disease. *Science*, **282**, 1075-1079.

Hay, D.G., Sathasivam, K., Tobaben, S., Stahl, B., Marber, M., Mestril, R., Mahal, A., Smith, D.L., Woodman, B. and Bates, G.P. (2004) Progressive decrease in chaperone protein levels in a mouse model of Huntington's disease and induction of stress proteins as a therapeutic approach. *Hum Mol Genet*, **13**, 1389-1405.

Hazeki, N., Tukamoto, T., Goto, J. and Kanazawa, I. (2000) Formic acid dissolves aggregates of an N-terminal huntingtin fragment containing an expanded polyglutamine tract: applying to quantification of protein components of the aggregates. *Biochem Biophys Res Commun*, **277**, 386-393.

Hoffner, G., Island, M.L. and Djian, P. (2005) Purification of neuronal inclusions of patients with Huntington's disease reveals a broad range of N-terminal fragments of expanded huntingtin and insoluble polymers. *J Neurochem*, **95**, 125-136.

Huen, N.Y. and Chan, H.Y. (2005) Dynamic regulation of molecular chaperone gene expression in polyglutamine disease. *Biochem Biophys Res Commun*, **334**, 1074-1084.

Huen, N.Y., Wong, S.L. and Chan, H.Y. (2007) Transcriptional malfunctioning of heat shock protein gene expression in spinocerebellar ataxias. *Cerebellum*, **6**, 111-117.

Iuchi, S., Hoffner, G., Verbeke, P., Djian, P. and Green, H. (2003) Oligomeric and polymeric aggregates formed by proteins containing expanded polyglutamine. *Proc Natl Acad Sci U S A*, **100**, 2409-2414.

Jackson, G.R., Salecker, I., Dong, X., Yao, X., Arnheim, N., Faber, P.W., MacDonald, M.E. and Zipursky, S.L. (1998) Polyglutamine-expanded human huntingtin transgenes induce degeneration of Drosophila photoreceptor neurons. *Neuron*, **21**, 633-642.

Jana, N.R., Tanaka, M., Wang, G. and Nukina, N. (2000) Polyglutamine length-dependent interaction of Hsp40 and Hsp70 family chaperones with truncated N-terminal huntingtin: their role in suppression of aggregation and cellular toxicity. *Hum Mol Genet*, **9**, 2009-2018.

Jana, N.R., Zemskov, E.A., Wang, G. and Nukina, N. (2001) Altered proteasomal function due to the expression of polyglutamine-expanded truncated N-terminal huntingtin induces apoptosis by caspase activation through mitochondrial cytochrome c release. *Hum Mol Genet*, **10**, 1049-1059.

Jiang, H., Poirier, M.A., Liang, Y., Pei, Z., Weiskittel, C.E., Smith, W.W., DeFranco, D.B. and Ross, C.A. (2006) Depletion of CBP is directly linked with cellular toxicity caused by mutant huntingtin. *Neurobiol Dis*, **23**, 543-551.

Kazemi-Esfarjani, P. and Benzer, S. (2000) Genetic suppression of polyglutamine toxicity in Drosophila. *Science*, **287**, 1837-1840.

Kim, S., Nollen, E.A., Kitagawa, K., Bindokas, V.P. and Morimoto, R.I. (2002) Polyglutamine protein aggregates are dynamic. *Nat Cell Biol*, **4**, 826-831.

Klucken, J., Shin, Y., Hyman, B.T. and McLean, P.J. (2004) A single amino acid substitution differentiates Hsp70-dependent effects on alpha-synuclein degradation and toxicity. *Biochem Biophys Res Commun*, **325**, 367-373.

Kobayashi, Y., Kume, A., Li, M., Doyu, M., Hata, M., Ohtsuka, K. and Sobue, G. (2000) Chaperones Hsp70 and Hsp40 suppress aggregate formation and apoptosis in cultured neuronal cells expressing truncated androgen receptor protein with expanded polyglutamine tract. *J Biol Chem*, **275**, 8772-8778.

Lam, Y.C., Bowman, A.B., Jafar-Nejad, P., Lim, J., Richman, R., Fryer, J.D., Hyun, E.D., Duvick, L.A., Orr, H.T., Botas, J. and Zoghbi, H.Y. (2006) ATAXIN-1 interacts with the repressor Capicua in its native complex to cause SCA1 neuropathology. *Cell*, **127**, 1335-1347.

Latouche, M., Lasbleiz, C., Martin, E., Monnier, V., Debeir, T., Mouatt-Prigent, A., Muriel, M.P., Morel, L., Ruberg, M., Brice, A., Stevanin, G. and Tricoire, H. (2007) A conditional pan-neuronal Drosophila model of spinocerebellar ataxia 7 with a reversible adult phenotype suitable for identifying modifier genes. *J Neurosci*, **27**, 2483-2492.

Lee, T. and Luo, L. (1999) Mosaic analysis with a repressible cell marker for studies of gene function in neuronal morphogenesis. *Neuron*, **22**, 451-461.

Li, M., Chevalier-Larsen, E.S., Merry, D.E. and Diamond, M.I. (2006) Soluble androgen receptor oligomers underlie pathology in a mouse model of SBMA. *J Biol Chem*, **282**, 3157-3164.

Lievens, J.C., Rival, T., Iche, M., Chneiweiss, H. and Birman, S. (2005) Expanded polyglutamine peptides disrupt EGF receptor signaling and glutamate transporter expression in Drosophila. *Hum Mol Genet*, **14**, 713-724.

Lin, M.T. and Beal, M.F. (2006) Mitochondrial dysfunction and oxidative stress in neurodegenerative diseases. *Nature*, **443**, 787-795.

Lohr, D., Venkov, P. and Zlatanova, J. (1995) Transcriptional regulation in the yeast GAL gene family: a complex genetic network. *Faseb J*, **9**, 777-787.

Lyubchenko, Y.L., Sherman, S., Shlyakhtenko, L.S. and Uversky, V.N. (2006) Nanoimaging for protein misfolding and related diseases. *J Cell Biochem*, **99**, 52-70.

Marsh, J.L. and Thompson, L.M. (2006) Drosophila in the study of

neurodegenerative disease. *Neuron*, **52**, 169-178.

Marsh, J.L., Walker, H., Theisen, H., Zhu, Y.Z., Fielder, T., Purcell, J. and Thompson, L.M. (2000) Expanded polyglutamine peptides alone are intrinsically cytotoxic and cause neurodegeneration in Drosophila. *Hum Mol Genet*, **9**, 13-25.

McCampbell, A., Taylor, J.P., Taye, A.A., Robitschek, J., Li, M., Walcott, J., Merry, D., Chai, Y., Paulson, H., Sobue, G. and Fischbeck, K.H. (2000) CREB-binding protein sequestration by expanded polyglutamine. *Hum Mol Genet*, **9**, 2197-2202.

McGuire, S.E., Le, P.T., Osborn, A.J., Matsumoto, K. and Davis, R.L. (2003) Spatiotemporal rescue of memory dysfunction in Drosophila. *Science*, **302**, 1765-1768.

McGuire, S.E., Mao, Z. and Davis, R.L. (2004) Spatiotemporal gene expression targeting with the TARGET and gene-switch systems in Drosophila. *Sci STKE*, **2004**, pl6.

Mergliano, J. and Minden, J.S. (2003) Caspase-independent cell engulfment mirrors cell death pattern in Drosophila embryos. *Development*, **130**, 5779-5789.

Michalik, A. and Van Broeckhoven, C. (2003) Pathogenesis of polyglutamine disorders: aggregation revisited. *Hum Mol Genet*, **12 Spec No 2**, R173-186.

Mitsui, K., Nakayama, H., Akagi, T., Nekooki, M., Ohtawa, K., Takio, K., Hashikawa, T. and Nukina, N. (2002) Purification of polyglutamine aggregates and identification of elongation factor-1alpha and heat shock protein 84 as aggregate-interacting proteins. *J Neurosci*, **22**, 9267-9277.

Morton, A.J., Lagan, M.A., Skepper, J.N. and Dunnett, S.B. (2000) Progressive formation of inclusions in the striatum and hippocampus of mice transgenic for the human Huntington's disease mutation. *J Neurocytol*, **29**, 679-702.

Muchowski, P.J., Schaffar, G., Sittler, A., Wanker, E.E., Hayer-Hartl, M.K. and Hartl, F.U. (2000) Hsp70 and hsp40 chaperones can inhibit self-assembly of polyglutamine proteins into amyloid-like fibrils. *Proc Natl Acad Sci U S A*, **97**, 7841-7846.

Muchowski, P.J. and Wacker, J.L. (2005) Modulation of neurodegeneration by molecular chaperones. *Nat Rev Neurosci*, **6**, 11-22.

Mukai, H., Isagawa, T., Goyama, E., Tanaka, S., Bence, N.F., Tamura, A., Ono, Y. and Kopito, R.R. (2005) Formation of morphologically similar globular aggregates from diverse aggregation-prone proteins in mammalian cells. *Proc Natl Acad Sci U S A*, **102**, 10887-10892.

Nagai, Y., Inui, T., Popiel, H.A., Fujikake, N., Hasegawa, K., Urade, Y., Goto, Y., Naiki, H. and Toda, T. (2007) A toxic monomeric conformer of the polyglutamine protein. *Nat Struct Mol Biol*, **14**, 332-340.

Nucifora, F.C., Jr., Sasaki, M., Peters, M.F., Huang, H., Cooper, J.K., Yamada, M., Takahashi, H., Tsuji, S., Troncoso, J., Dawson, V.L., Dawson, T.M. and Ross, C.A. (2001) Interference by huntingtin and atrophin-1 with cbp-mediated transcription leading to cellular toxicity. *Science*, **291**, 2423-2428.

O'Kane, C.J. (2003) Modelling human diseases in Drosophila and Caenorhabditis. *Semin Cell Dev Biol*, **14**, 3-10.

Ordway, J.M., Tallaksen-Greene, S., Gutekunst, C.A., Bernstein, E.M., Cearley, J.A., Wiener, H.W., Dure, L.S.t., Lindsey, R., Hersch, S.M., Jope, R.S., Albin, R.L. and Detloff, P.J. (1997) Ectopically expressed CAG repeats cause intranuclear inclusions and a progressive late onset neurological phenotype in the mouse. *Cell*, **91**, 753-763.

Osterwalder, T., Yoon, K.S., White, B.H. and Keshishian, H. (2001) A conditional tissue-specific transgene expression system using inducible GAL4. *Proc Natl Acad Sci U S A*, **98**, 12596-12601.

Palop, J.J., Chin, J. and Mucke, L. (2006) A network dysfunction perspective on neurodegenerative diseases. *Nature*, **443**, 768-773.

Perutz, M.F., Johnson, T., Suzuki, M. and Finch, J.T. (1994) Glutamine repeats as polar zippers: their possible role in inherited neurodegenerative diseases. *Proc Natl Acad Sci U S A*, **91**, 5355-5358.

Poirier, M.A., Li, H., Macosko, J., Cai, S., Amzel, M. and Ross, C.A. (2002) Huntingtin spheroids and protofibrils as precursors in polyglutamine fibrilization. *J Biol Chem*, **277**, 41032-41037.

Reiter, L.T., Potocki, L., Chien, S., Gribskov, M. and Bier, E. (2001) A systematic analysis of human disease-associated gene sequences in Drosophila melanogaster. *Genome Res*, **11**, 1114-1125.

Riley, B.E. and Orr, H.T. (2006) Polyglutamine neurodegenerative diseases and regulation of transcription: assembling the puzzle. *Genes Dev*, **20**, 2183-2192.

Roman, G., Endo, K., Zong, L. and Davis, R.L. (2001) P[Switch], a system for spatial and temporal control of gene expression in Drosophila melanogaster. *Proc Natl Acad Sci U S A*, **98**, 12602-12607.

Rosenbaum, E.E., Hardie, R.C. and Colley, N.J. (2006) Calnexin is essential for rhodopsin maturation, Ca2+ regulation, and photoreceptor cell survival. *Neuron*, **49**, 229-241.

Ross, C.A. (2002) Polyglutamine pathogenesis: emergence of unifying mechanisms for Huntington's disease and related disorders. *Neuron*, **35**, 819-822.

Ross, C.A. and Poirier, M.A. (2004) Protein aggregation and neurodegenerative disease. *Nat Med*, **10 Suppl**, S10-17.

Ross, C.A. and Poirier, M.A. (2005) Opinion: What is the role of protein aggregation in neurodegeneration? *Nat Rev Mol Cell Biol*, **6**, 891-898.

Rub, U., de Vos, R.A., Brunt, E.R., Sebesteny, T., Schols, L., Auburger, G., Bohl, J., Ghebremedhin, E., Gierga, K., Seidel, K., den Dunnen, W., Heinsen, H., Paulson, H. and Deller, T. (2006) Spinocerebellar ataxia type 3 (SCA3): thalamic neurodegeneration occurs independently from thalamic ataxin-3 immunopositive neuronal intranuclear inclusions. *Brain Pathol*, **16**, 218-227.

Rubin, G.M., Yandell, M.D., Wortman, J.R., Gabor Miklos, G.L., Nelson, C.R., Hariharan, I.K., Fortini, M.E., Li, P.W., Apweiler, R., Fleischmann, W., Cherry, J.M., Henikoff, S., Skupski, M.P., Misra, S., Ashburner, M., Birney, E., Boguski, M.S., Brody, T., Brokstein, P., Celniker, S.E., Chervitz, S.A., Coates, D., Cravchik, A., Gabrielian, A., Galle, R.F., Gelbart, W.M., George, R.A., Goldstein, L.S., Gong, F., Guan, P., Harris, N.L., Hay, B.A., Hoskins, R.A., Li, J., Li, Z., Hynes, R.O., Jones, S.J., Kuehl, P.M., Lemaitre, B., Littleton, J.T., Morrison, D.K., Mungall, C., O'Farrell, P.H., Pickeral, O.K., Shue, C., Vosshall, L.B., Zhang, J., Zhao, Q., Zheng, X.H. and Lewis, S. (2000) Comparative genomics of the eukaryotes. *Science*, **287**, 2204-2215.

Rubinsztein, D.C. (2006) The roles of intracellular protein-degradation pathways in neurodegeneration. *Nature*, **443**, 780-786.

Ryder, E. and Russell, S. (2003) Transposable elements as tools for genomics and genetics in Drosophila. *Brief Funct Genomic Proteomic*, **2**, 57-71.

Sanchez-Soriano, N., Tear, G., Whitington, P. and Prokop, A. (2007) Drosophila as a genetic and cellular model for studies on axonal growth. *Neural Develop*, **2**, 9.

Sang, T.K. and Jackson, G.R. (2005) Drosophila models of neurodegenerative disease. *NeuroRx*, **2**, 438-446.

Sang, T.K., Li, C., Liu, W., Rodriguez, A., Abrams, J.M., Zipursky, S.L. and Jackson, G.R. (2005) Inactivation of Drosophila Apaf-1 related killer suppresses formation of polyglutamine aggregates and blocks polyglutamine pathogenesis. *Hum Mol Genet*, **14**, 357-372.

Schaffar, G., Breuer, P., Boteva, R., Behrends, C., Tzvetkov, N., Strippel, N., Sakahira, H., Siegers, K., Hayer-Hartl, M. and Hartl, F.U. (2004) Cellular toxicity of polyglutamine expansion proteins: mechanism of transcription factor deactivation. *Mol Cell*, **15**, 95-105.

Scherzinger, E., Sittler, A., Schweiger, K., Heiser, V., Lurz, R., Hasenbank, R., Bates, G.P., Lehrach, H. and Wanker, E.E. (1999) Self-assembly of polyglutamine-containing huntingtin fragments into amyloid-like fibrils: implications for Huntington's disease pathology. *Proc Natl Acad Sci U S A*, **96**, 4604-4609.

Schiffer, N.W., Broadley, S.A., Hirschberger, T., Tavan, P., Kretzschmar, H.A., Giese, A., Haass, C., Hartl, F.U. and Schmid, B. (2007) Identification of anti-prion

compounds as efficient inhibitors of polyglutamine protein aggregation in a zebrafish model. *J Biol Chem*, **282**, 9195-9203.

Schrodel, A. and de Marco, A. (2005) Characterization of the aggregates formed during recombinant protein expression in bacteria. *BMC Biochem*, **6**, 10.

Shiga, Y., Tanaka-Matakatsu, M. and Hayashi, S. (1996) A nuclear GFP/β-galactosidase fusion protein as a marker for morphogenesis in living Drosophila. *Development, Growth & Differentiation*, **38**, 99-106.

Shulman, J.M., Shulman, L.M., Weiner, W.J. and Feany, M.B. (2003) From fruit fly to bedside: translating lessons from Drosophila models of neurodegenerative disease. *Curr Opin Neurol*, **16**, 443-449.

Slepko, N., Bhattacharyya, A.M., Jackson, G.R., Steffan, J.S., Marsh, J.L., Thompson, L.M. and Wetzel, R. (2006) Normal-repeat-length polyglutamine peptides accelerate aggregation nucleation and cytotoxicity of expanded polyglutamine proteins. *Proc Natl Acad Sci U S A*, **103**, 14367-14372.

Slow, E.J., Graham, R.K. and Hayden, M.R. (2006) To be or not to be toxic: aggregations in Huntington and Alzheimer disease. *Trends Genet*, **22**, 408-411.

Slow, E.J., Graham, R.K., Osmand, A.P., Devon, R.S., Lu, G., Deng, Y., Pearson, J., Vaid, K., Bissada, N., Wetzel, R., Leavitt, B.R. and Hayden, M.R. (2005) Absence of behavioral abnormalities and neurodegeneration in vivo despite widespread neuronal huntingtin inclusions. *Proc Natl Acad Sci U S A*, **102**, 11402-11407.

Steffan, J.S., Bodai, L., Pallos, J., Poelman, M., McCampbell, A., Apostol, B.L., Kazantsev, A., Schmidt, E., Zhu, Y.Z., Greenwald, M., Kurokawa, R., Housman, D.E., Jackson, G.R., Marsh, J.L. and Thompson, L.M. (2001) Histone deacetylase inhibitors arrest polyglutamine-dependent neurodegeneration in Drosophila. *Nature*, **413**, 739-743.

Steffan, J.S., Kazantsev, A., Spasic-Boskovic, O., Greenwald, M., Zhu, Y.Z., Gohler, H., Wanker, E.E., Bates, G.P., Housman, D.E. and Thompson, L.M. (2000) The Huntington's disease protein interacts with p53 and CREB-binding protein and represses transcription. *Proc Natl Acad Sci U S A*, **97**, 6763-6768.

Stenoien, D.L., Cummings, C.J., Adams, H.P., Mancini, M.G., Patel, K., DeMartino, G.N., Marcelli, M., Weigel, N.L. and Mancini, M.A. (1999) Polyglutamine-expanded androgen receptors form aggregates that sequester heat shock proteins, proteasome components and SRC-1, and are suppressed by the HDJ-2 chaperone. *Hum Mol Genet*, **8**, 731-741.

Stenoien, D.L., Mielke, M. and Mancini, M.A. (2002) Intranuclear ataxin1 inclusions contain both fast- and slow-exchanging components. *Nat Cell Biol*, **4**, 806-810.

Suhr, S.T., Senut, M.C., Whitelegge, J.P., Faull, K.F., Cuizon, D.B. and Gage, F.H. (2001) Identities of sequestered proteins in aggregates from cells with induced polyglutamine expression. *J Cell Biol*, **153**, 283-294.

Takahashi, J., Fujigasaki, H., Zander, C., El Hachimi, K.H., Stevanin, G., Durr, A., Lebre, A.S., Yvert, G., Trottier, Y., de The, H., Hauw, J.J., Duyckaerts, C. and Brice, A. (2002) Two populations of neuronal intranuclear inclusions in SCA7 differ in size and promyelocytic leukaemia protein content. *Brain*, **125**, 1534-1543.

Takeyama, K., Ito, S., Yamamoto, A., Tanimoto, H., Furutani, T., Kanuka, H., Miura, M., Tabata, T. and Kato, S. (2002) Androgen-dependent neurodegeneration by polyglutamine-expanded human androgen receptor in Drosophila. *Neuron*, **35**, 855-864.

Taylor, J.P., Tanaka, F., Robitschek, J., Sandoval, C.M., Taye, A., Markovic-Plese, S. and Fischbeck, K.H. (2003a) Aggresomes protect cells by enhancing the degradation of toxic polyglutamine-containing protein. *Hum Mol Genet*, **12**, 749-757.

Taylor, J.P., Taye, A.A., Campbell, C., Kazemi-Esfarjani, P., Fischbeck, K.H. and Min, K.T. (2003b) Aberrant histone acetylation, altered transcription, and retinal degeneration in a Drosophila model of polyglutamine disease are rescued by CREB-binding protein. *Genes Dev*, **17**, 1463-1468.

Tsai, H.F., Lin, S.J., Li, C. and Hsieh, M. (2005) Decreased expression of Hsp27 and Hsp70 in transformed lymphoblastoid cells from patients with spinocerebellar ataxia type 7. *Biochem Biophys Res Commun*, **334**, 1279-1286.

Venken, K.J. and Bellen, H.J. (2005) Emerging technologies for gene manipulation in Drosophila melanogaster. *Nat Rev Genet*, **6**, 167-178.

Vidal, M. and Cagan, R.L. (2006) Drosophila models for cancer research. *Curr Opin Genet Dev*, **16**, 10-16.

Wacker, J.L., Zareie, M.H., Fong, H., Sarikaya, M. and Muchowski, P.J. (2004) Hsp70 and Hsp40 attenuate formation of spherical and annular polyglutamine oligomers by partitioning monomer. *Nat Struct Mol Biol*, **11**, 1215-1222.

Wager-Smith, K. and Kay, S.A. (2000) Circadian rhythm genetics: from flies to mice to humans. *Nat Genet*, **26**, 23-27.

Walsh, D.M., Klyubin, I., Fadeeva, J.V., Cullen, W.K., Anwyl, R., Wolfe, M.S., Rowan, M.J. and Selkoe, D.J. (2002) Naturally secreted oligomers of amyloid beta protein potently inhibit hippocampal long-term potentiation in vivo. *Nature*, **416**, 535-539.

Wanderer, J. and Morton, A.J. (2007) Differential morphology and composition of inclusions in the R6/2 mouse and PC12 cell models of Huntington's disease. *Histochem Cell Biol*, **127**, 473-484.

Wanker, E.E., Scherzinger, E., Heiser, V., Sittler, A., Eickhoff, H. and Lehrach, H. (1999) Membrane filter assay for detection of amyloid-like polyglutamine-containing protein aggregates. *Methods Enzymol*, **309**, 375-386.

Warrick, J.M., Chan, H.Y., Gray-Board, G.L., Chai, Y., Paulson, H.L. and Bonini, N.M. (1999) Suppression of polyglutamine-mediated neurodegeneration in Drosophila by the molecular chaperone HSP70. *Nat Genet*, **23**, 425-428.

Warrick, J.M., Morabito, L.M., Bilen, J., Gordesky-Gold, B., Faust, L.Z., Paulson, H.L. and Bonini, N.M. (2005) Ataxin-3 suppresses polyglutamine neurodegeneration in Drosophila by a ubiquitin-associated mechanism. *Mol Cell*, **18**, 37-48.

Warrick, J.M., Paulson, H.L., Gray-Board, G.L., Bui, Q.T., Fischbeck, K.H., Pittman, R.N. and Bonini, N.M. (1998) Expanded polyglutamine protein forms nuclear inclusions and causes neural degeneration in Drosophila. *Cell*, **93**, 939-949.

Watase, K., Weeber, E.J., Xu, B., Antalffy, B., Yuva-Paylor, L., Hashimoto, K., Kano, M., Atkinson, R., Sun, Y., Armstrong, D.L., Sweatt, J.D., Orr, H.T., Paylor, R. and Zoghbi, H.Y. (2002) A long CAG repeat in the mouse Sca1 locus replicates SCA1 features and reveals the impact of protein solubility on selective neurodegeneration. *Neuron*, **34**, 905-919.

Wen, F.C., Li, Y.H., Tsai, H.F., Lin, C.H., Li, C., Liu, C.S., Lii, C.K., Nukina, N. and Hsieh, M. (2003) Down-regulation of heat shock protein 27 in neuronal cells and non-neuronal cells expressing mutant ataxin-3. *FEBS Lett*, **546**, 307-314.

Wolfgang, W.J., Miller, T.W., Webster, J.M., Huston, J.S., Thompson, L.M., Marsh, J.L. and Messer, A. (2005) Suppression of Huntington's disease pathology in Drosophila by human single-chain Fv antibodies. *Proc Natl Acad Sci U S A*, **102**, 11563-11568.

Wong, S.L., Chen, Y., Chan, C.M., Chan, C.S., Chan, P.K., Chui, Y.L., Fung, K.P., Waye, M.M., Tsui, S.K. and Chan, H.Y. (2005) In vivo functional characterization of the SARS-Coronavirus 3a protein in Drosophila. *Biochem Biophys Res Commun*, **337**, 720-729.

Wyttenbach, A., Swartz, J., Kita, H., Thykjaer, T., Carmichael, J., Bradley, J., Brown, R., Maxwell, M., Schapira, A., Orntoft, T.F., Kato, K. and Rubinsztein, D.C. (2001) Polyglutamine expansions cause decreased CRE-mediated transcription and early gene expression changes prior to cell death in an inducible cell model of Huntington's disease. *Hum Mol Genet*, **10**, 1829-1845.

Yoshihara, M., Ensminger, A.W. and Littleton, J.T. (2001) Neurobiology and the Drosophila genome. *Funct Integr Genomics*, **1**, 235-240.

Young, J.C., Agashe, V.R., Siegers, K. and Hartl, F.U. (2004) Pathways of

chaperone-mediated protein folding in the cytosol. *Nat Rev Mol Cell Biol*, **5**, 781-791.

Yu, Z.X., Li, S.H., Nguyen, H.P. and Li, X.J. (2002) Huntingtin inclusions do not deplete polyglutamine-containing transcription factors in HD mice. *Hum Mol Genet*, **11**, 905-914.

Zoghbi, H.Y. and Orr, H.T. (2000) Glutamine repeats and neurodegeneration. *Annu Rev Neurosci*, **23**, 217-247.

CUHK Libraries
004433442